The Galactic cycle
-
The importance of statistical studies of Galactic plane survey data

Davide Elia
INAF-IAPS, Rome (Italy)

The baryon cycle in galactic ecosystems

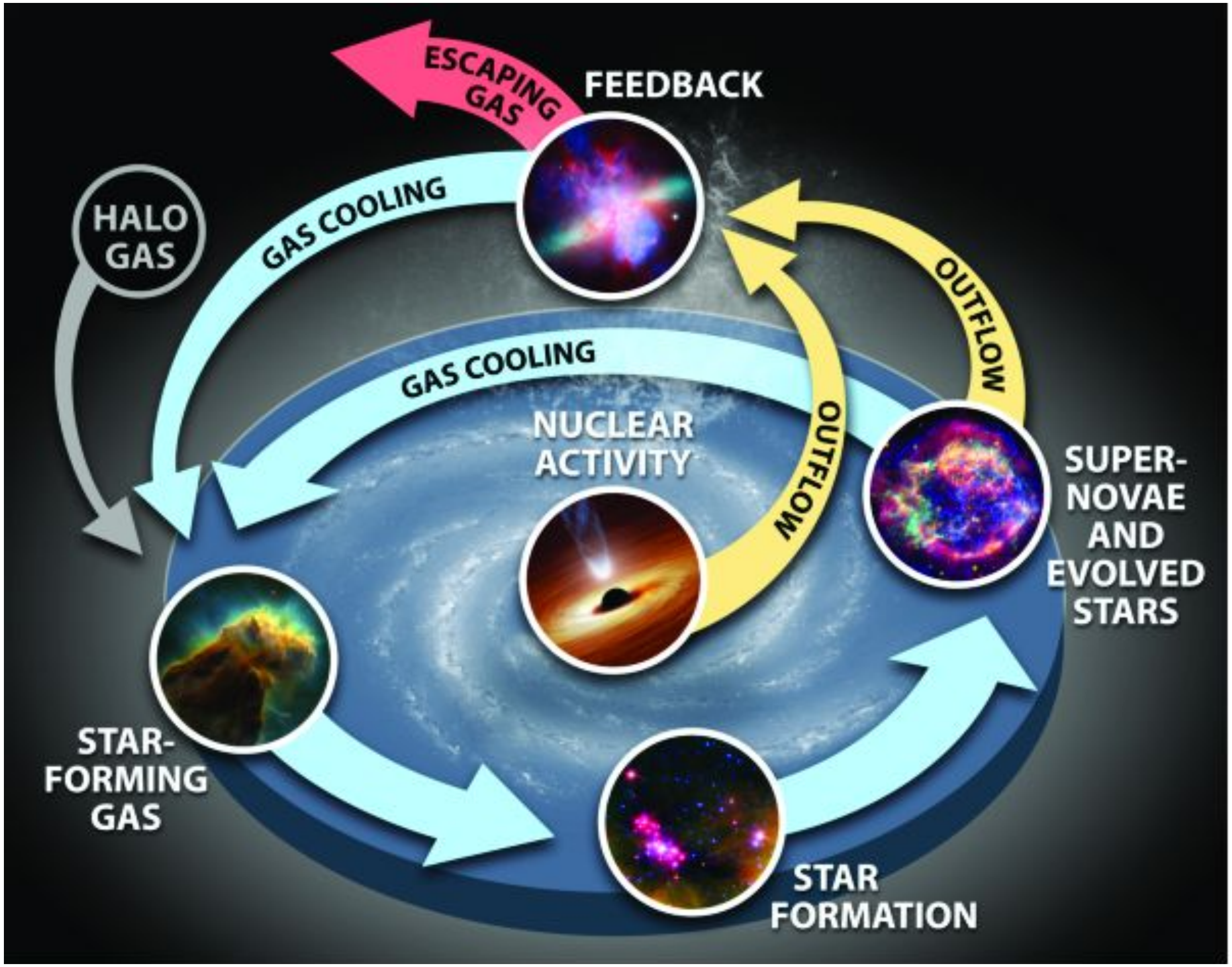

The baryon cycle is a complex phenomenon that encapsulates all the ways in which gas gets perpetually processed in overdensities.

Energetic processes that shape galaxies and the circumgalactic medium together define this ecosystem.

The lifecycle of interstellar clouds

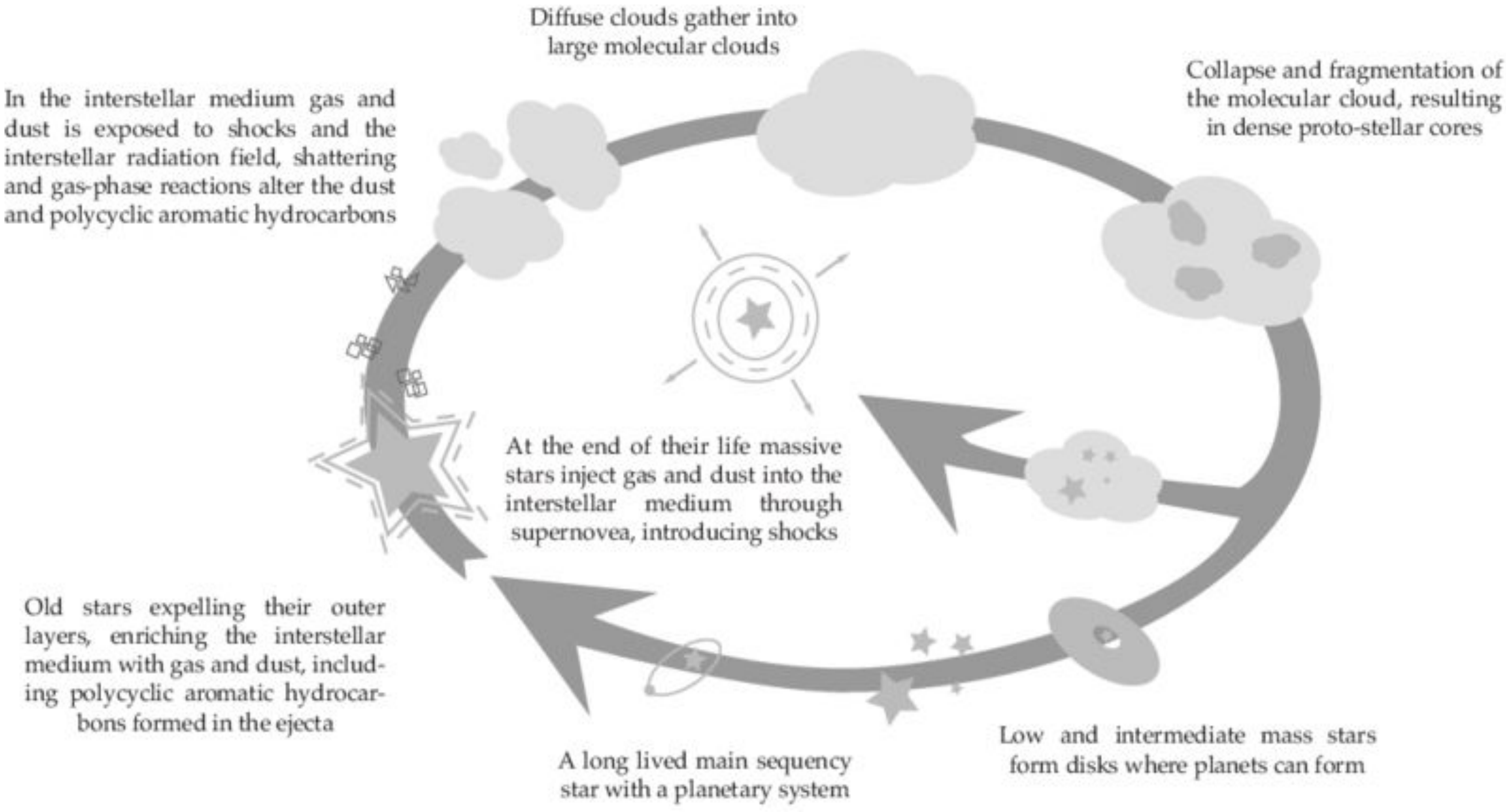

The lifecycle of interstellar dust

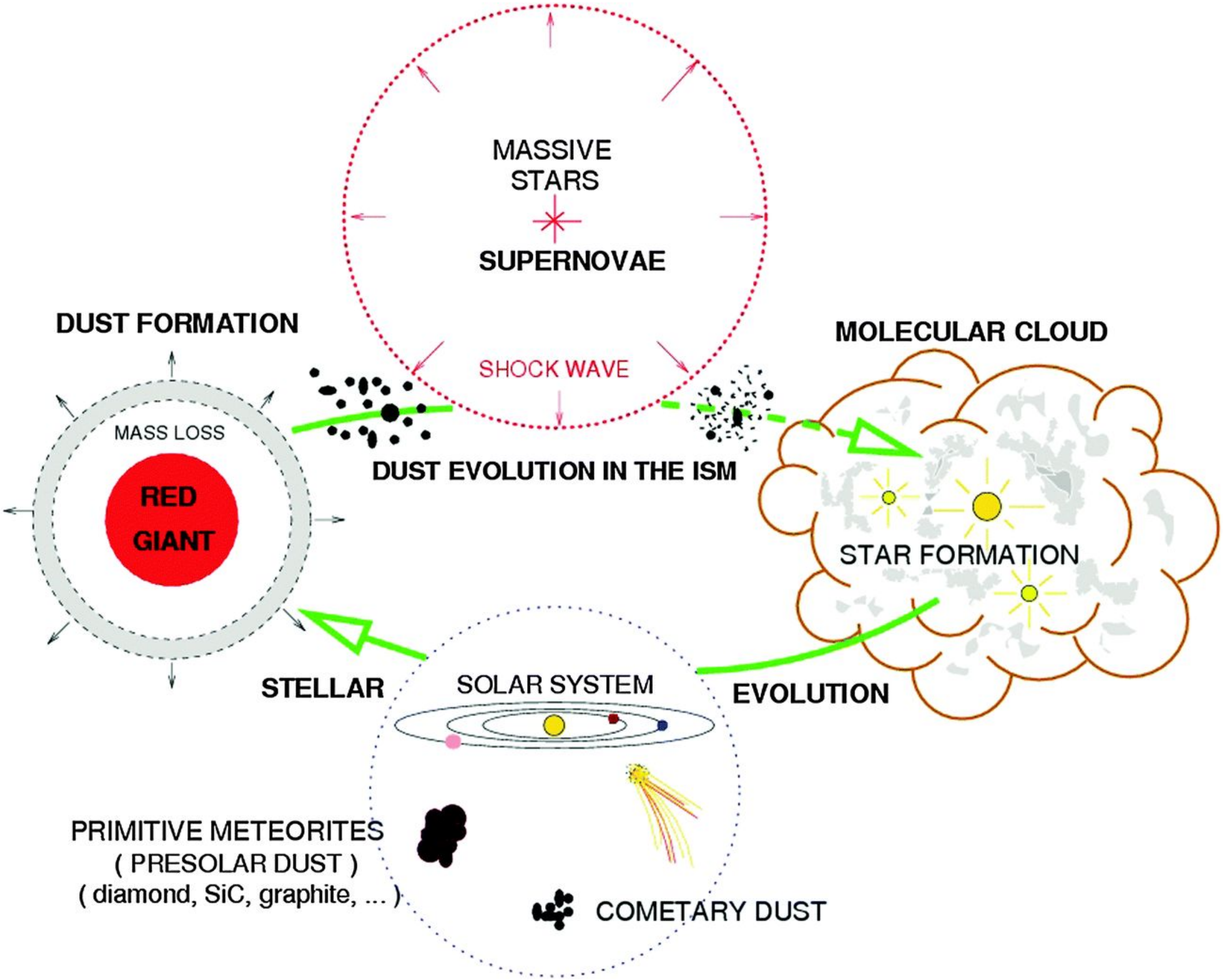

The cycle of carbon in gas phase

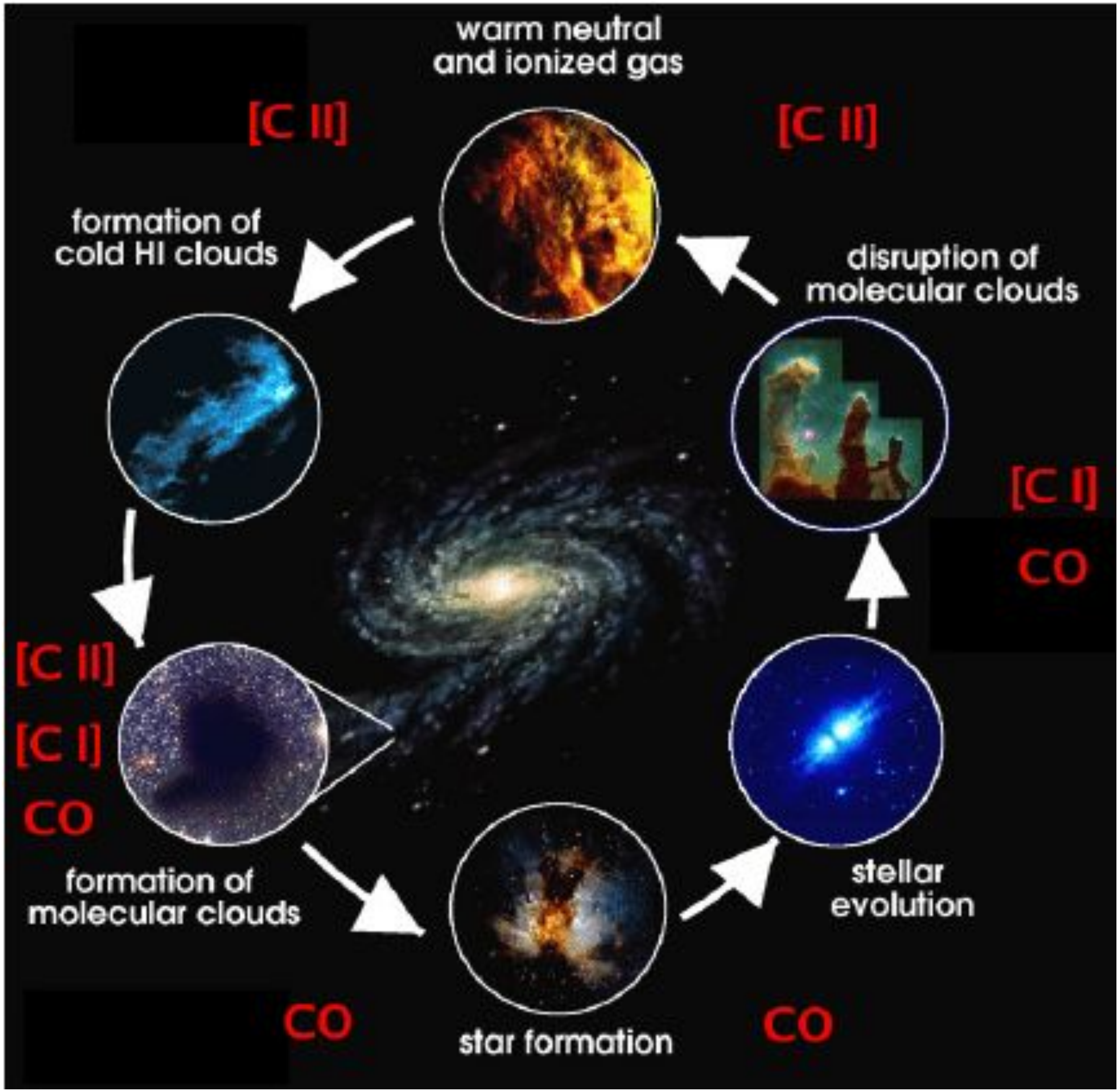

…but carbon is present also in carbonaceous grains!

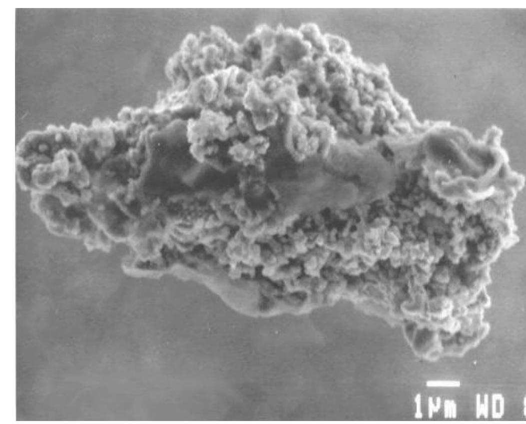

The Milky Way - Our Parent Galaxy

From Earth, we see few stars when looking out of galaxy (red arrows), many when looking in (blue and white arrows).

The Milky Way is how our Galaxy appears in the night sky (b).

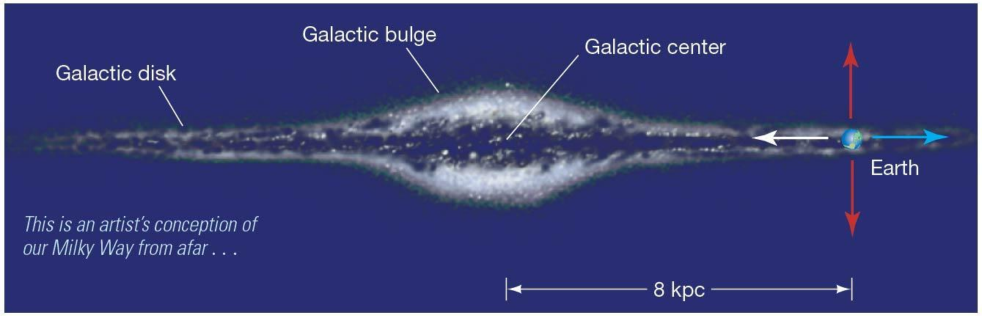

(a)

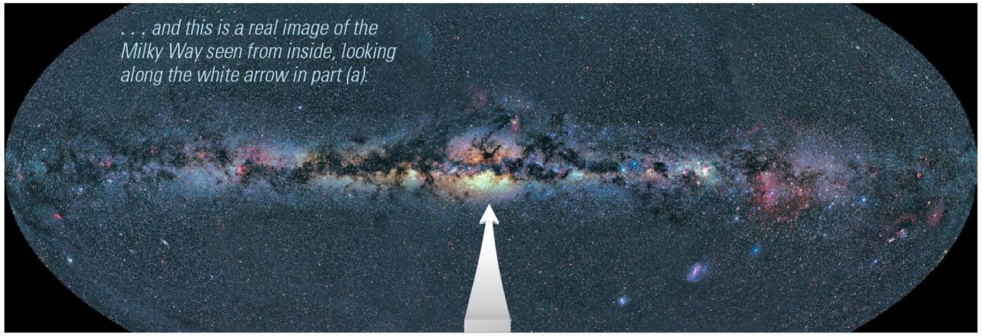

(b)

(b)

Hypotheses we build about the structure of our Galaxy (especially spiral arm structure) are inspired by the observation of external galaxies.

Recent Milky Way CO surveys

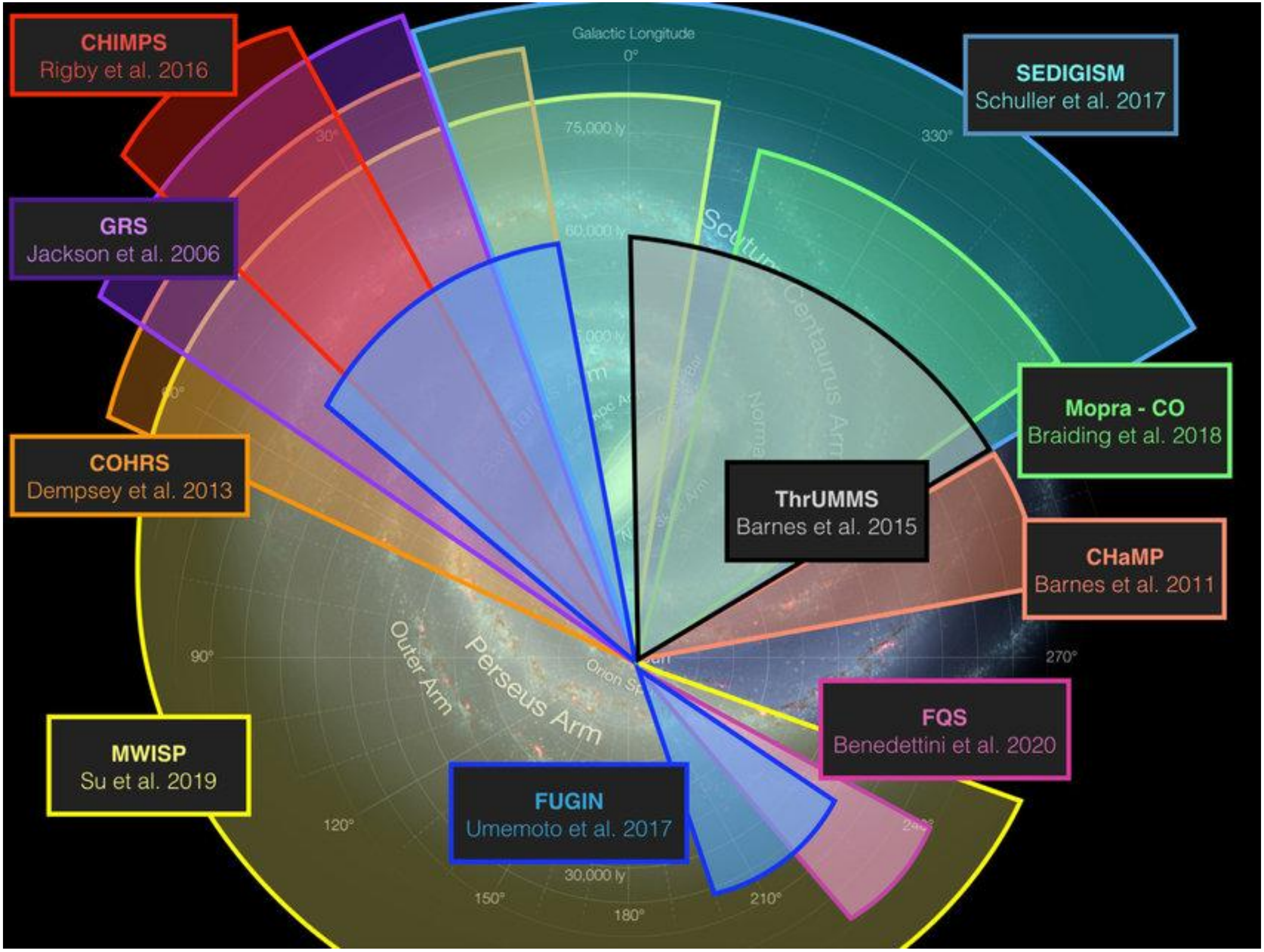

The value of Milky Way CO surveys

Tracer of molecular clouds.

Kinematic information, useful for:

- Disentangling different components along the l.o.s.
- Studying cloud internal dynamics.
- Estimating velocity dispersion
- Obtaining heliocentric and Galactocentric distances.

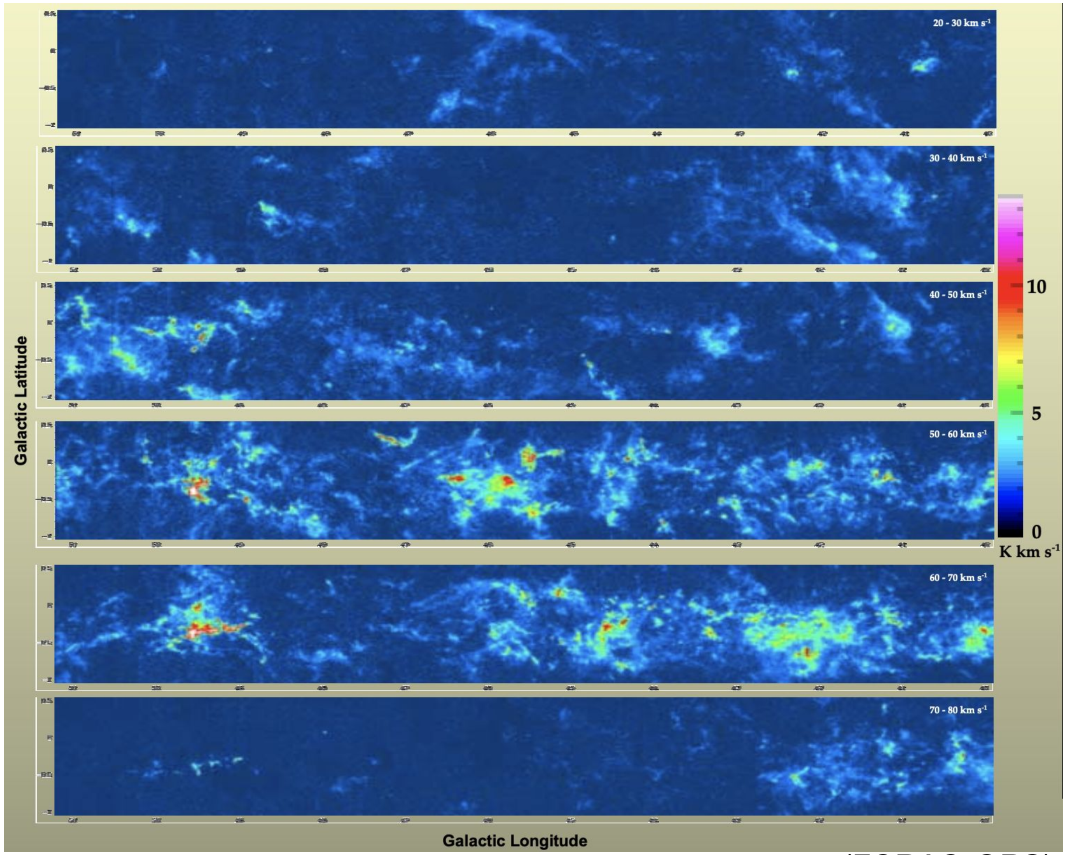

(FCRAO-GRS)

But…

CO low rotational lines are optically thick already at low densities…

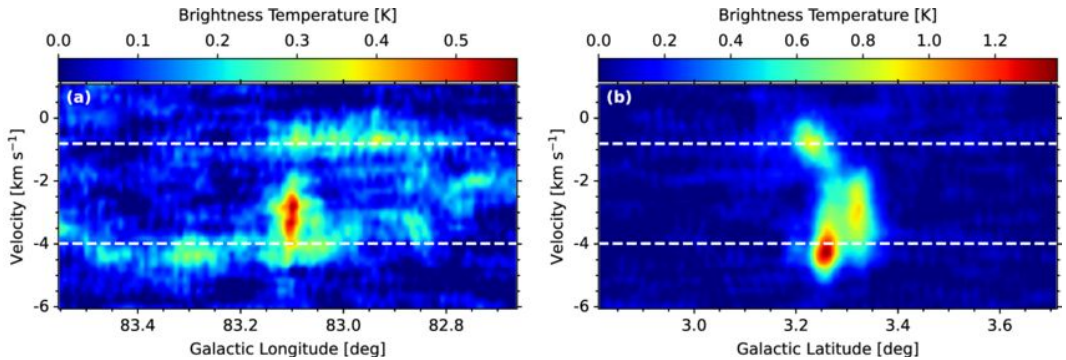

The value of Milky Way CO surveys

…nevertheless, a strong correlation is found between the CO(1-0) intensity and the H_2 column density N_{H2} , allowing quantitative studies.

$$N_{H2} = X_{CO} \, W_{CO}$$

$$\text{with } X_{CO} \simeq 2 \times 10^{20} \text{ cm}^{-2} \text{ K}^{-1} \text{ km}^{-1} \text{ s}$$

Actually, a X_{CO} variable with R_{GC} (due to metallicity gradient, see below) is reasonable. E.g.,

$$\log(X_{CO} / X_{CO,\odot}) = 0.08 \text{ kpc}^{-1} (R_{GC} - R_0)$$

(Arimoto+1996)

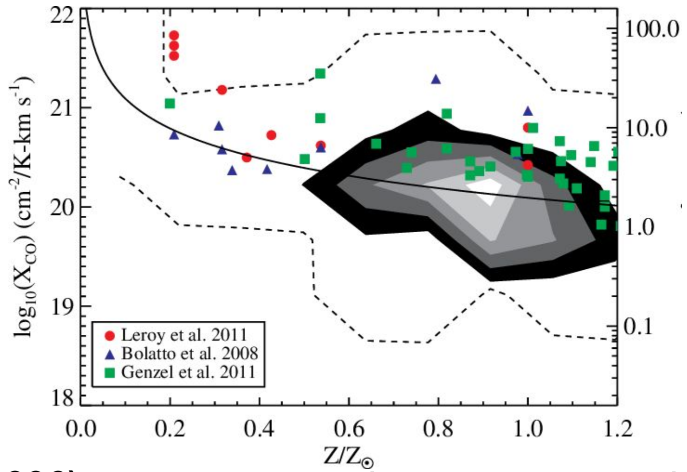

(Narayanan+2012)

$$X_{CO} = 83 \times 10^{20} / [54.5 - 3.7 (R_{GC} / \text{kpc})], \; 2<d<10 \text{ kpc}$$
$$X_{CO} = 6\text{x}10^{20} \; d > 10 \text{ kpc}$$

(Lada & Dame 2020)

Measuring the Milky Way

- Measuring heliocentric distances of astronomical sources/regions is fundamental for a fully quantitative analysis of them.
- One of the first attempts to measure the Milky Way was performed by Herschel using visible stars.
- Unfortunately, he was not aware that most of the Galaxy, particularly the center, is blocked from view by vast clouds of gas and dust.

Early models of the Galaxy placed the Sun near the center of a relatively small system.

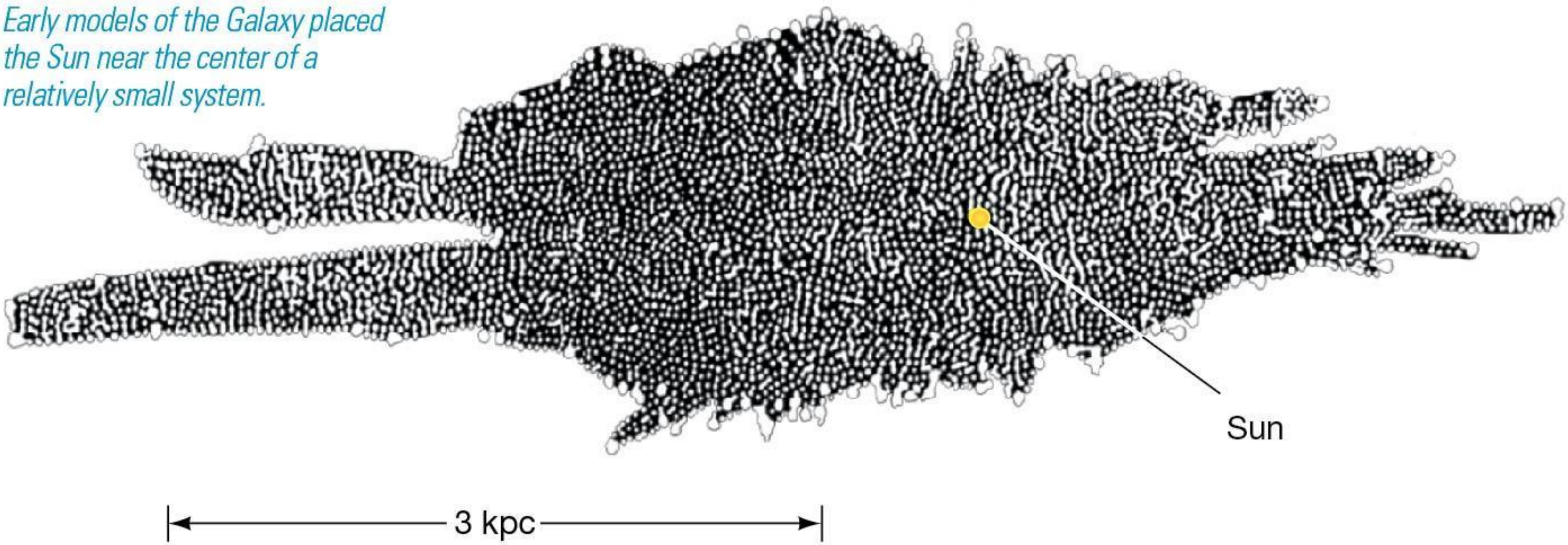

Measuring the Milky Way

Measuring distances through stars:

- **Variable stars—novae, supernovae, and related phenomena—which are called cataclysmic variables.**
- **There are other stars whose luminosity varies in a regular way, but much more softly. These are called intrinsic variables: RR Lyrae stars and Cepheids.**

$$5 \log_{10} (D / \mathrm{kpc}) = m - M + 5$$

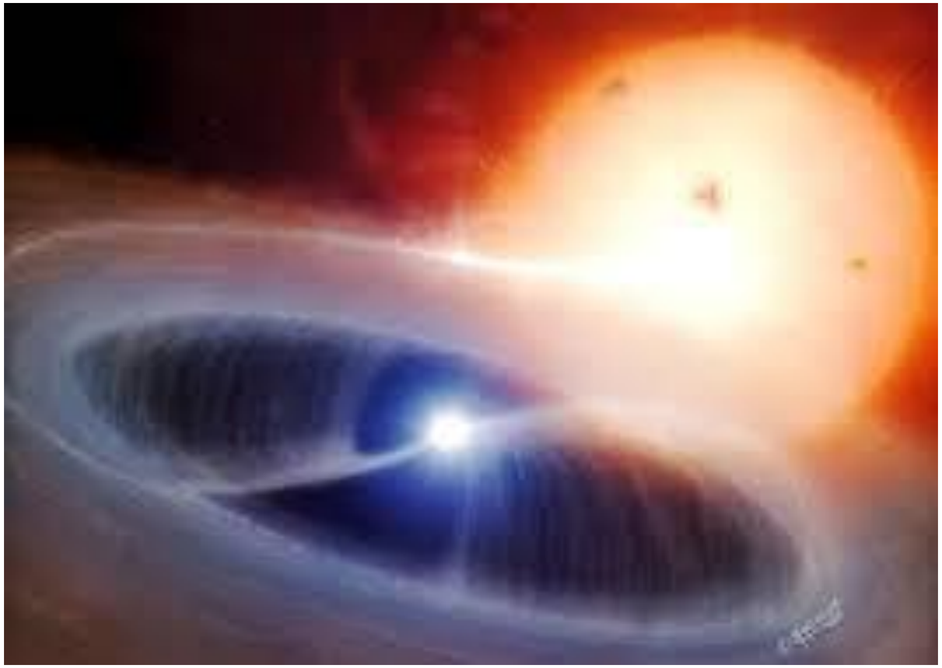

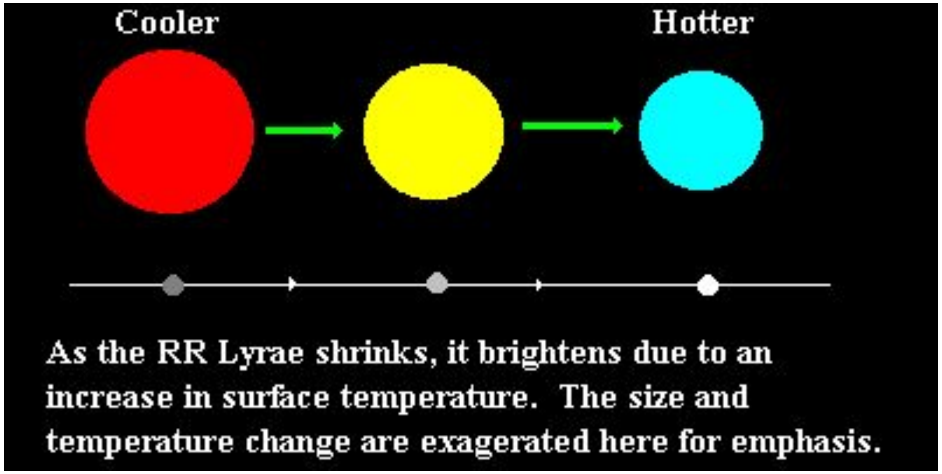

Measuring the Milky Way

RR Lyrae star. All such stars have essentially the same luminosity curve, with periods from 0.5 to 1 day.

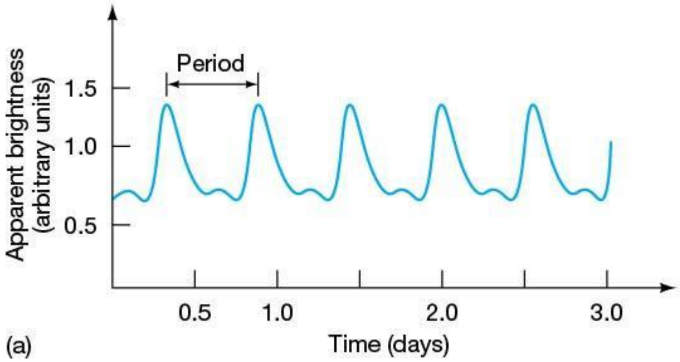

Cepheid variable; Cepheid periods range from about 1 to 100 days.

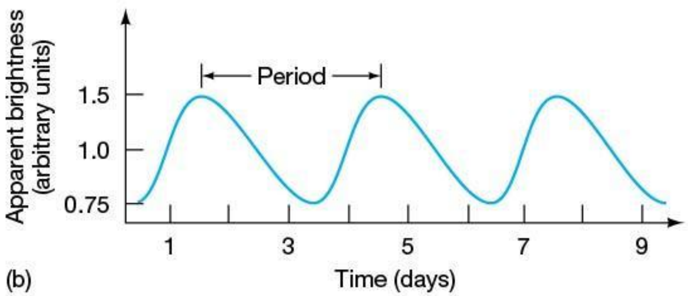

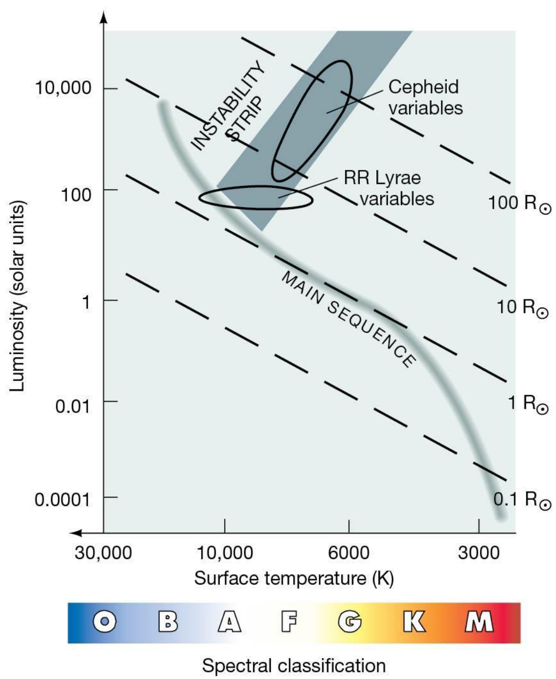

The variability of these stars comes from a dynamic balance between gravity and pressure. They have large oscillations around stability.

Measuring the Milky Way

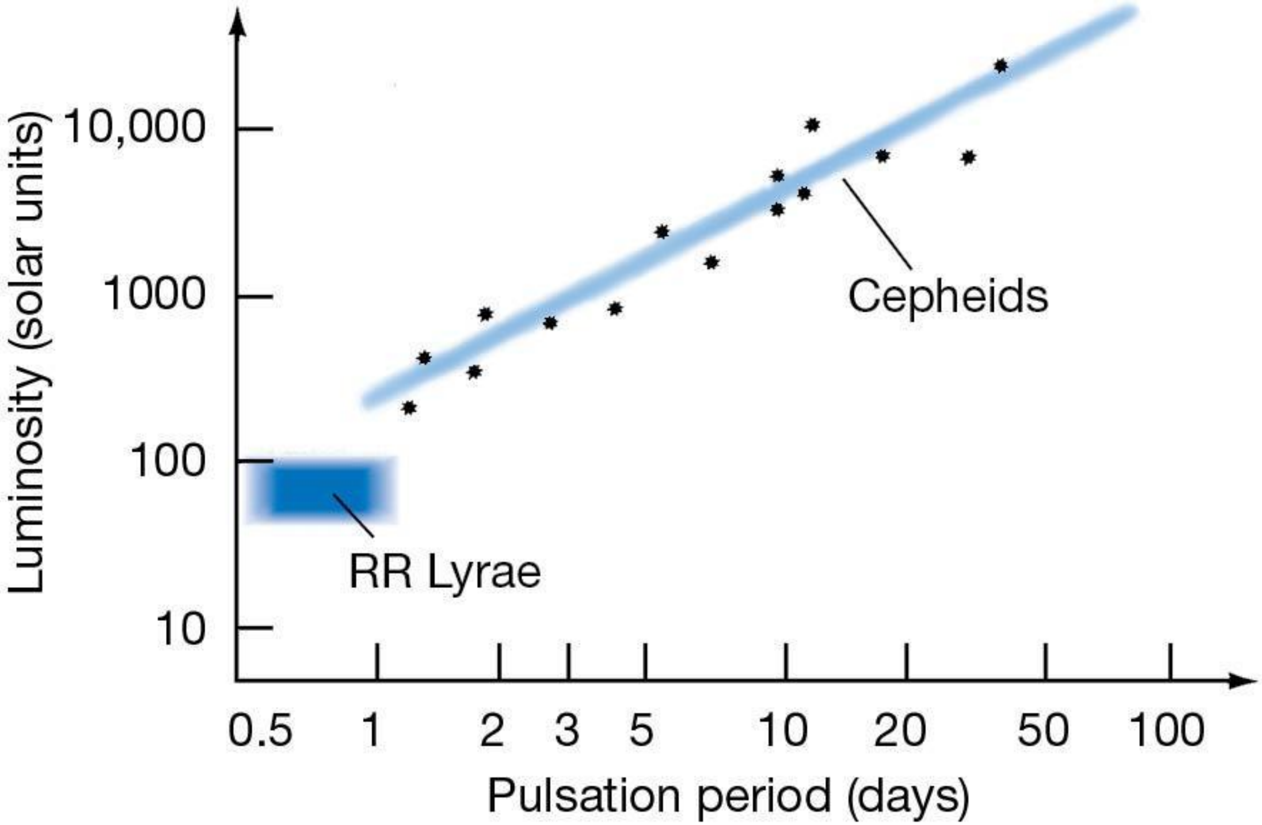

- RR Lyrae stars all have about the same luminosity; knowing their apparent magnitude allows us to calculate the distance.

- Cepheids have a luminosity that is strongly correlated with the period of their oscillations; once the period is measured.

Measuring the Milky Way

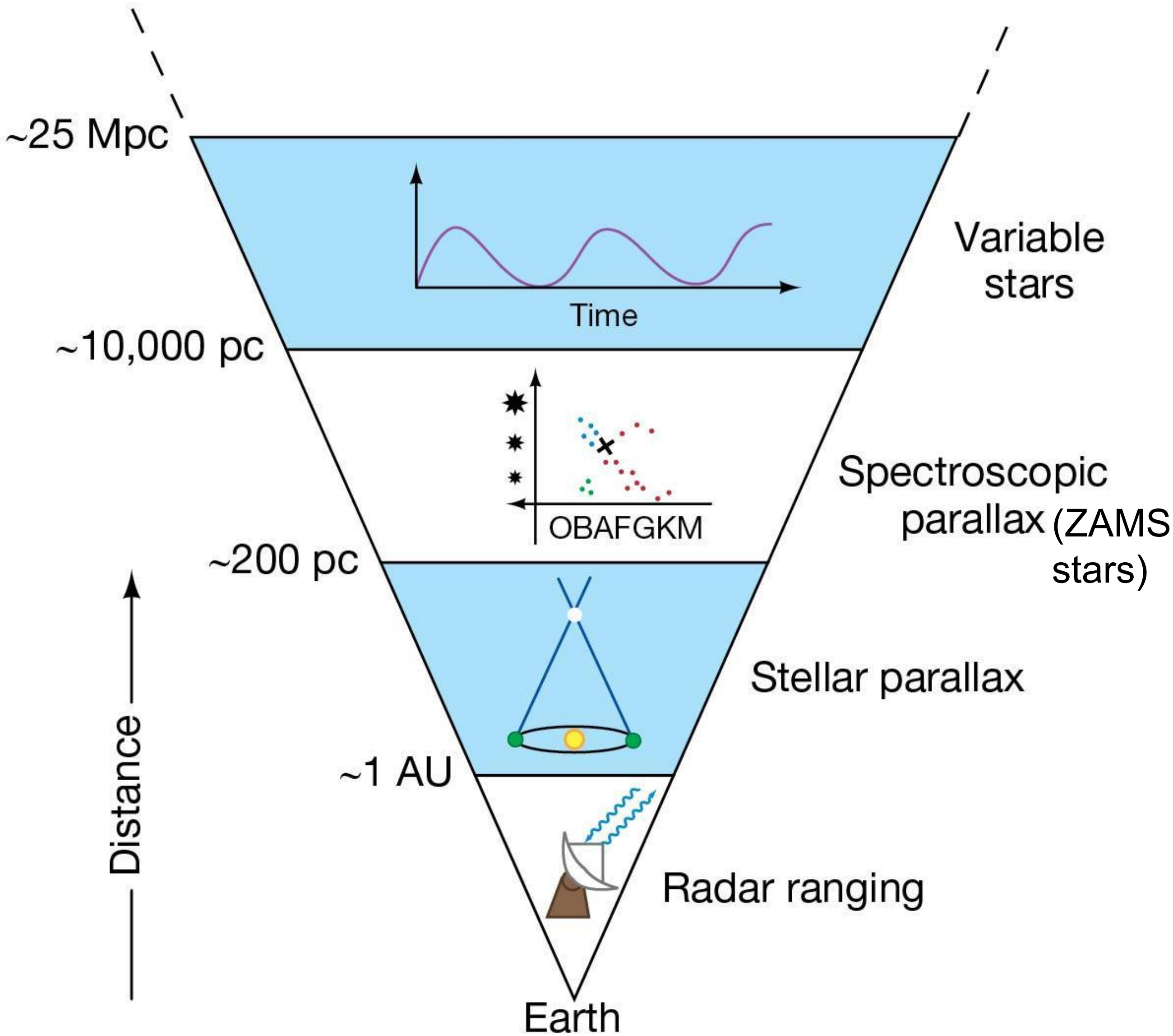

Kinematic distance

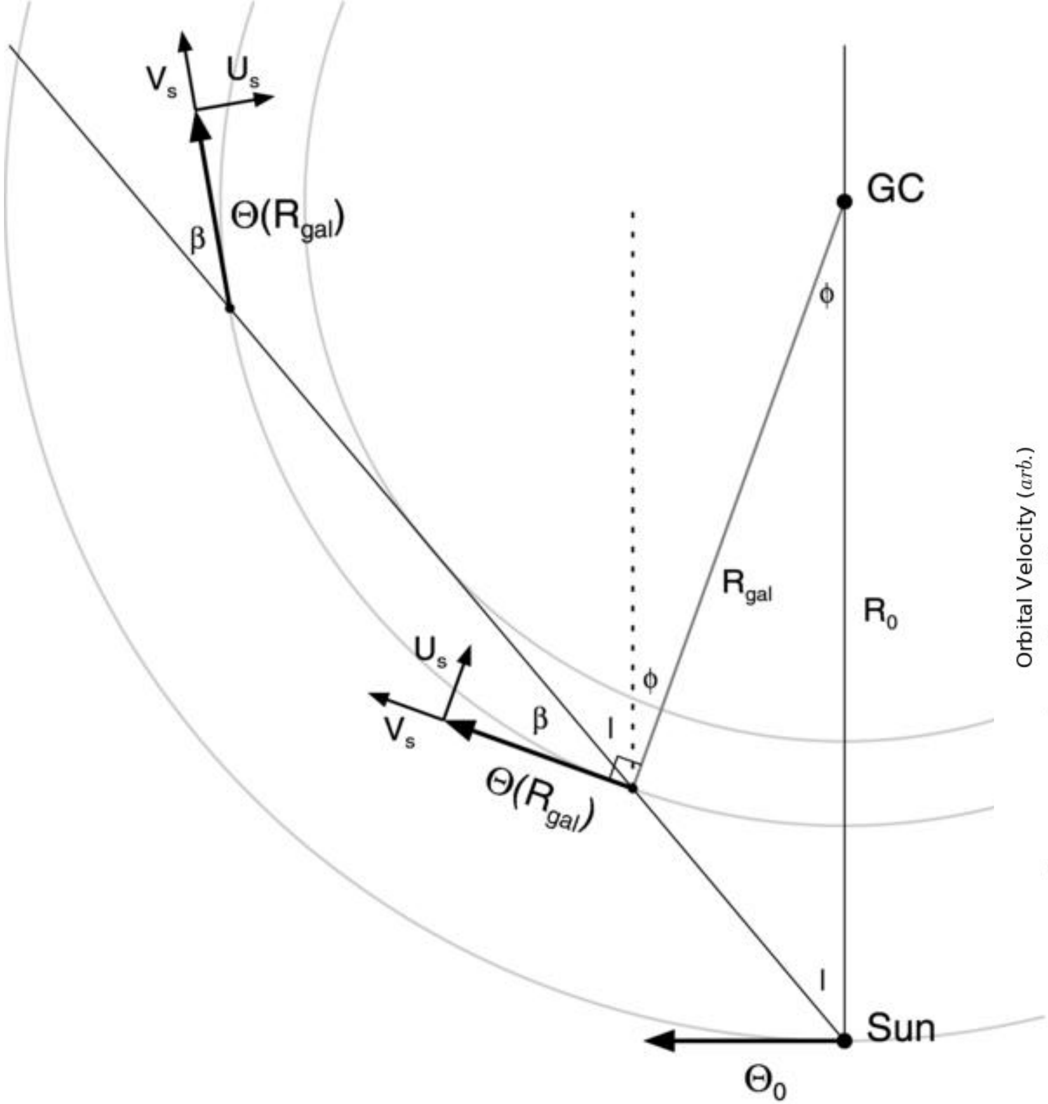

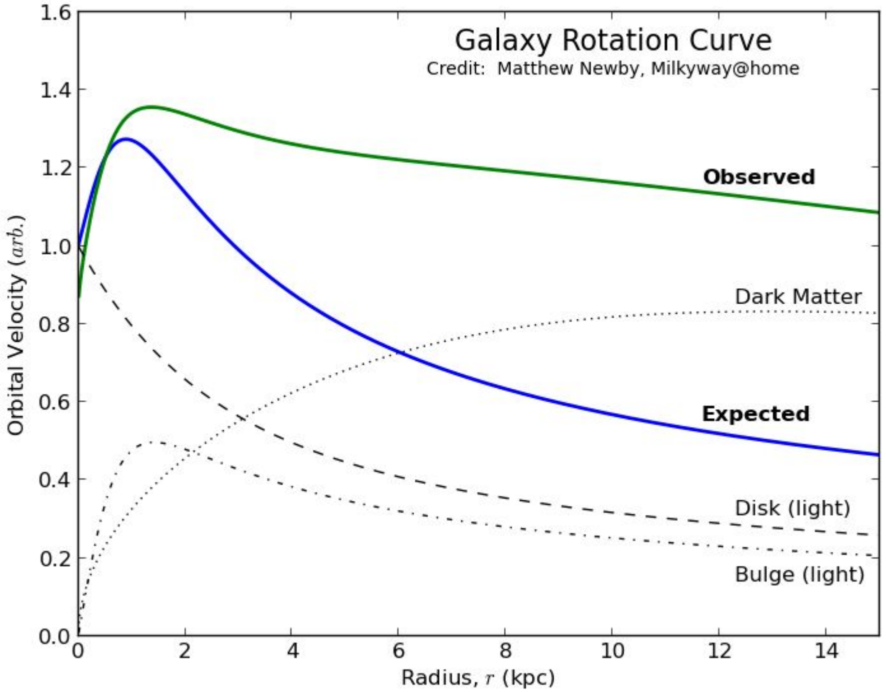

Inverting the law of cosines can be used to derive *d*, but the quadratic equation typically has two solutions…

Issues in measuring the V_{LSR}

Local Standard of Rest: ideally, the mean velocity of a circular orbit at the Solar distance from the Galactic centre.

Multiple peaks along the l.o.s.

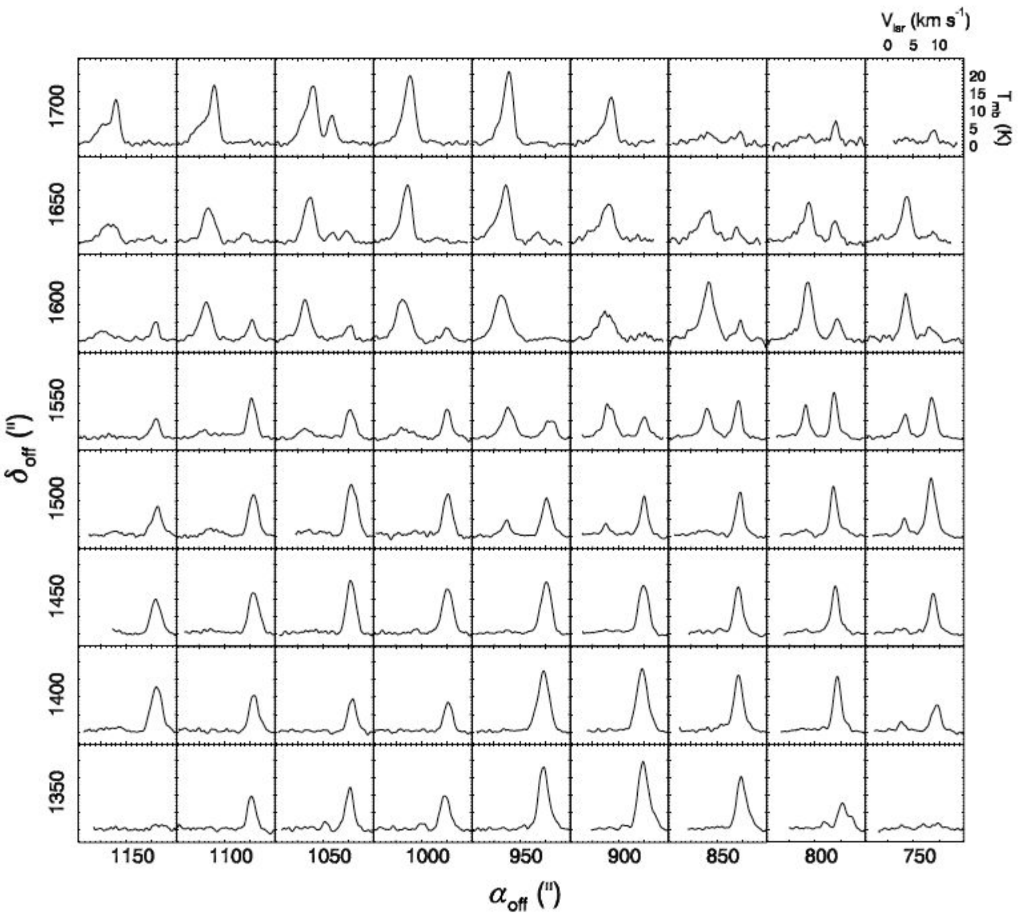

CO self-absorption

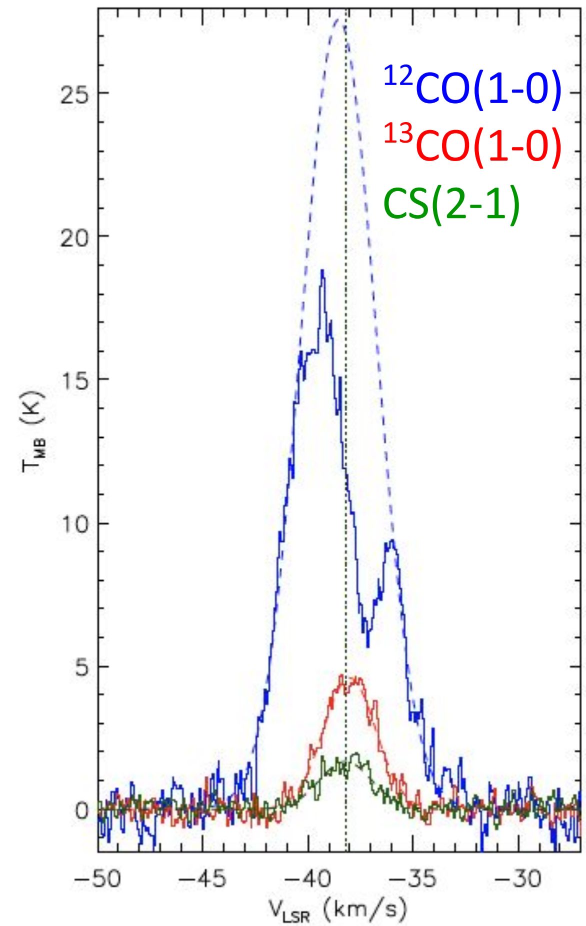

Trying to solve the near/far ambiguity

Priority order	Method used for disambiguation
1	Maser distance [(a)]
2	Stellar distance from grouping (optical H II regions, literature [(b)])
3	Kinematic distance from spectral abs. line (literature [(c)])
4	Kinematic distance from grouping (radio HII regions, literature [(b)])
5	Kinematic distance from IRDC/dark clouds (literature [(d)])
6	Kinematic distance from daughter clouds (for Q1 only, Brunt et al. [(e)])
7	Kinematic distance from Extinction datacubes
8	Kinematic distance from HI profile self-absorption analysis
9	Kinematic distance from Solomon [(f)] method (distance above the galactic plane)

Cold foreground HI will absorb against warmer background HI at the same velocity

Galactic molecular clouds contain residual HI, which is cold (~10 K) compared the the warm HI in the ISM (~100 K). The HI inside a molecular cloud at the near distance will absorb against the warm background HI at the same LSR velocity that lies at the far distance. The HI inside a molecular cloud at the far distance shows no such absorption as there is no background HI at the same velocity. Thus the signature of a cloud at the near distance is molecular emission at the same velocity and with the same line width as an HI absorption feature.

Distances of BGPS sources

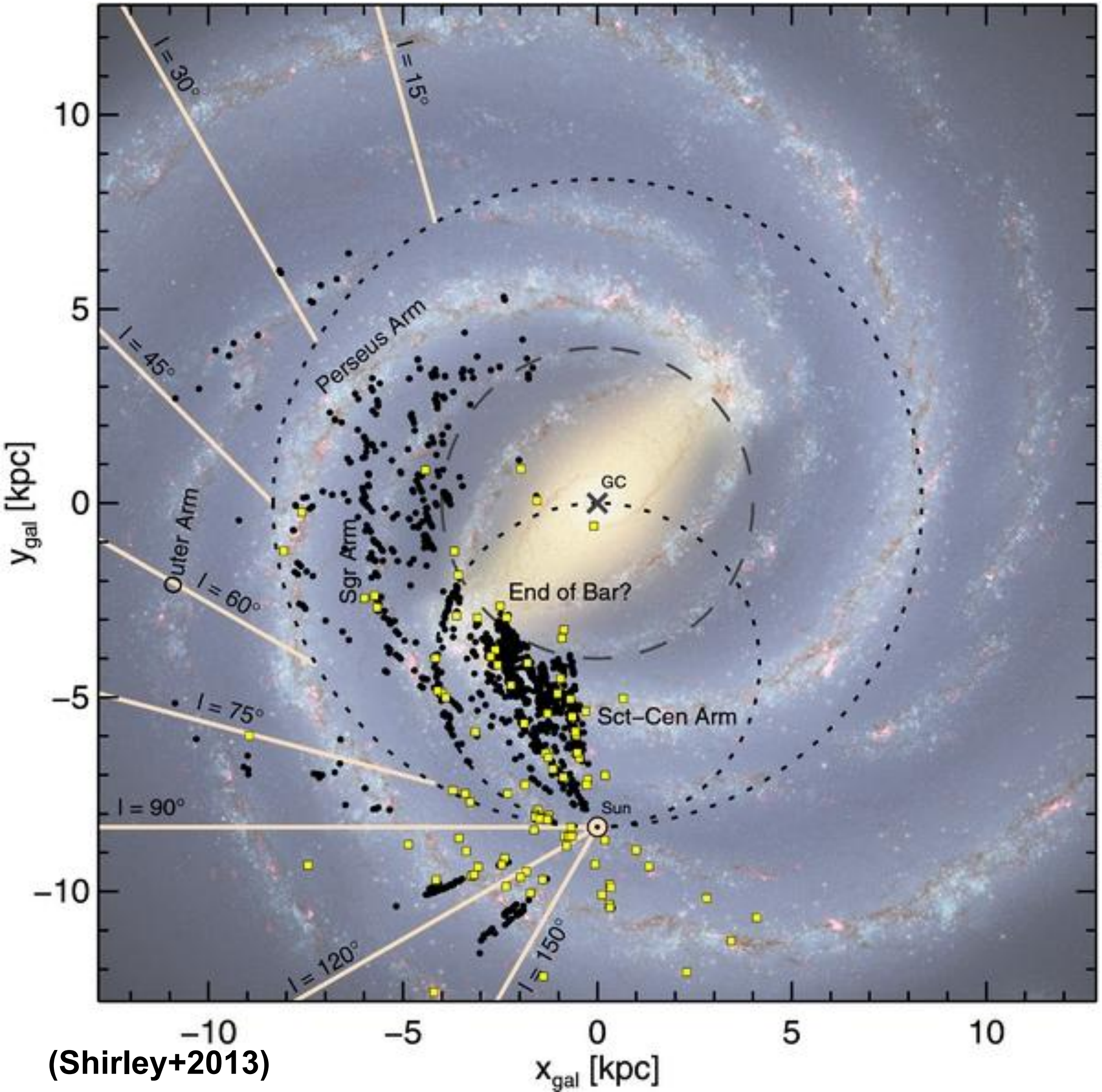

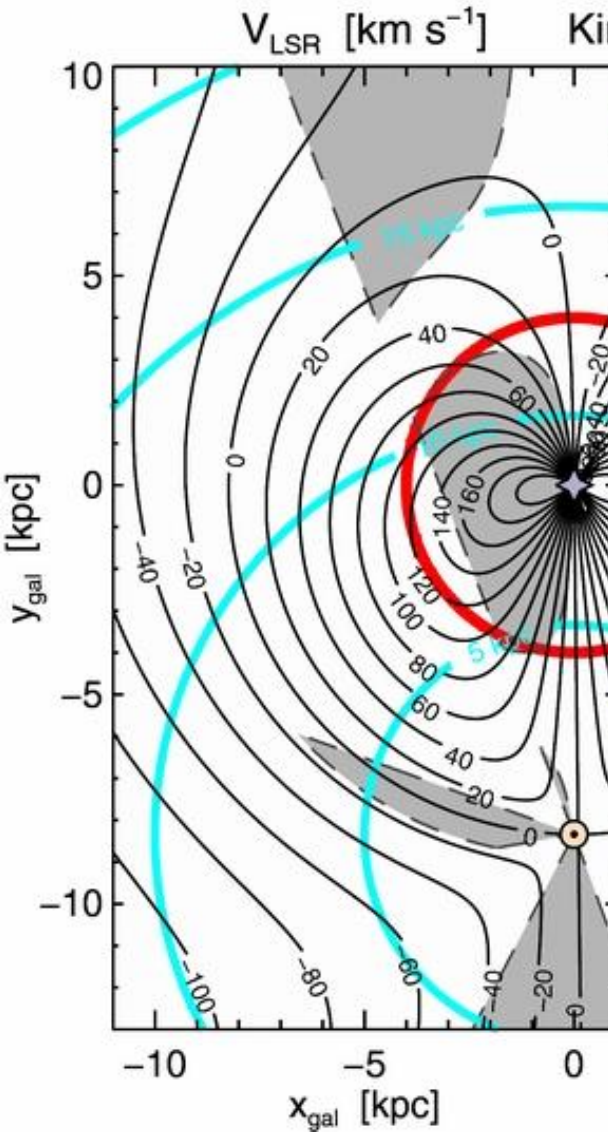

(Shirley+2013)

Distances of Hi-GAL sources

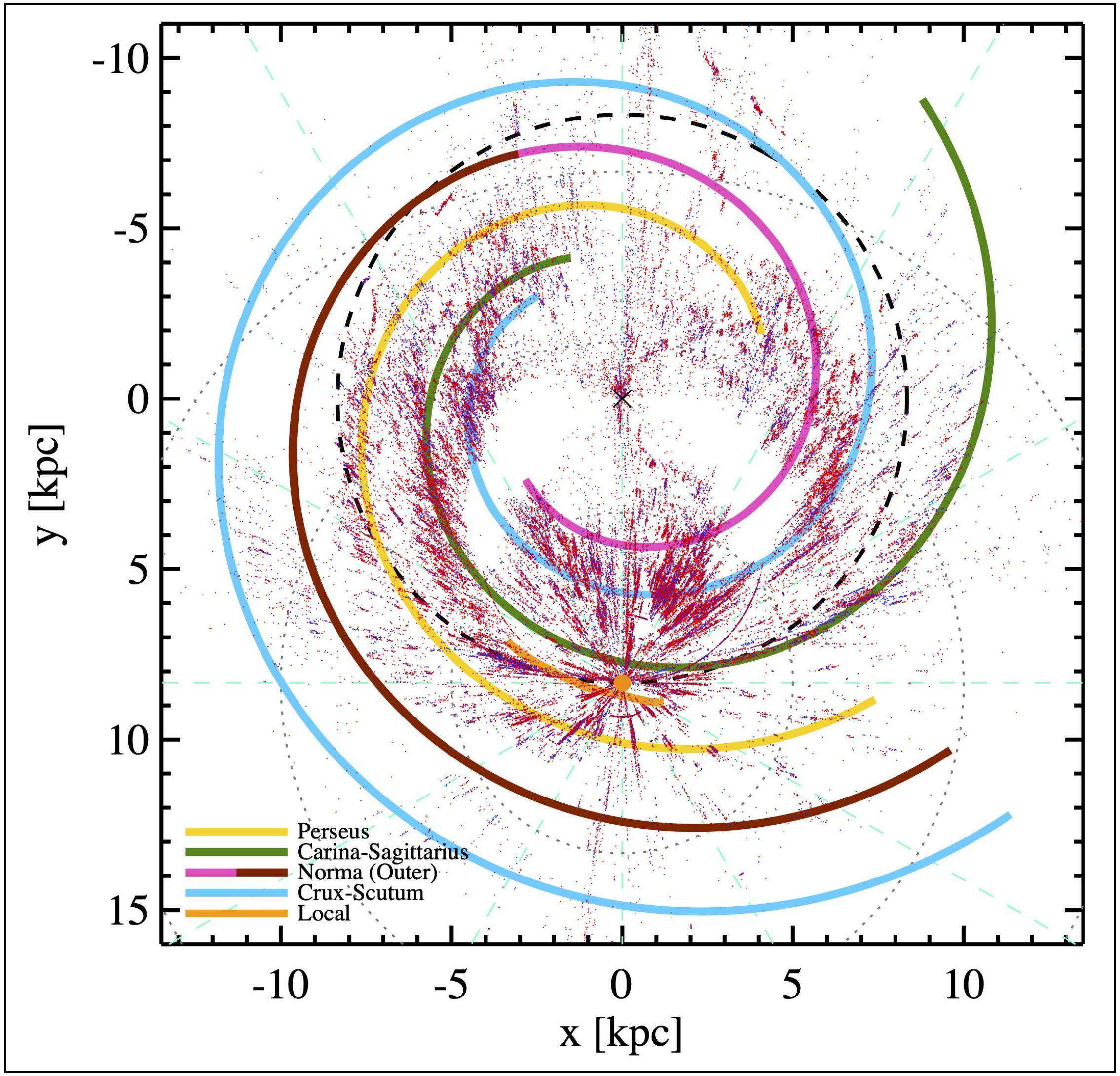

◆ Proto-stellar
◆ Pre-stellar

Arm prescription by Hou, Han & Shi (2009)

Distances for ~1.2x10^5 sources estimated by Mège+2021

For ATLASGAL survey distances, see Wienen+(2015), Urquhart+(2018)
For BGPS, Ellsworth-Bowers+(2013, 2015)

Galactic plane surveys

Survey	λ or lines	Notes
		Ground-based
Columbia/CfA	CO, ^{13}CO	9 - 25′ resolution (*Dame et al.*, 2001)
DRAO/ATCA/VLA	HI-21 cm	IGPS: unbiased 255°$\leq l \leq$ 357° and 18°$\leq l \leq$ 147° (*McClure-Griffiths et al.*, 2001; *Gibson et al.*, 2000; *Stil et al.*, 2006)
FCRAO 14 m	CO, ^{13}CO	55″ resolution. Galactic Ring Survey (*Jackson et al.*, 2006) + Outer Galaxy Survey (*Heyer et al.*, 1998)
Mopra 22 m	CO, ^{13}CO, N_2H^+, (NH_3 + H_2O) maser, HCO^+/$H^{13}CO^+$ + others	HOPS: (*Walsh et al.*, 2011; *Purcell et al.*, 2012), MALT90: ~ 2000 clumps 20° $\geq l \geq -60°$ (*Foster et al.*, 2013), Southern GPS CO: unbiased 305°$\leq l \leq$ 345° (*Burton et al.*, 2013), ThrUMMS: unbiased 300°$\leq l \leq$ 358° (*Barnes et al.*, 2013), CMZ: (*Jones et al.*, 2012, 2013)
Parkes	CH_3OH maser	Methanol MultiBeam Survey (*Green et al.*, 2009)
NANTEN/ NANTEN2	CO, ^{13}CO, $C^{18}O$	NGPS: unbiased, 200° $\leq l \leq$ 60° (*Mizuno and Fukui*, 2004) + NASCO: unbiased in progress, 160° $\leq l \leq$ 80°
CSO 10 m	1.3 mm continuum	Bolocam Galactic Plane Survey (BGPS), 33″ (*Aguirre et al.*, 2011)
APEX 12 m	870 μm continuum	ATLASGAL, 60°$\geq l \geq -80°$ (*Schuller et al.*, 2009)
		Space-borne
IRAS	12, 25, 60 and 100 μm cont.	3-5′, 96% of the sky
MSX	8.3, 12.1, 14.7, 21.3 μm cont.	Full Galactic Plane (*Price et al.*, 2001)
WISE	3.4, 4.6, 11, 22 μm continuum	All-sky (*Wright et al.*, 2010)
Akari	65, 90, 140, 160 μm continuum	All-sky (*Ishihara et al.*, 2010)
Spitzer	3.6, 4.5, 6, 8, 24 μm continuum	GLIMPSE+GLIMPSE360: Full Galactic Plane (*Benjamin et al.*, 2003), (*Benjamin and GLIMPSE360 Team*, 2013) + MIPSGAL, 63°$\geq l \geq -62°$ (*Carey et al.*, 2009)
Planck	350, 550, 850, 1382, 2098, 3000, 4285, 6820, 10^4 μm cont.	All-sky, resolution $\geq$5′ (*Planck Collaboration et al.*, 2013a)
Herschel	70, 160, 250, 350, 500 μm cont.	Hi-GAL: Full Galactic Plane (*Molinari et al.*, 2010a)

Molinari+(2014)

The value of Galactic plane surveys

Studying the star formation in Milky Way as a whole.

Need for large surveys both in line and in continuum…
…and for combining them.

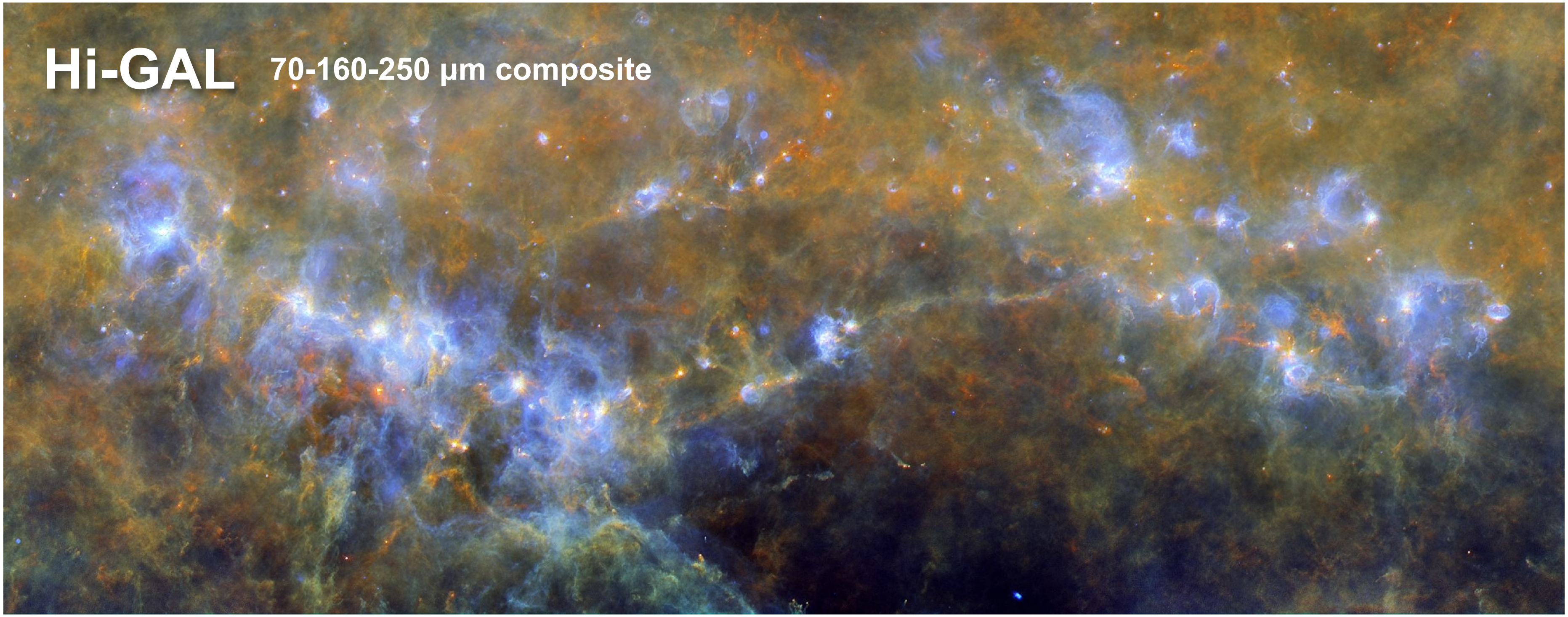

BOLOCAM Galactic Plane Survey

@ 1.1 mm

$-10.5° \leq \ell \leq 90.5°$, $|b| \leq 0.5°$
($|b| \leq 1.5°$ for $75.5° \leq \ell \leq 87.5°$ and at $\ell = 3°, 15°, 30°$ and $31°$.)
Total area: <u>133 sq. deg.</u>

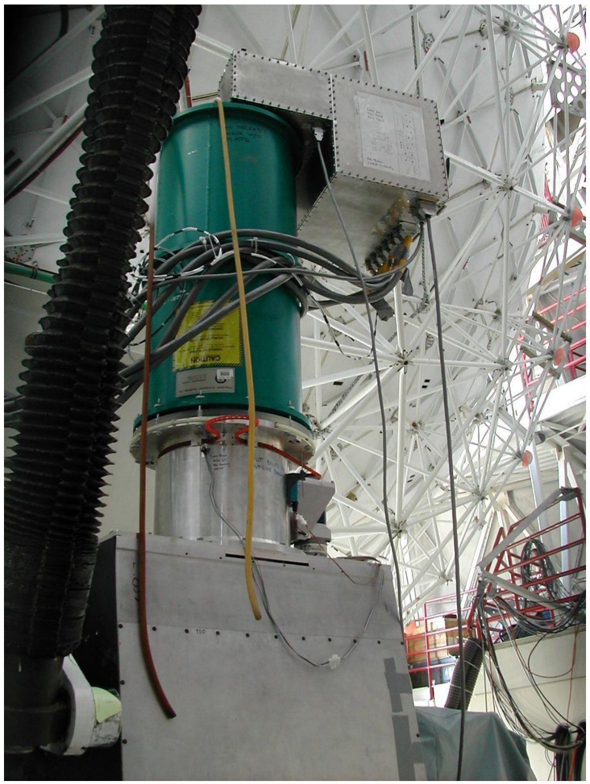

Caltech
Submillimeter
Observatory

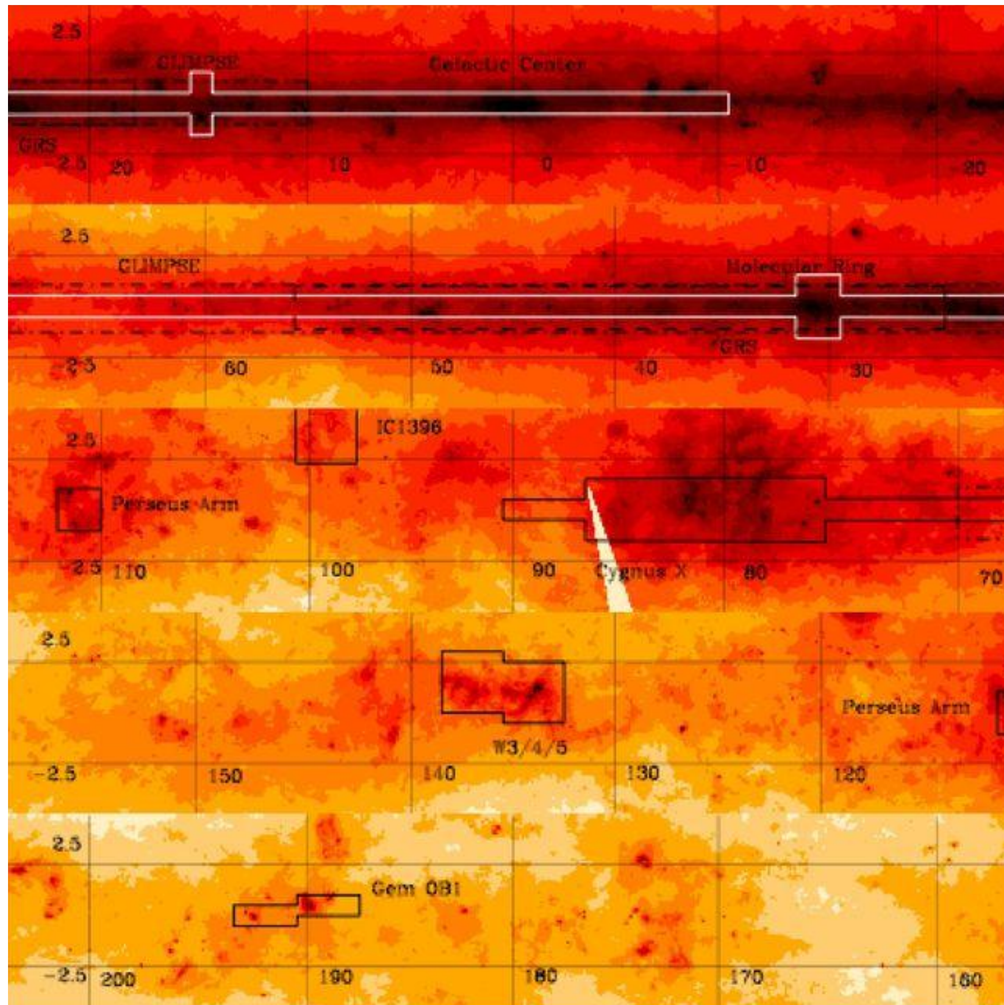

ATLASGAL Survey

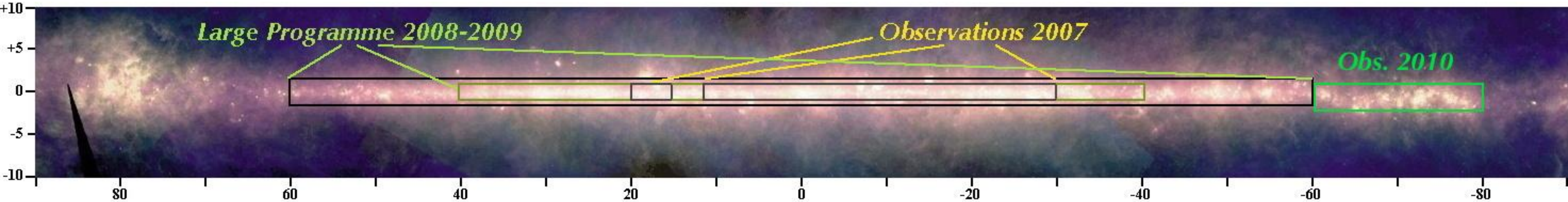

@ 870 μm

$|l| \leq 80°, |b| \leq 1°$

Atacama Pathfinder EXperiment

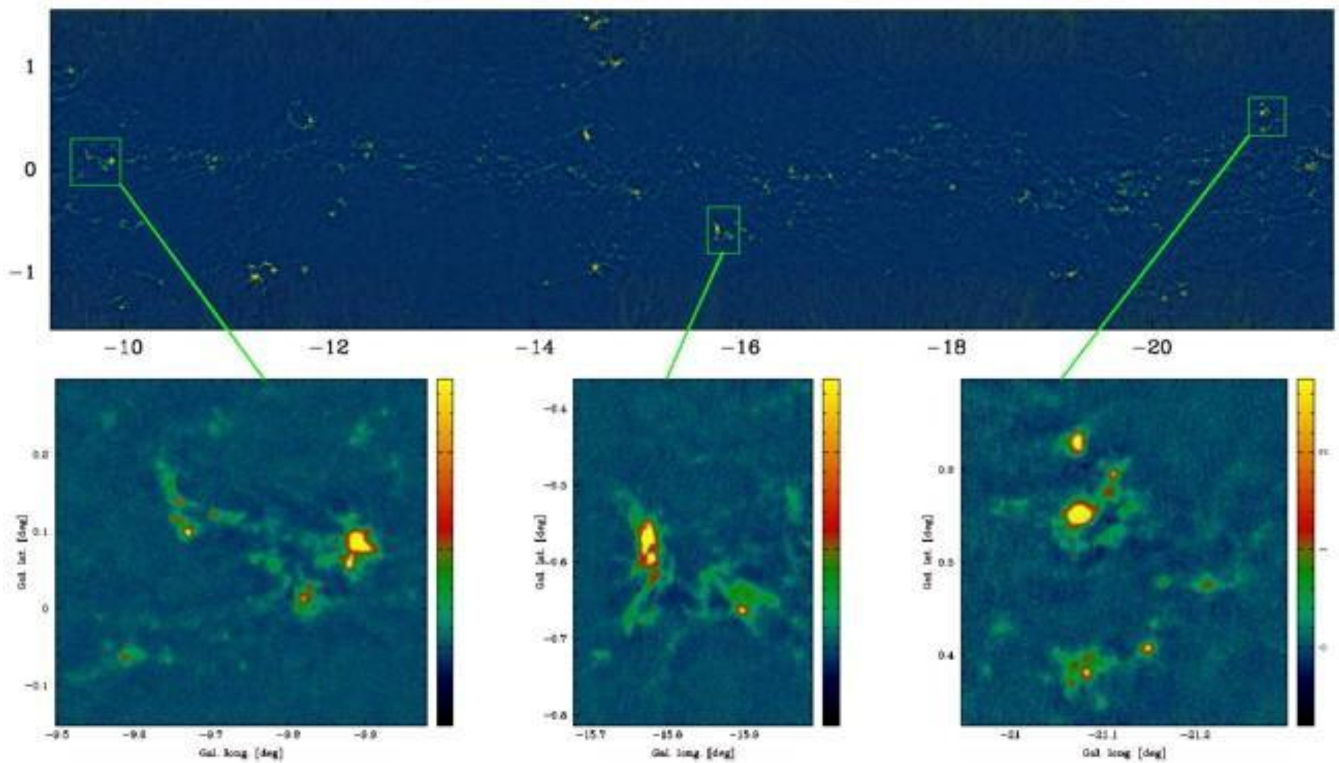

Spitzer GP surveys

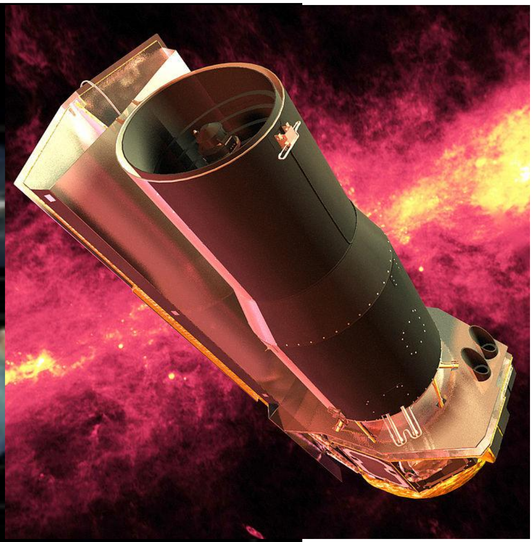

GLIMPSE (IRAC)
3.6
4.5
5.8
8 µm

MIPSGAL (MIPS)
24 µm

WISE all sky survey

3.4 µm 4.6 µm 12 µm 22 µm

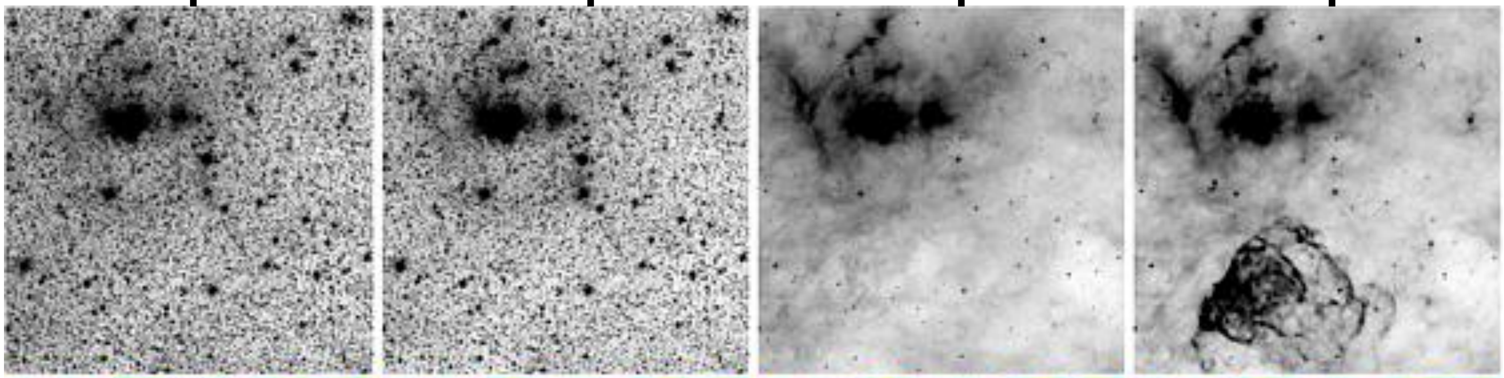

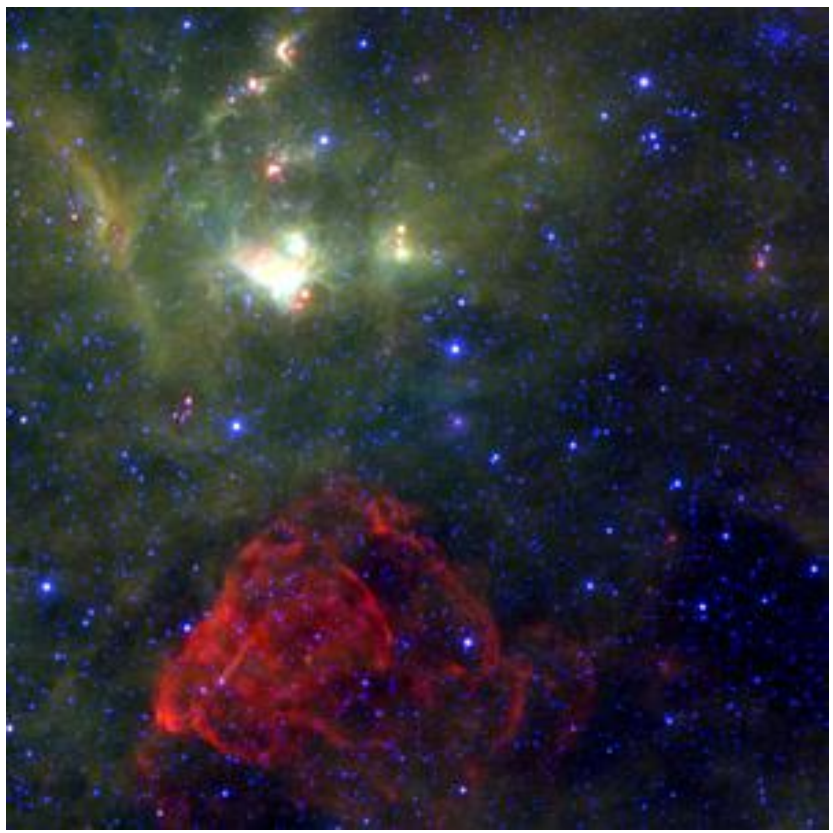

Herschel Space Observatory

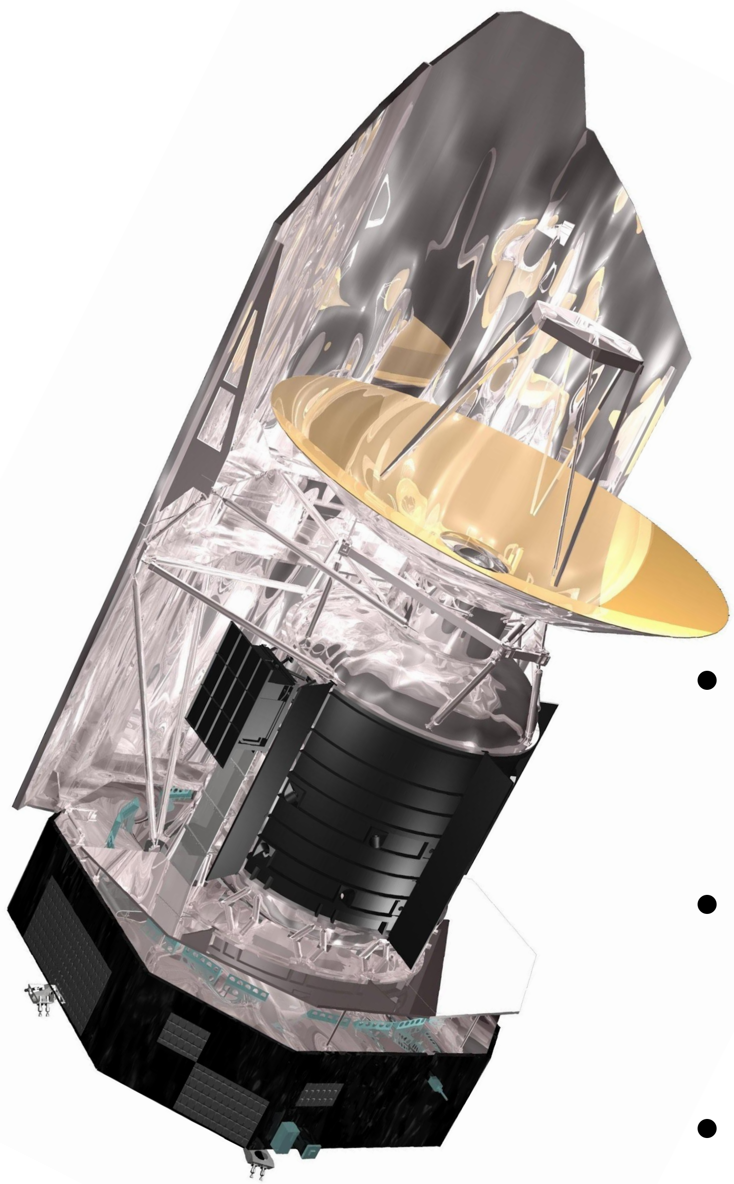

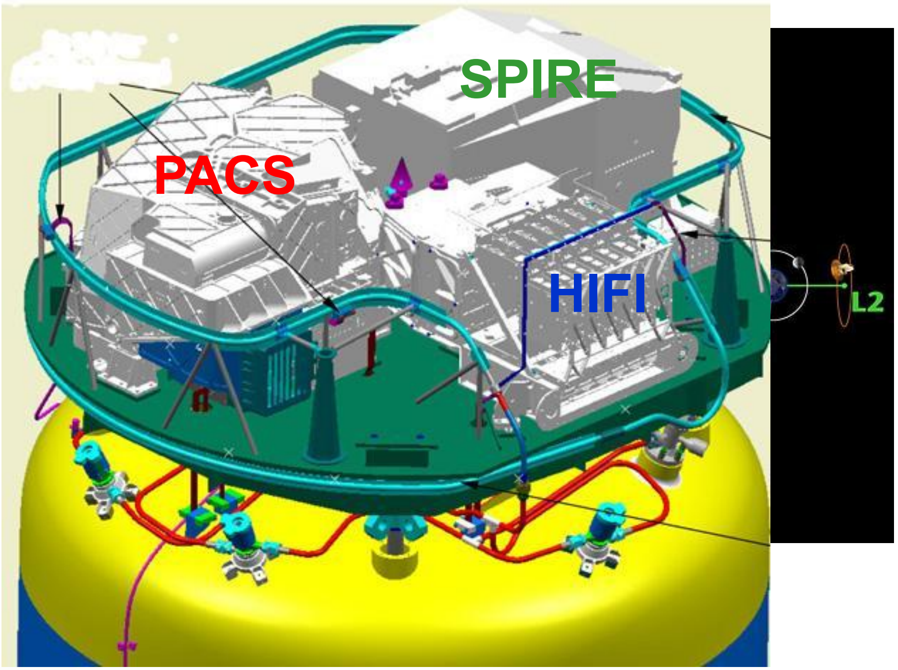

- **PACS (57 - 210 µm)**
  - **Imaging photometer**
  - **Grating spectrometer**
- **SPIRE (200 - 670 µm)**
  - **Imaging photometer**
  - **Fourier transform spectrometer**
- **HIFI (157- 212 µm and 240 - 625 µm)**
  - **Heterodyne spectrometer**

Star formation science with Herschel

The wavelength range covered by the cameras on board Herschel (70-500 μm) contains the emission peak of the cold dust.

It is suited for studying the dense clouds and the early stages of star formation.

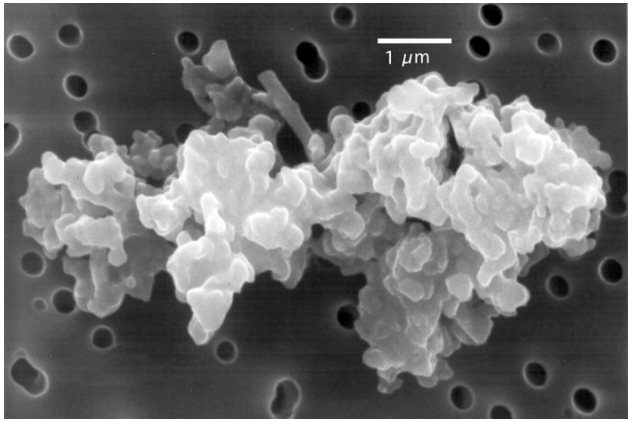

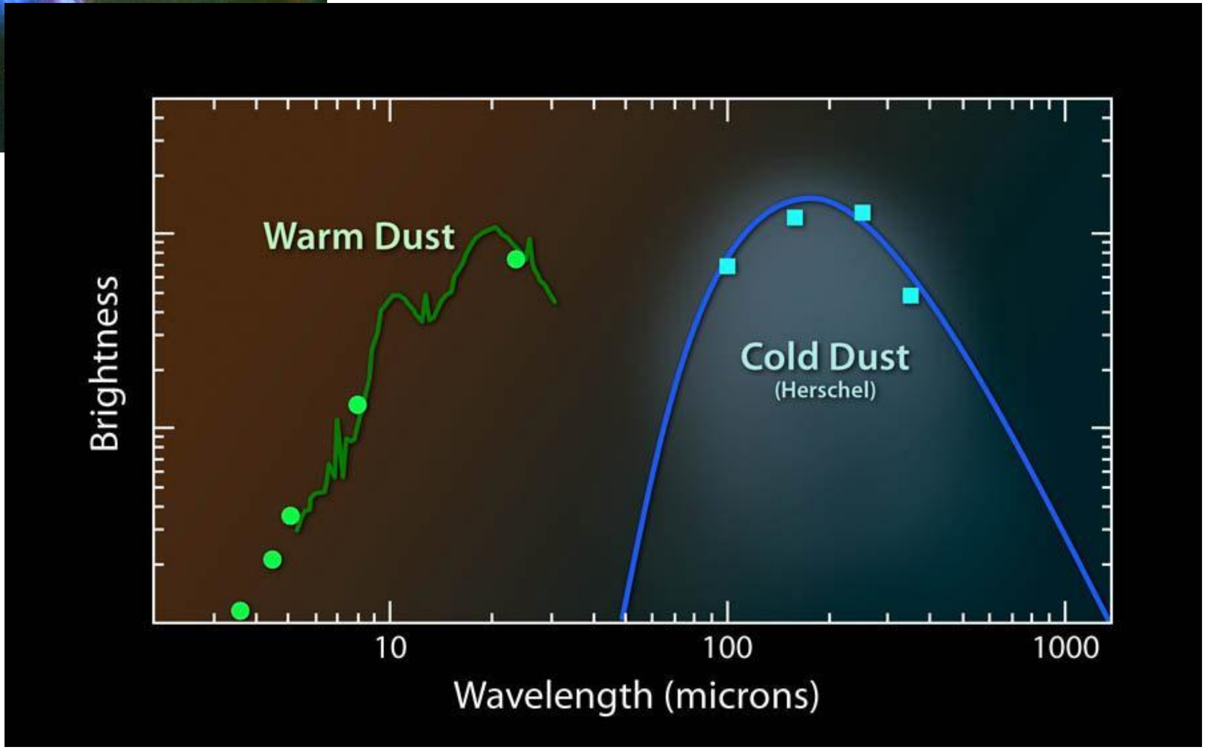

Star formation science with Herschel

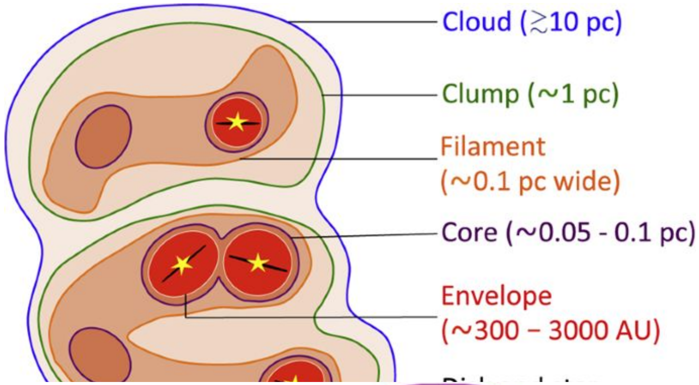

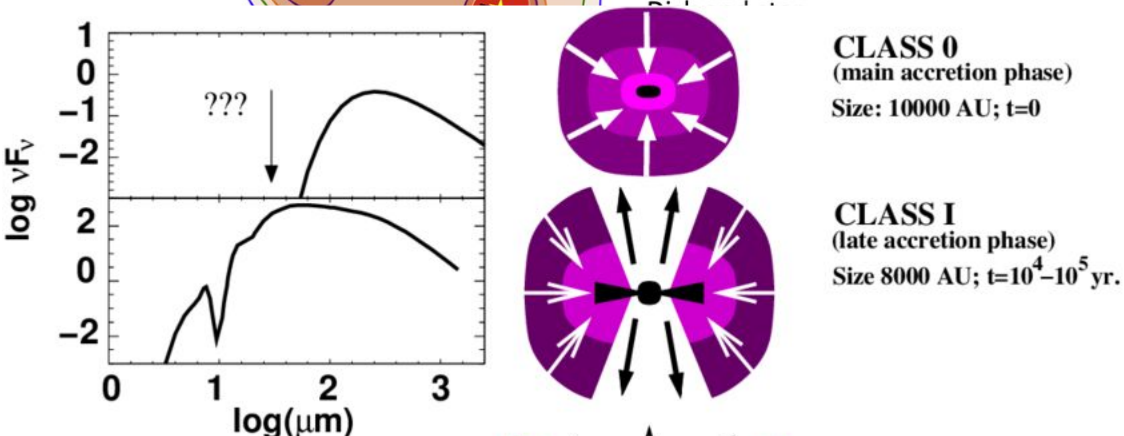

Herschel

Launhardt et al. (2013)

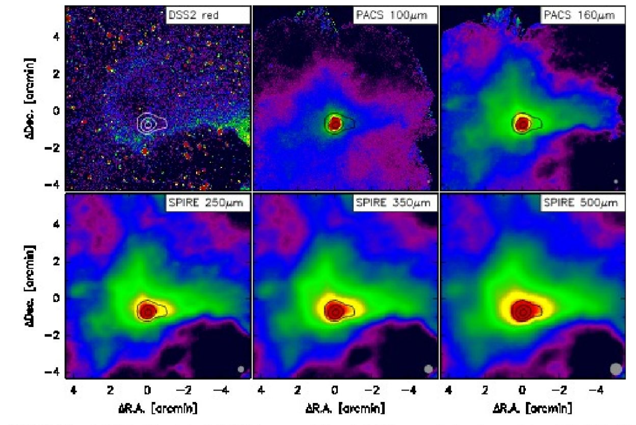

Tapia et al. (2020)

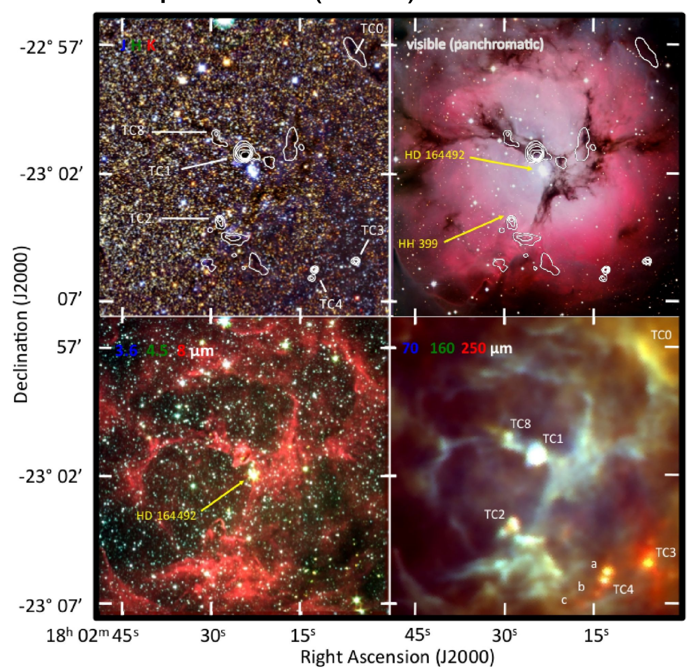

Compact sources in the Herschel maps

Let's consider point-like or poorly resolved sources (i.e. $1 \times PSF_\lambda \leq FWHM_\lambda \leq 3 \times PSF_\lambda$)

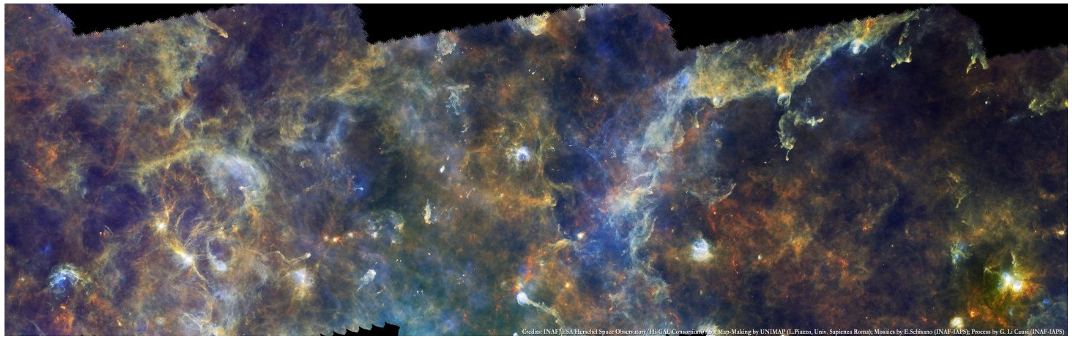

…how to detect them?

PSF photometry wouldn't be adequate, Clumpfind-2D wouldn't be flexible in estimating the background.

CuTEx (Rome, IT; based on curvature analysis)
Molinari et al. 2011, A&A, 530, A133

Getsources (Saclay, FR; based on multi-scale spatial decomposition)
Men'shchikov et al. 2012, A&A, 542, A81

CSAR (Cardiff, UK; based on Clumpfind)
Kirk et al. 2013, MNRAS, 432, 1424

Hi-GAL Photometric Catalogues

Source statistics

	$0^\circ < l < 360^\circ$
70 µm	141994
160 µm	322827
250 µm	355924
350 µm	215134
500 µm	110991

Created using CuTEx package (Molinari+2011)

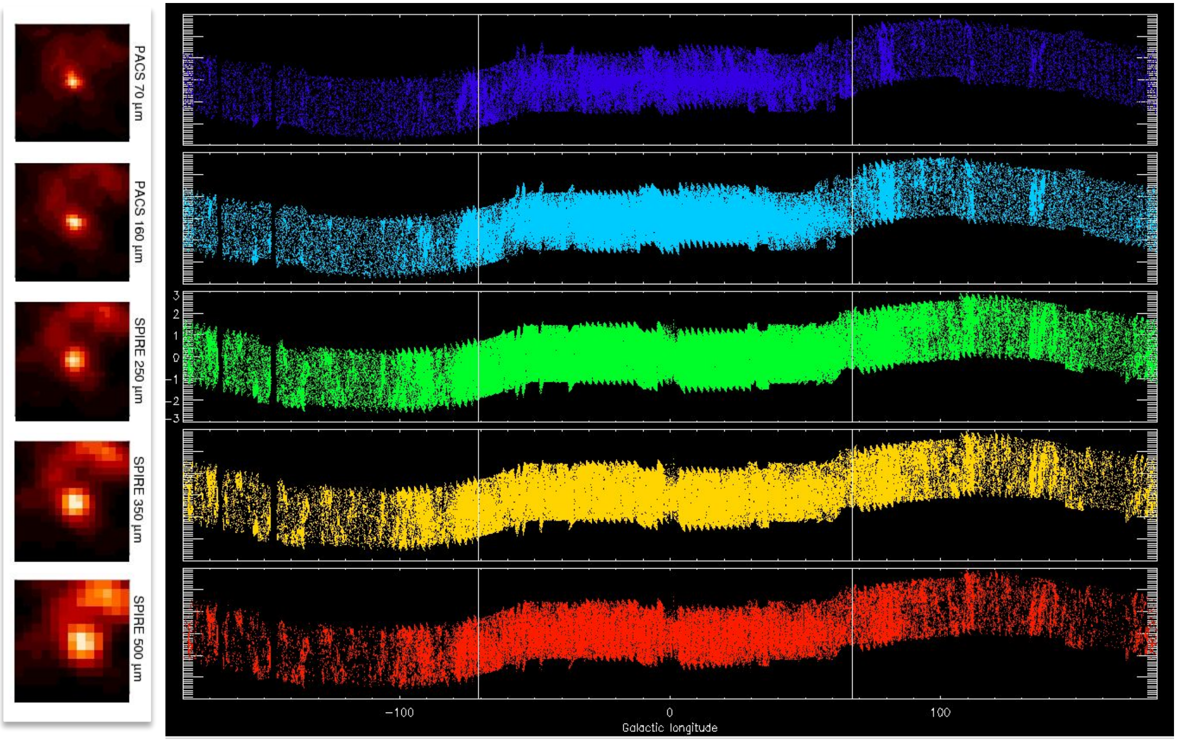

After band-merging and filtering, <u>$\sim 1.5 \times 10^5$</u> reliable SEDs are available for greybody fit and physical properties determination (Elia+2021).

For comparison: ATLASGAL and BGPS catalogs have $\sim 10^4$ and 8×10^3 sources, respectively; clumps detected in GRS survey are $\sim 6 \times 10^3$.

Starless sources vs Proto-stellar

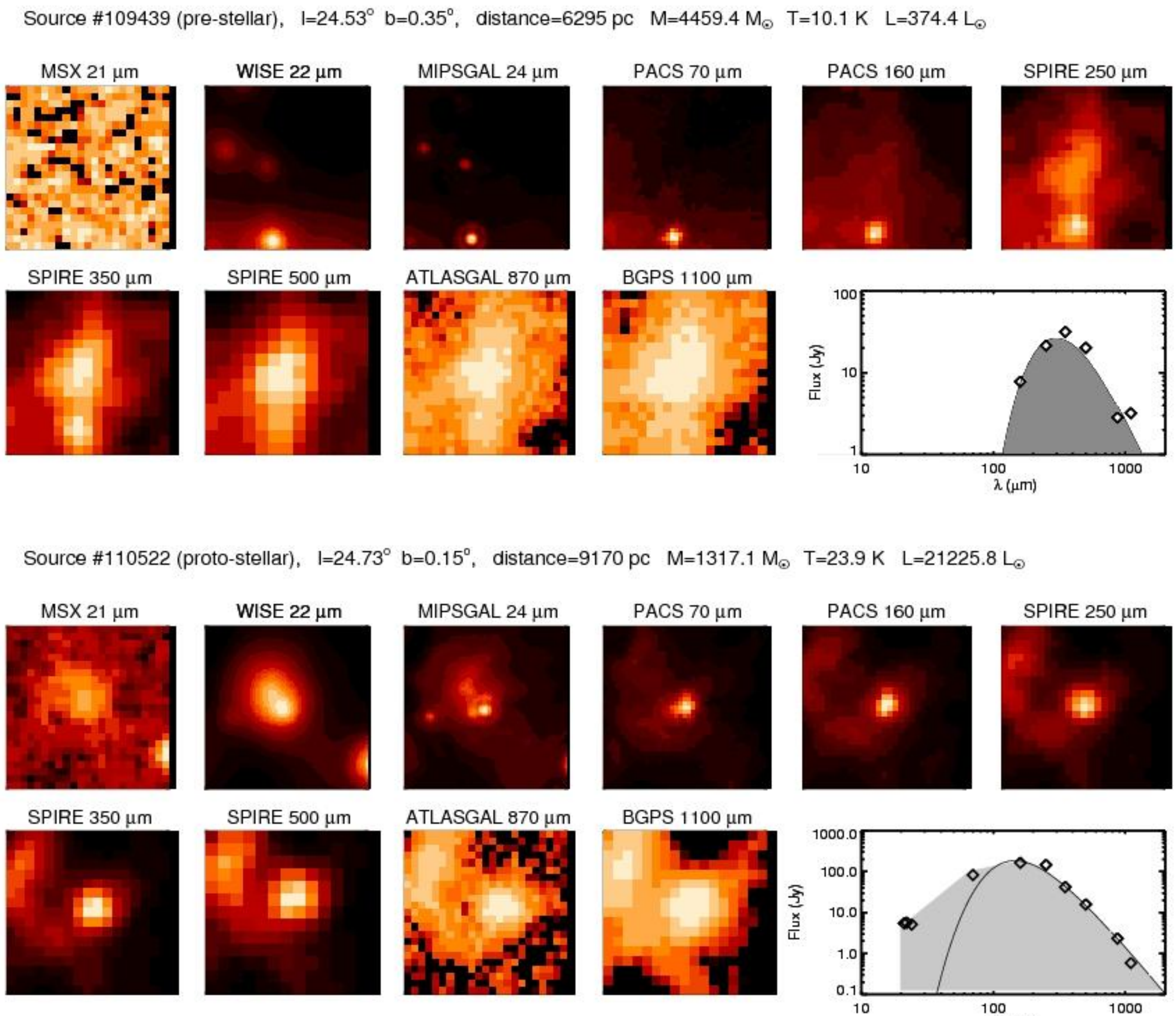

MSX ***21 µm***
+
WISE
+
MIPSGAL
+
Hi-GAL
+
ATLASGAL
+
BGPS ***1100 µm***

Elia+(2017)

SED building

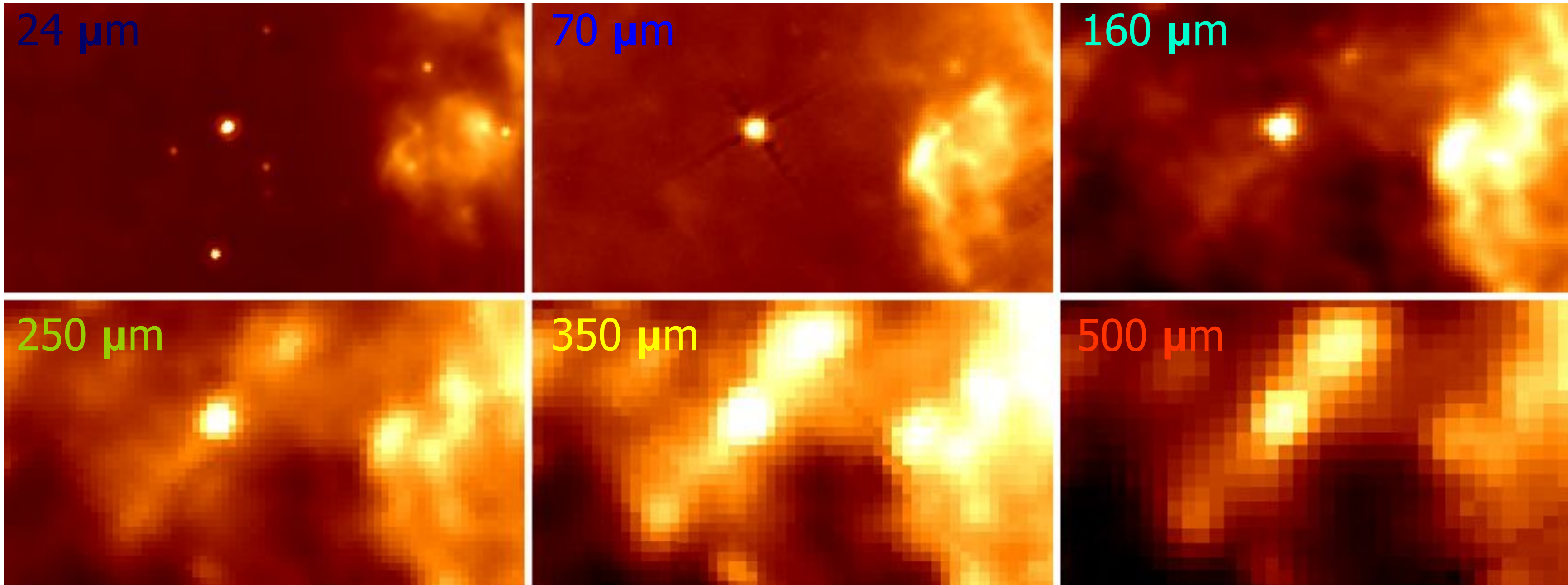

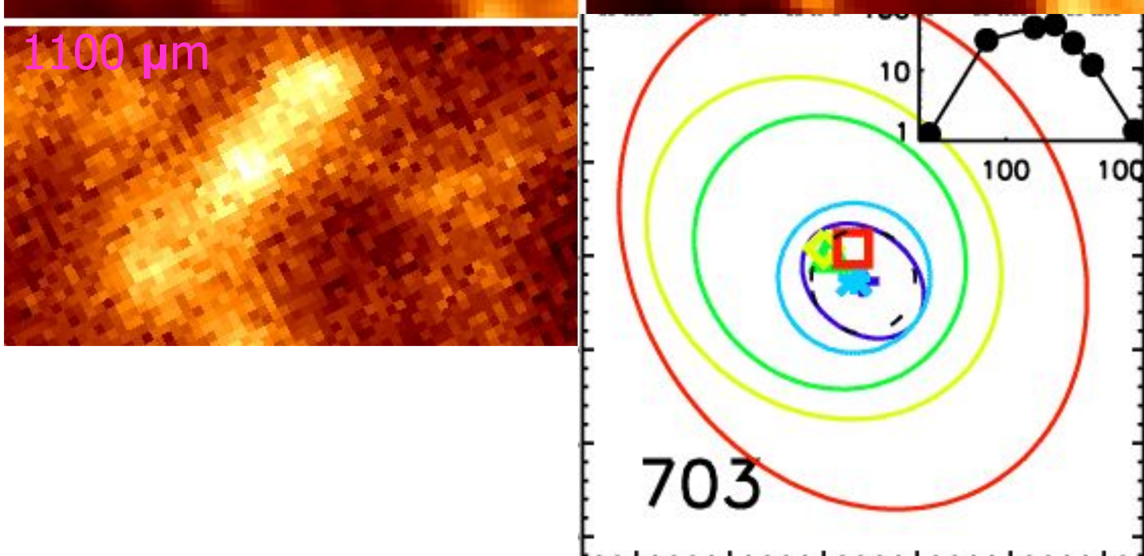

Association based on positional criteria

SED building

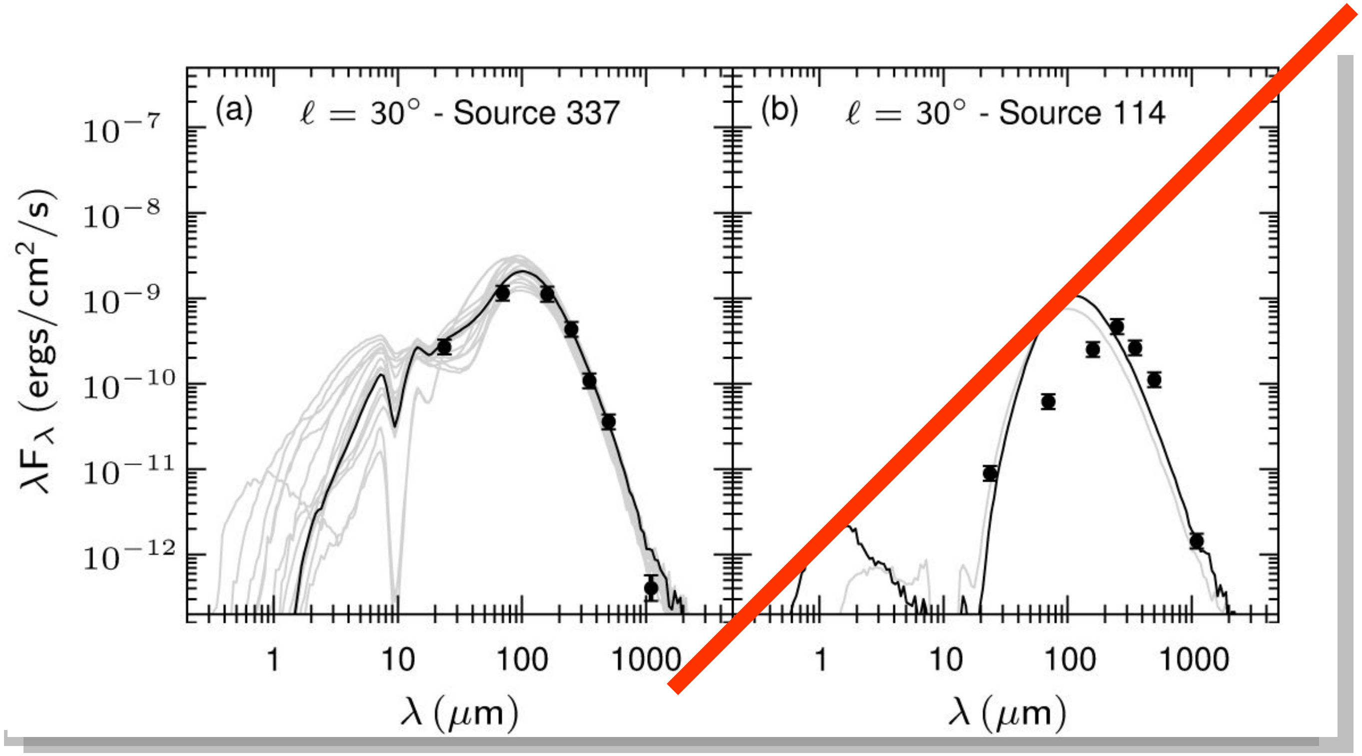

If Mid-Infrared ancillary photometry is available, a protostar+disk+envelope (e.g. Robitaille et al. 2006, ApJS, 167, 256) can be fitted to the SED…

…otherwise let's fit a greybody to the λ ≥ 160 μm portion of the SED to derive the properties of the envelope.

Greybody fitting

$$F_\nu = \Omega\left(1 - e^{-\tau_\nu}\right) B_\nu\left(T\right)$$

$$\tau_\nu = \left(\nu / \nu_0\right)^\beta = \left(\lambda_0 / \lambda\right)^\beta \ . \ \text{For } \lambda = \lambda_0 \ , \ \tau = 1$$

Four free parameters (Ω, λ_0, T, β)

The solid angle can be constrained by using the observed size.
β can also be fixed (e.g., $\beta = 2$).

Greybody fitting (optically thin at any λ)

For $\tau \ll 1$, $\left(1-e^{-\tau}\right) \approx \tau$

and $\tau_\nu = \int K ds = \int \kappa \rho ds \approx \kappa_{ref} \left(\lambda_{ref} / \lambda\right)^\beta M / \left(d^2 \Omega\right)$

where $k_{ref} =$ opacity at λ_{ref} (already containing dust/gas)

$$\Rightarrow M = \frac{d^2 \Omega}{k_{ref}} \left(\frac{\lambda_0}{\lambda_{ref}} \right)^\beta$$

$$F_\nu = \frac{M \kappa_{ref}}{d^2} \left(\frac{\lambda_{ref}}{\lambda} \right)^\beta B_\nu (T)$$

Three free parameters (M, T, β)

Greybody fitting (thin vs «thick»)

Differences between temperatures (left) and masses (right) obtained through the two different fits.

No differences if λ_0 is such that $\tau \leq 0.1$ for $\lambda \geq 160$ μm (for $\beta = 2$, this happens for $\lambda_0 \leq 50.6$ μm).

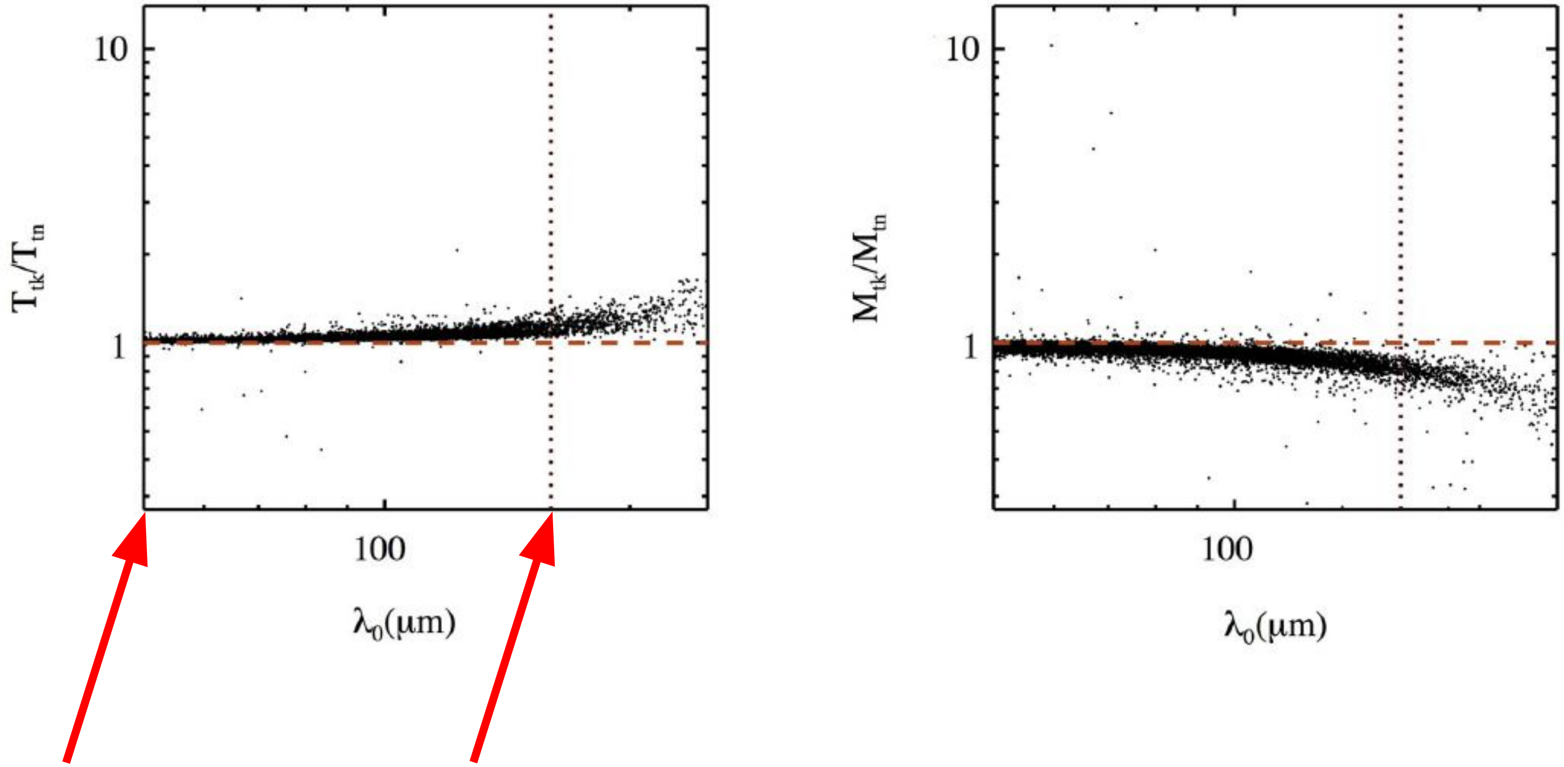

λ_0 = 50.6 μm **λ_0 = 160 μm**

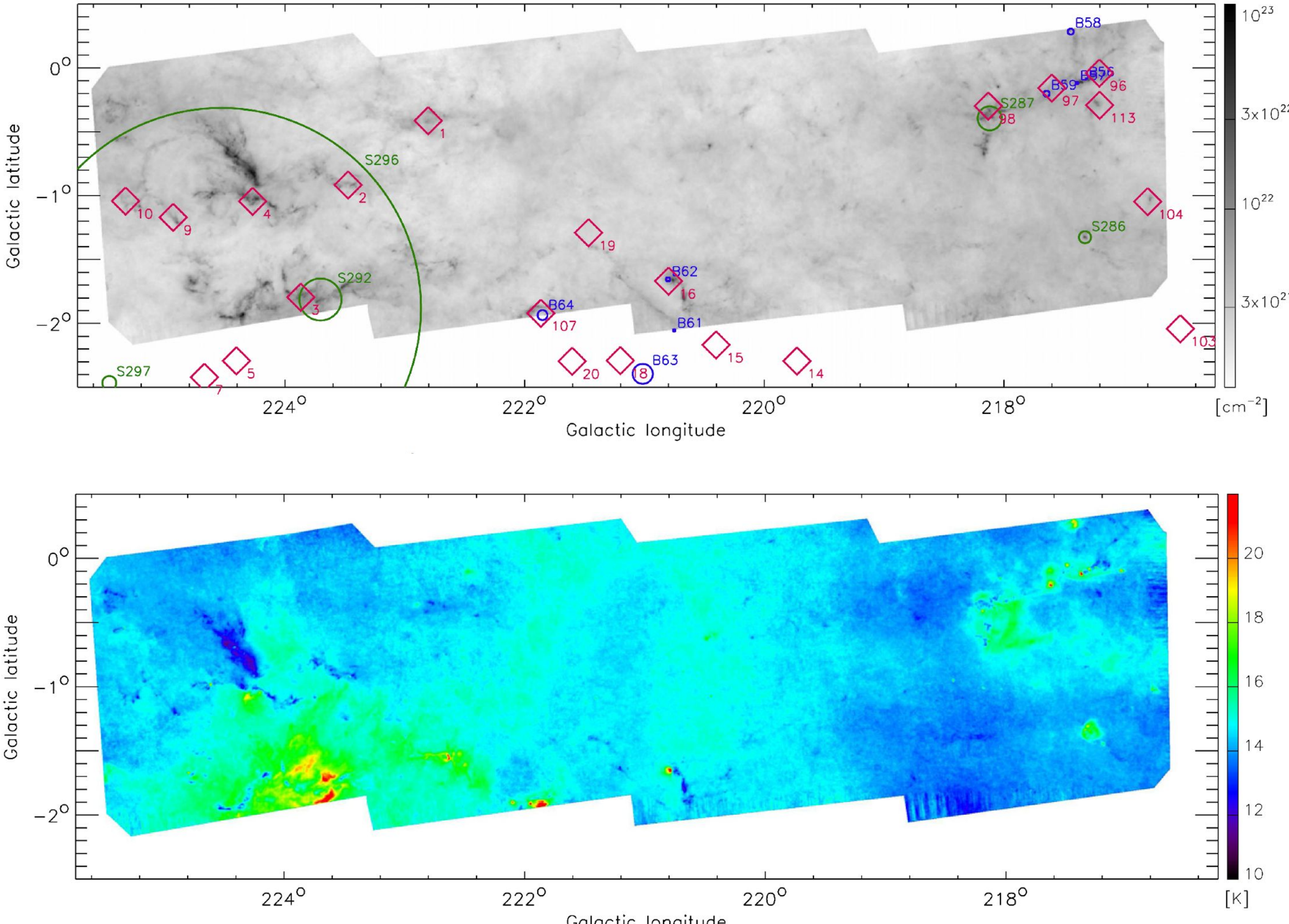
Galactic latitude
Galactic longitude
0°
−1°
−2°
224°
222°
220°
218°
10²³
3x10²²
10²²
3x10²¹
[cm⁻²]
S296
S292
S297
S287
S286
B58
B56
B57
B59
B62
B64
B61
B63
1
2
3
4
5
7
9
10
14
15
16
18
19
20
96
97
98
103
104
107
113
20
18
16
14
12
10
[K]

Source sizes

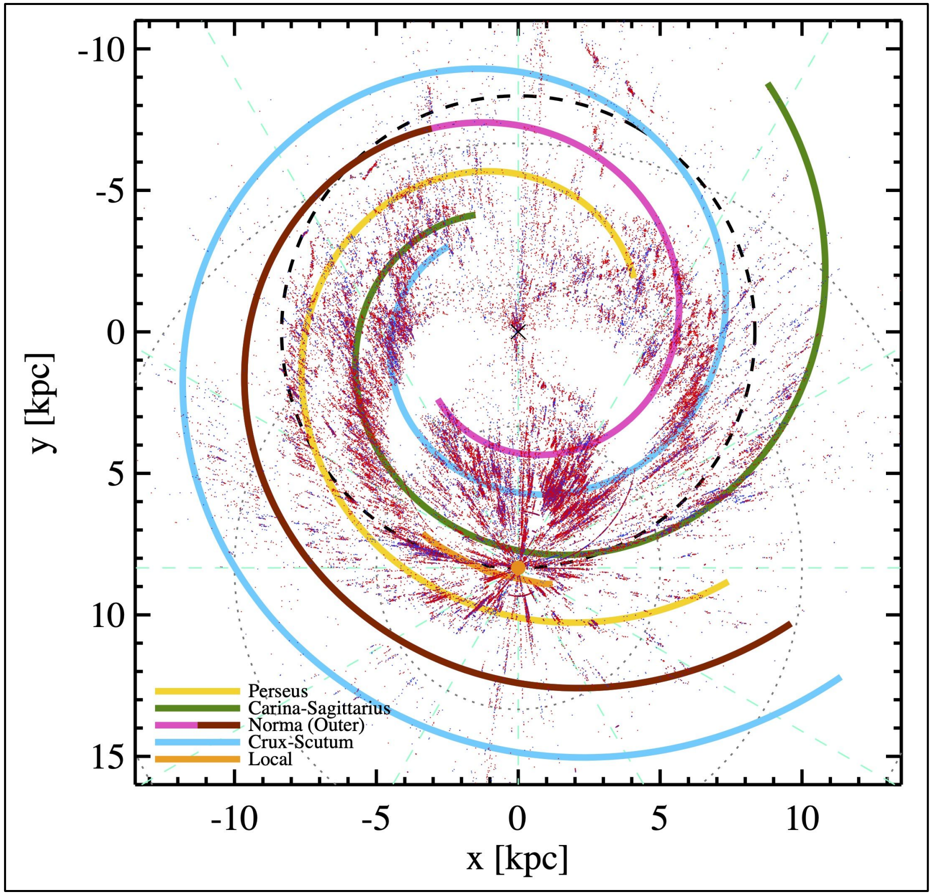

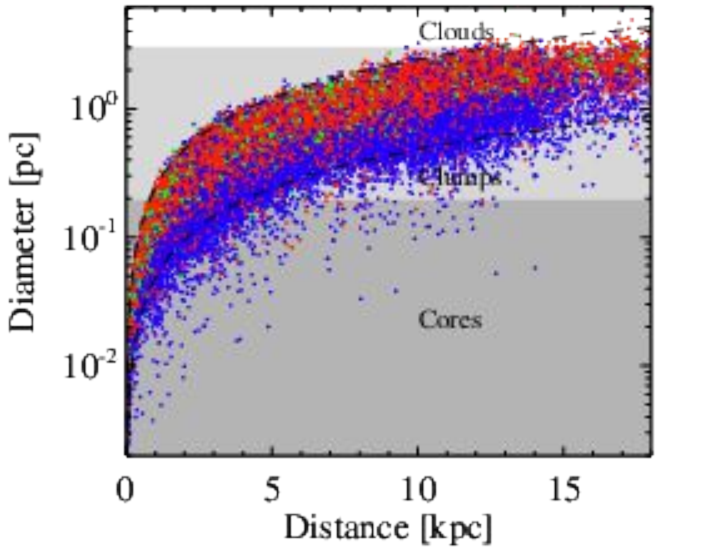

Source sizes estimated at 250 μm

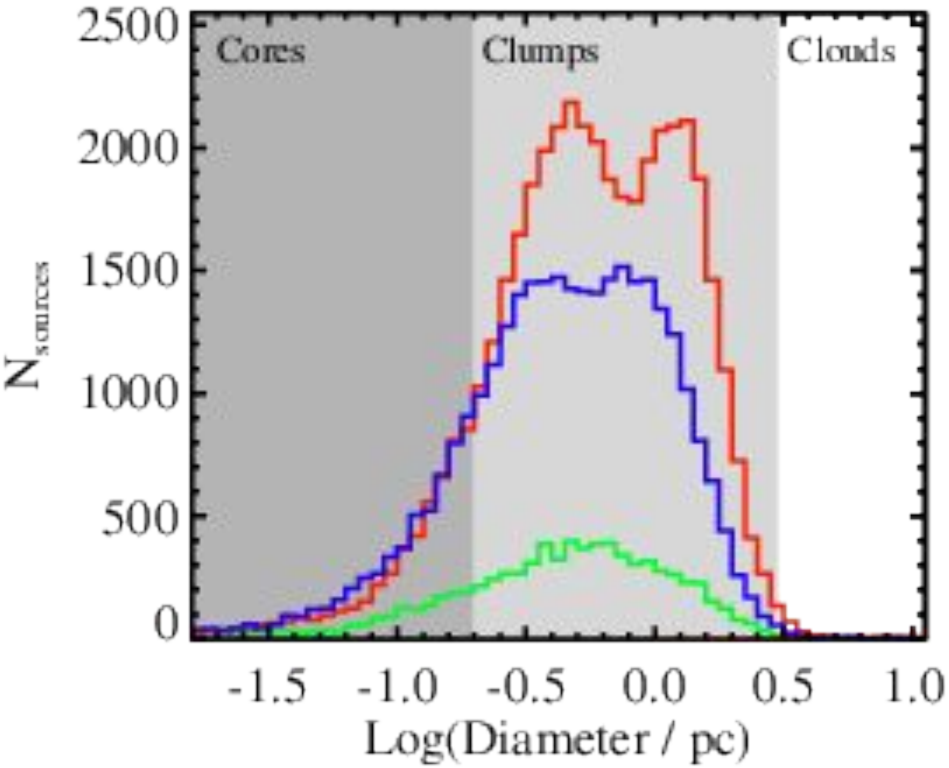

◆ **Proto-stellar**
◆ **Pre-stellar**

Arm prescription by
Hou, Han & Shi (2009)

What Hi-GAL sources…

…are not:

Single YSOs (in most cases)

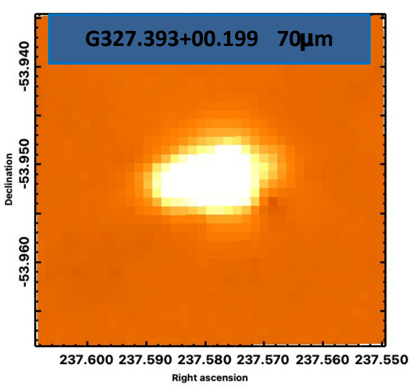

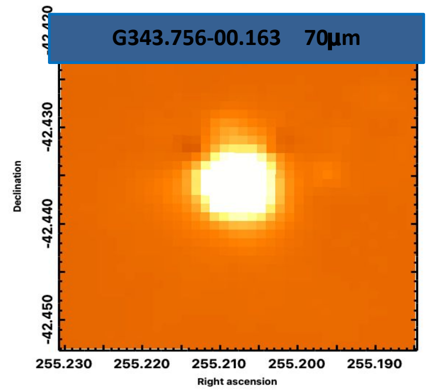

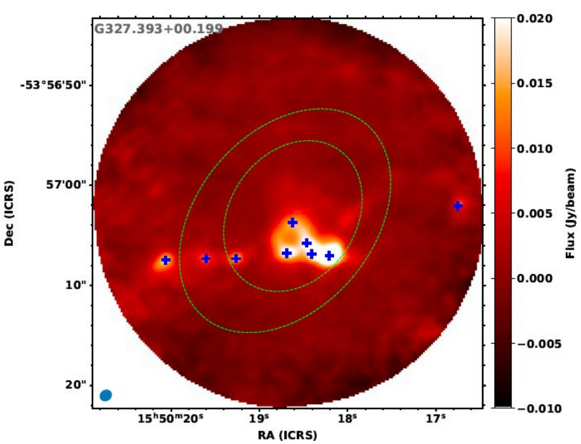

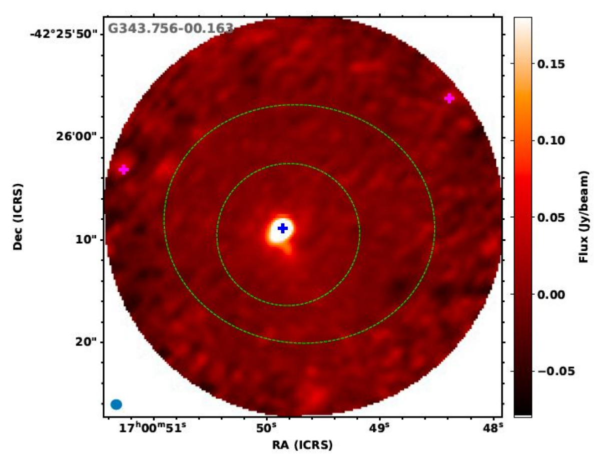

Traficante+(2023)

…are:

Structures with size from several arcsec to few tens of, so that:
- cores (at *d* ≲ 1 kpc)
- clumps at larger *d* (or even clouds, at largest distances)

They are forming / can form a number of stars

Resolving Hi-GAL sources with ALMA

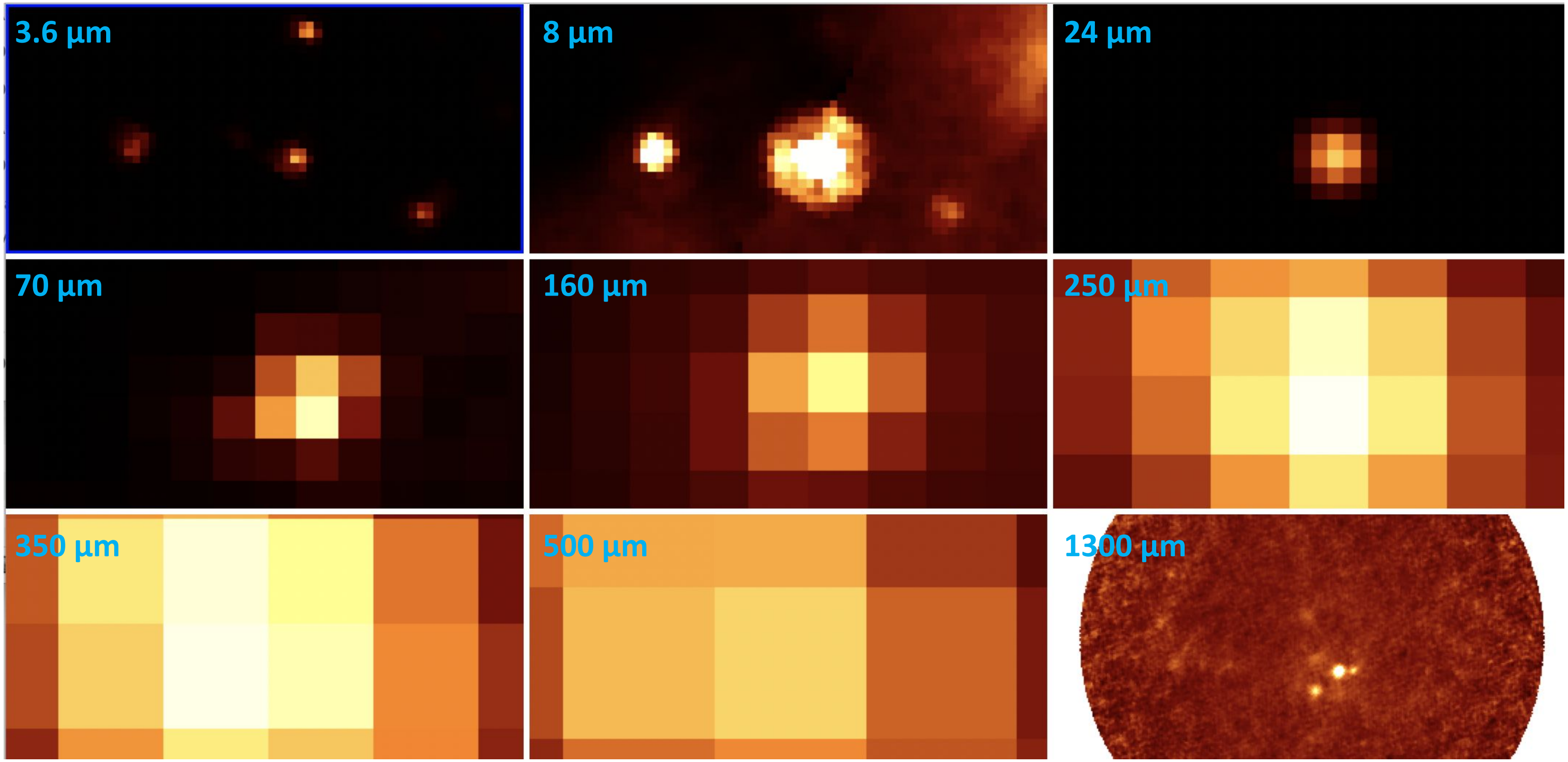

ALMAGAL: ALMA (Band 6) large project to observe, both in continuum and lines, 1000+ Hi-GAL clumps candidate to form massive stars with a spatial resolution of ~1000 AU.

Temperature is the average temperature of the structure, dominated by the large-scale envelope.

Mass is the total mass of the structure, mostly contained the large-scale envelope. Consequently, **Surface Density** is the average surface density.

Evolutionary parameters, such as the **Mass/Luminosity** ratio, as well as the **Temperature** itself, are single numbers summarizing an underlying (and unresolved) variety of conditions across the internal structure of the clump (star-forming vs quiescent part, the inter-core medium, etc.). It's hard to understand if they mirror the average properties of the population of contained cores, or are dominated by the most luminous core(s).

Distance bias on clump parameters
"Moving away" SF regions (Baldeschi et al. 2017, I)

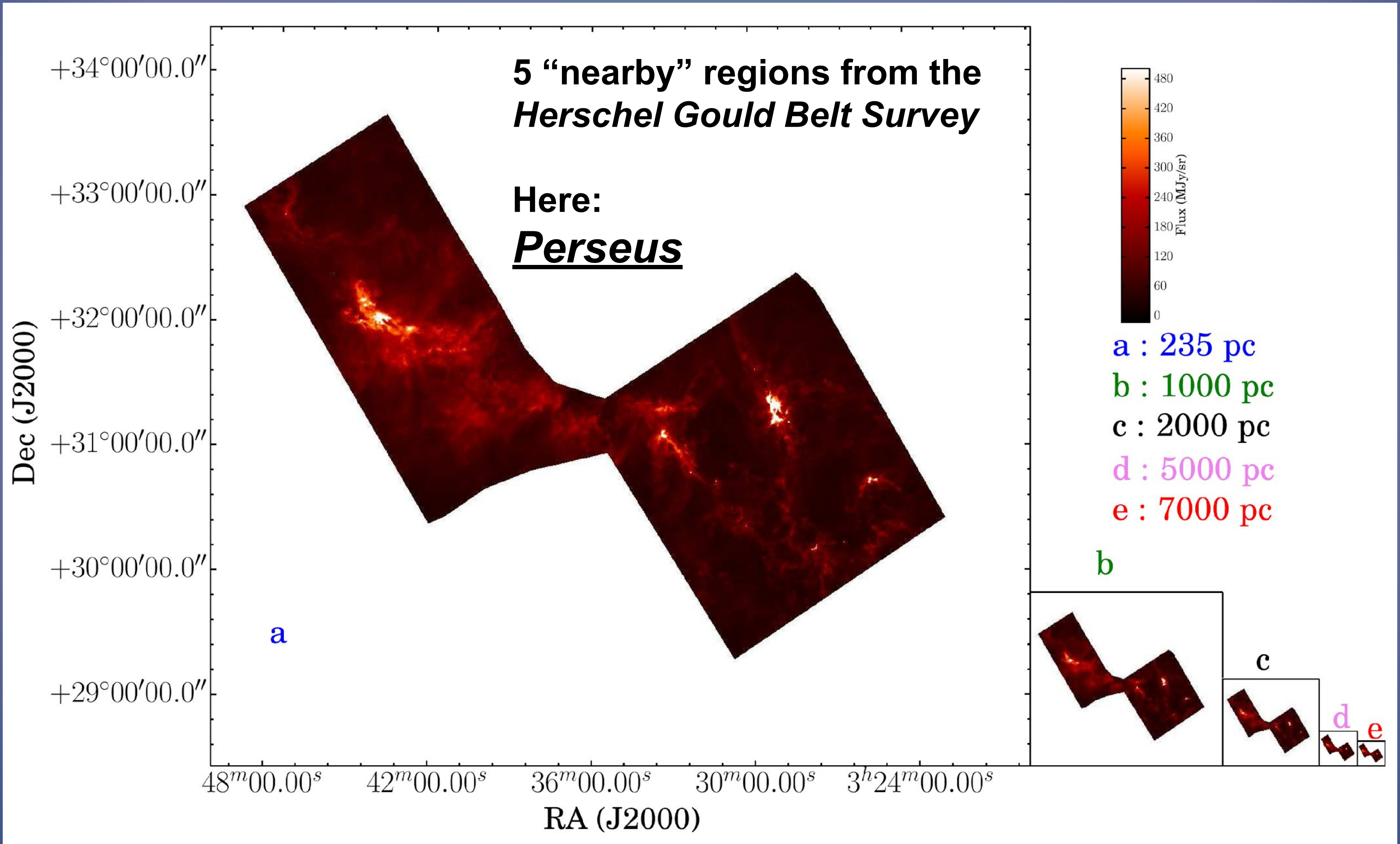

Distance bias - “Moving away” SF regions (Baldeschi et al. 2017, I)

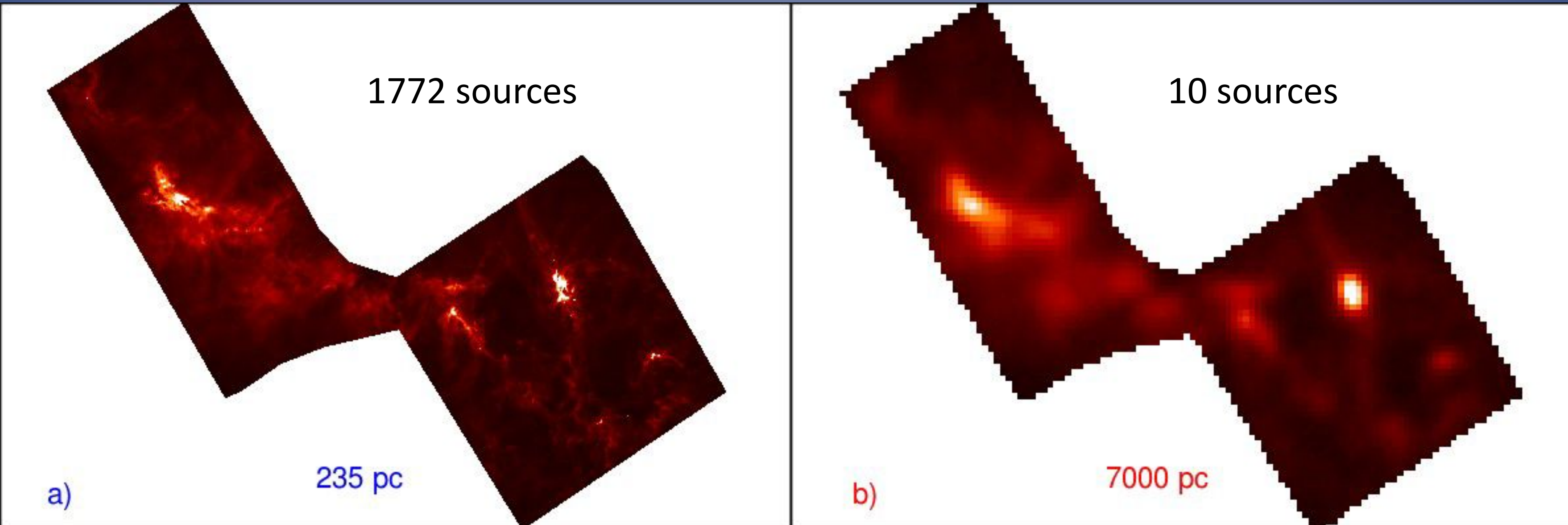

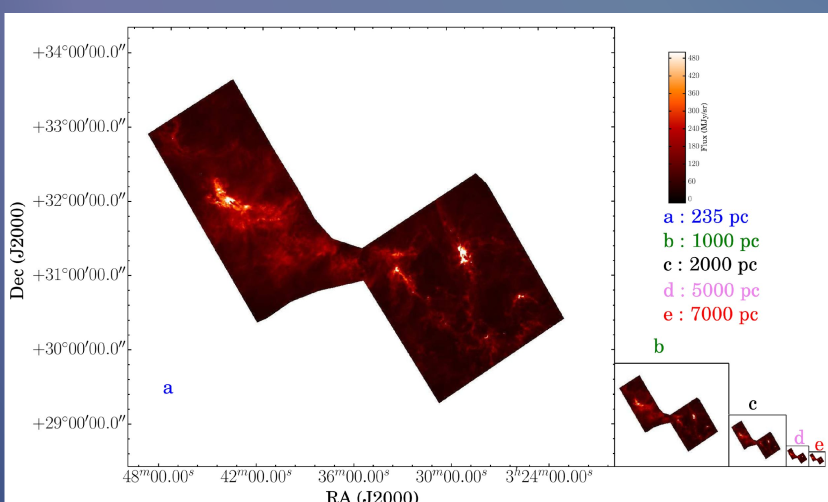

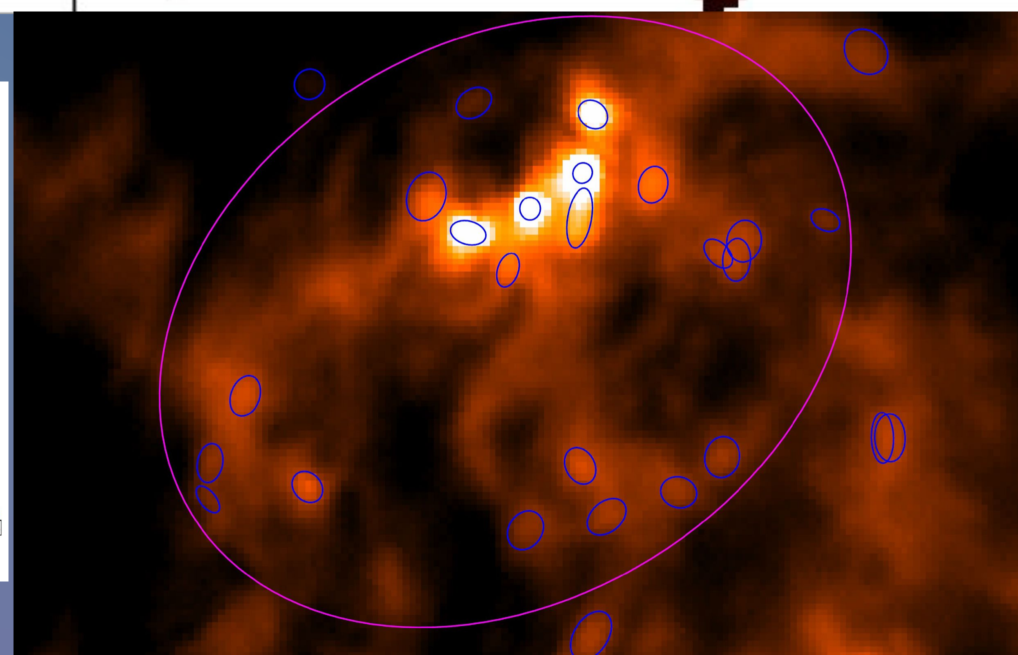

Mass and luminosity regimes

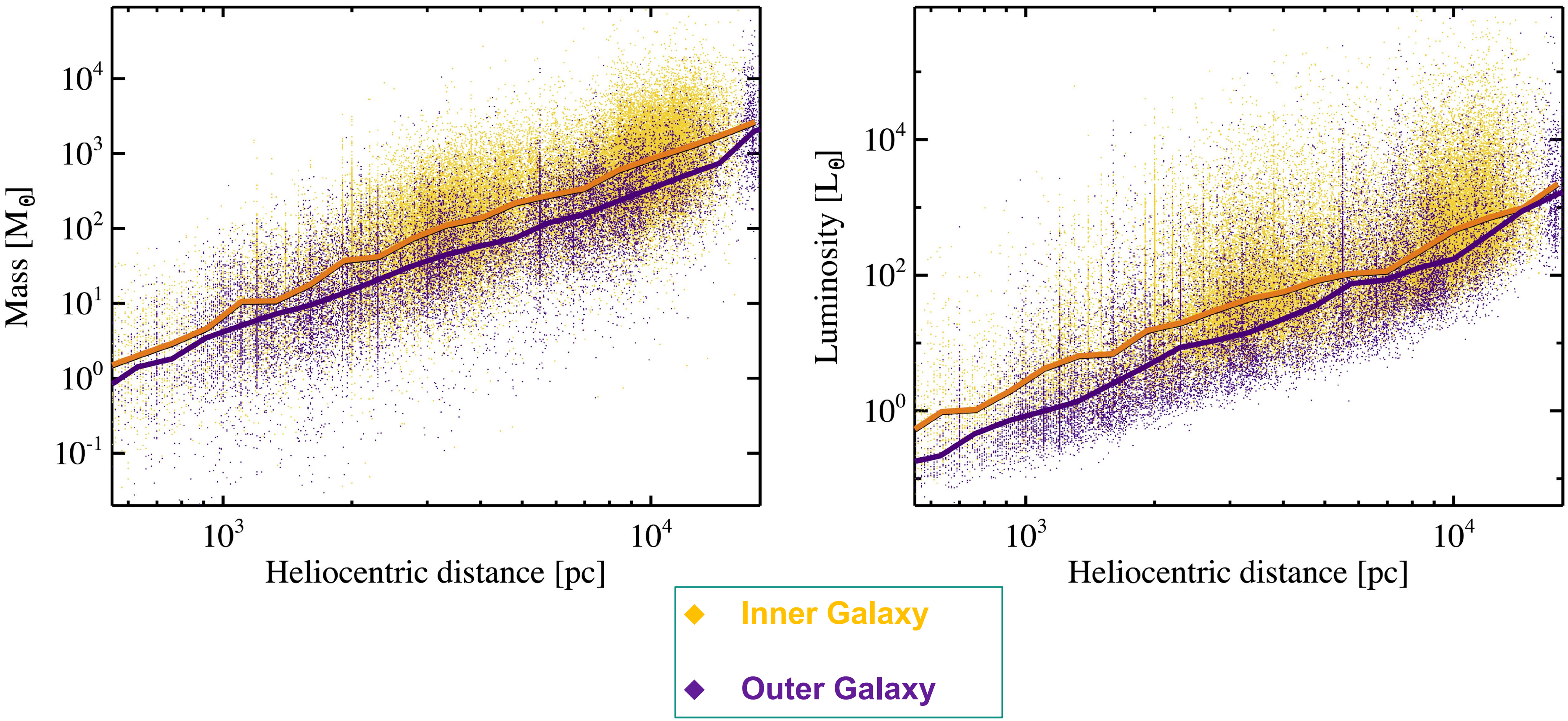

For a given distance bin, median masses and luminosities are typically higher in the inner than in the outer Galaxy.

Greybody temperature

		<*T*> [K]	+/- [K]
Pre-stellar	inner	11.6	1.3
Proto-stellar		15.1	2.8
Pre-stellar	outer	10.4	1.1
Proto-stellar		15.6	3.1

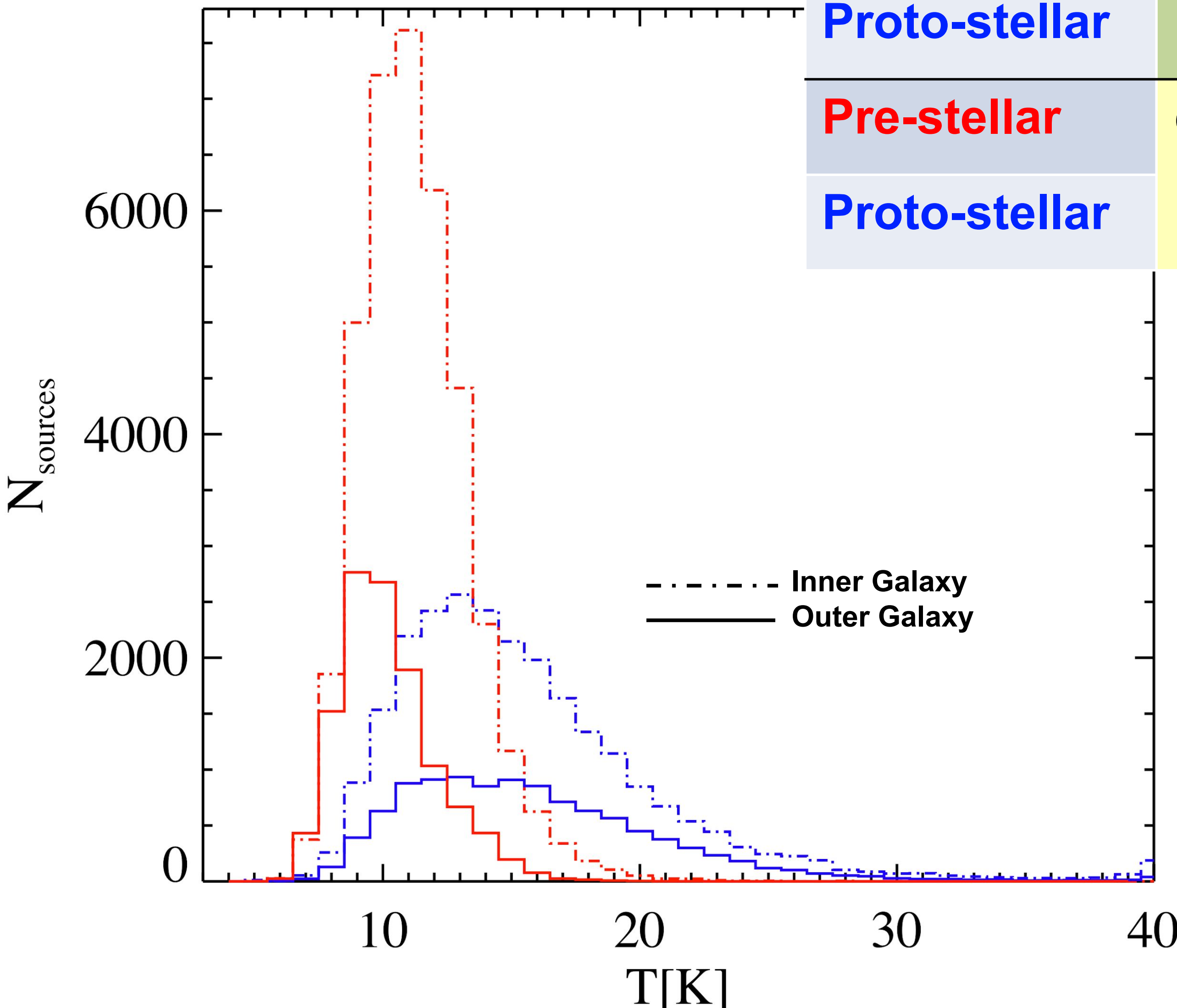

<*T*>:
median *T*

+/-:
Median absolute deviation <|*T*-<*T*>|>

Mass-radius relation

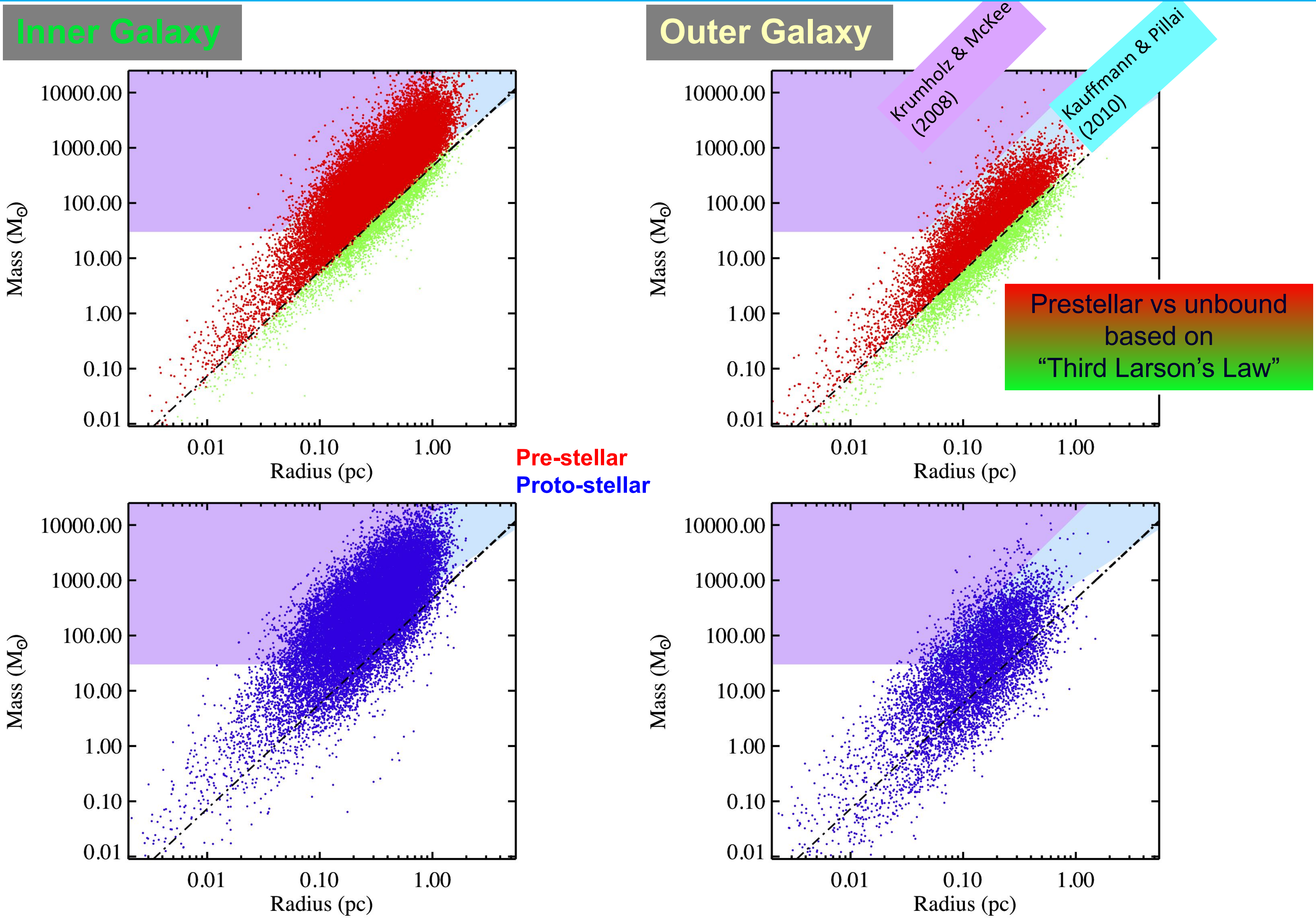

Surface density

KP10 = Kauffmann & Pillai (2010)
B+17 = Baldeschi et al. (2017)
KM08= Krumholz & McKee (2008)

		KP10	B+17	KM08
Pre-stellar	inner	20076	16219	1188
Proto-stellar		15191	13589	3156
Pre-stellar	outer	2011	1367	85
Proto-stellar		2192	1794	297

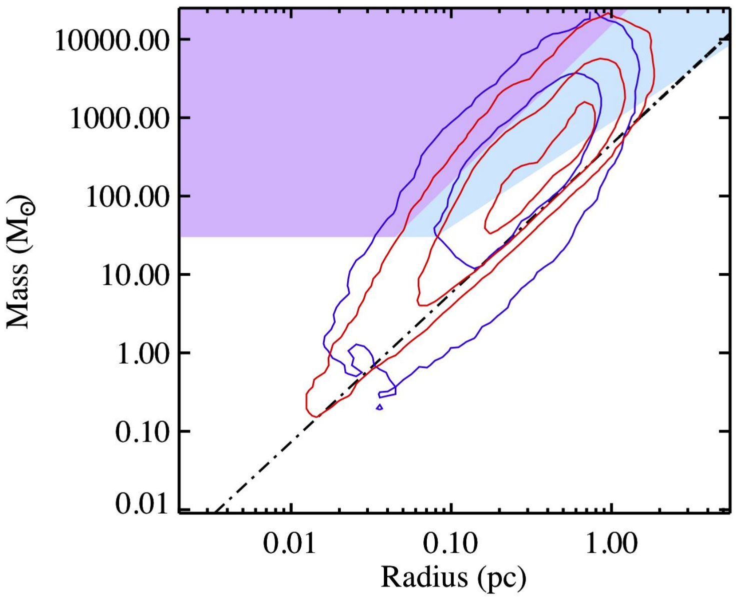

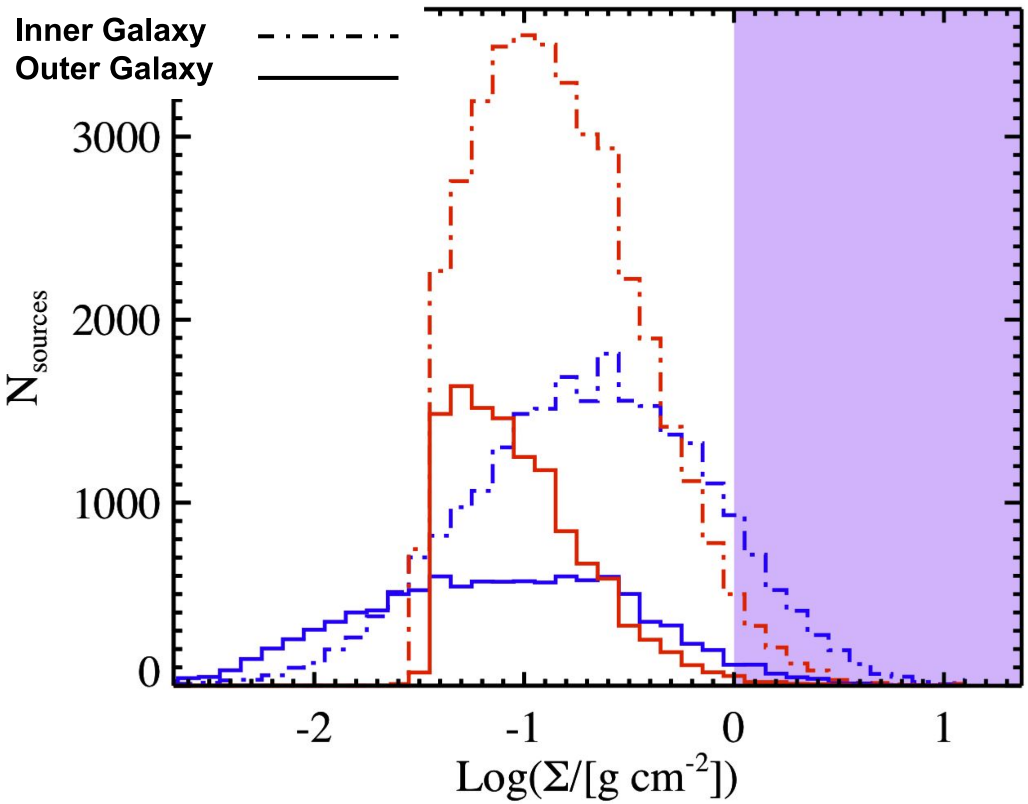

		<Σ/[g cm^{-2}]>
Pre-stellar	inner	0.27
Proto-stellar		0.53
Pre-stellar	outer	0.16
Proto-stellar		0.23

Distance bias on *M* - *r* relation

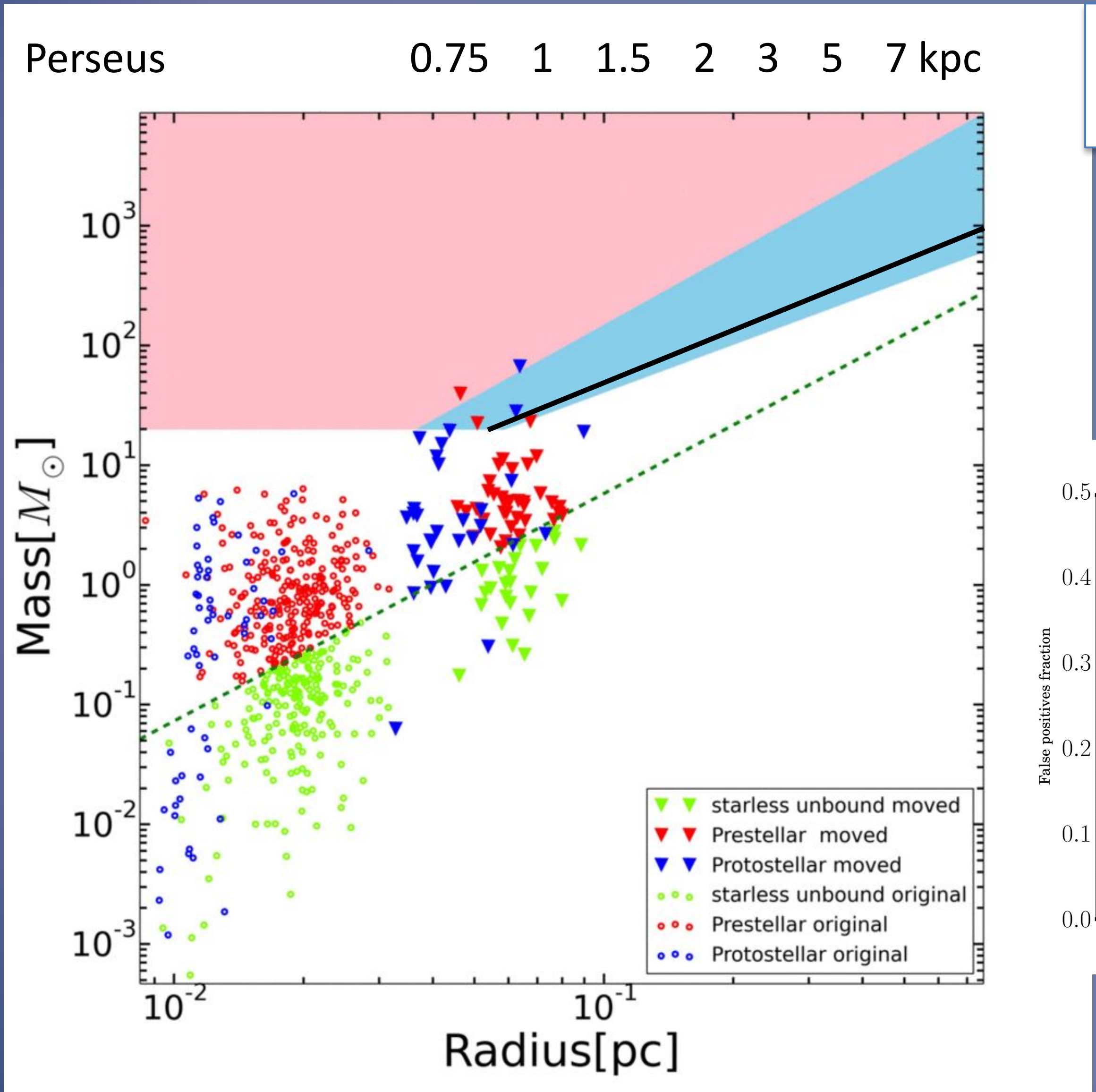

KM08: $M \propto r^2$

KP10: $M \propto r^{1.33}$

$$M > 1282\left(\frac{r}{\mathrm{pc}}\right)^{1.42} \mathrm{M_{sun}}$$

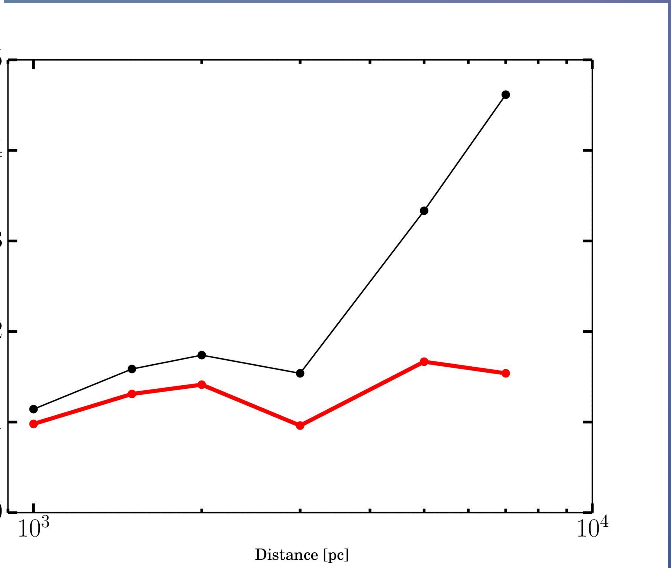

Baldeschi+(2017a)

Evolutionary diagnostics through the L_{bol} vs M relation

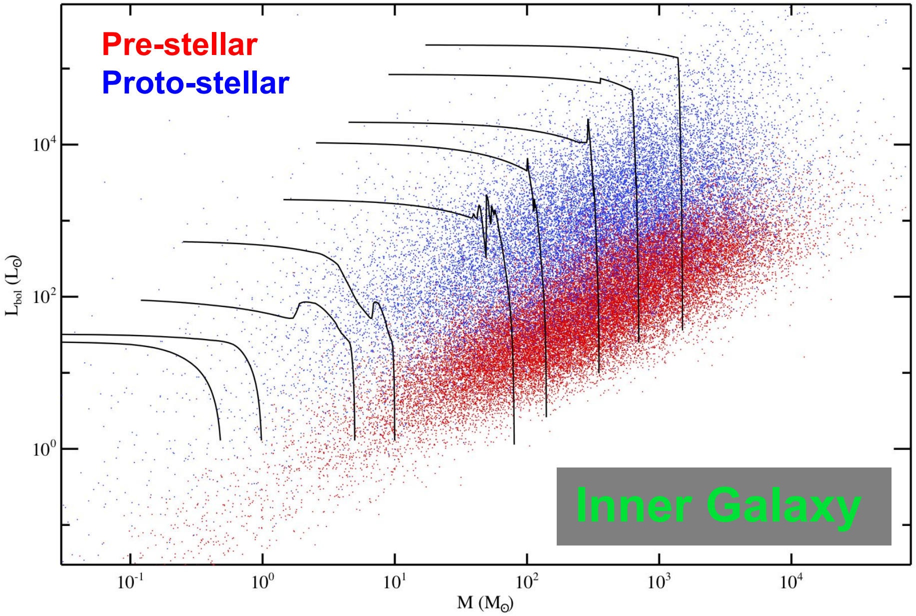

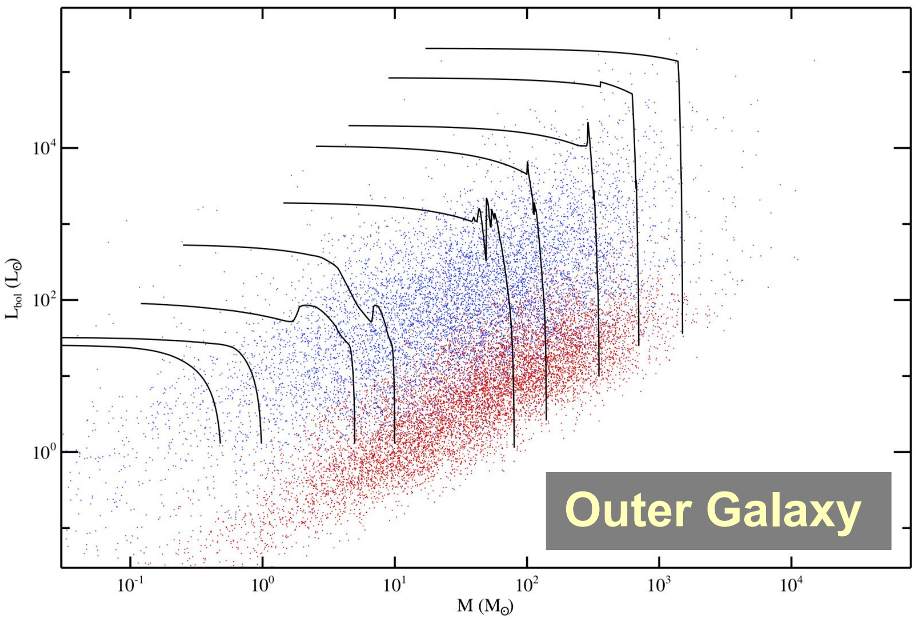

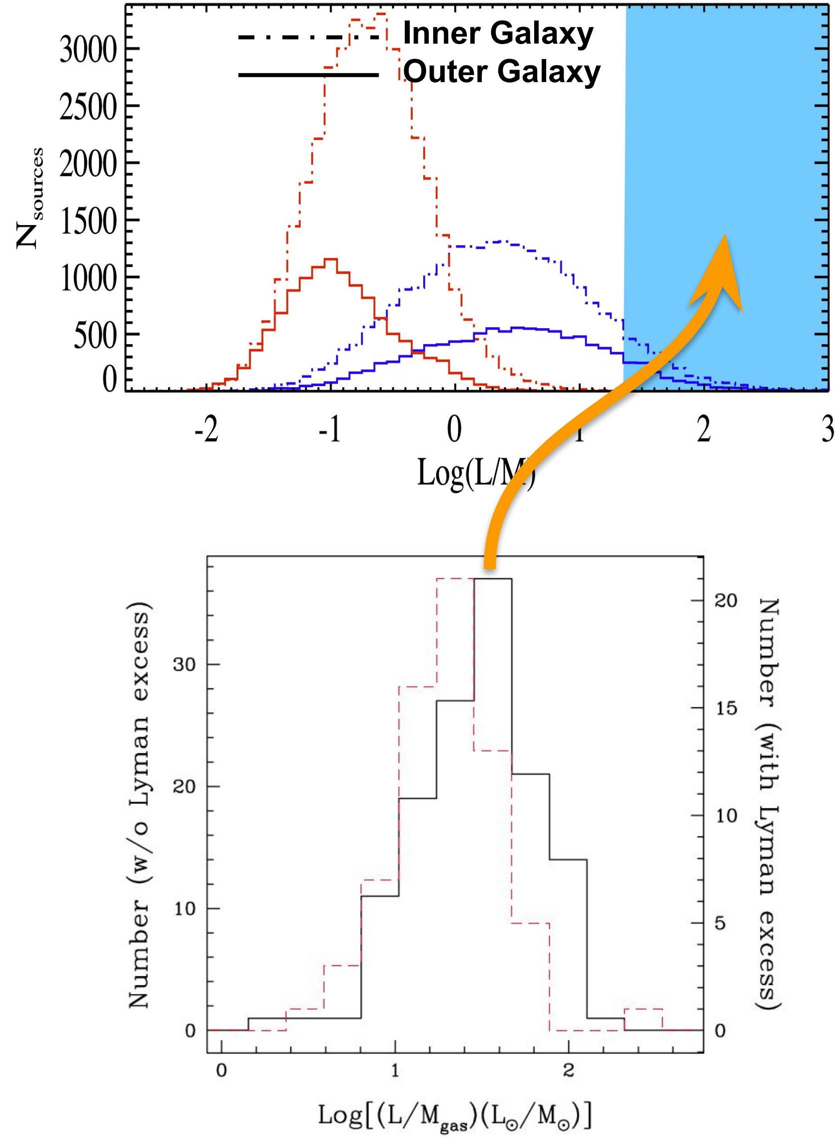

Cesaroni+(2015), Hi-GAL sources detected in CORNISH

L/*M* for SF regions "moved away" (Baldeschi et al. 2017, II)

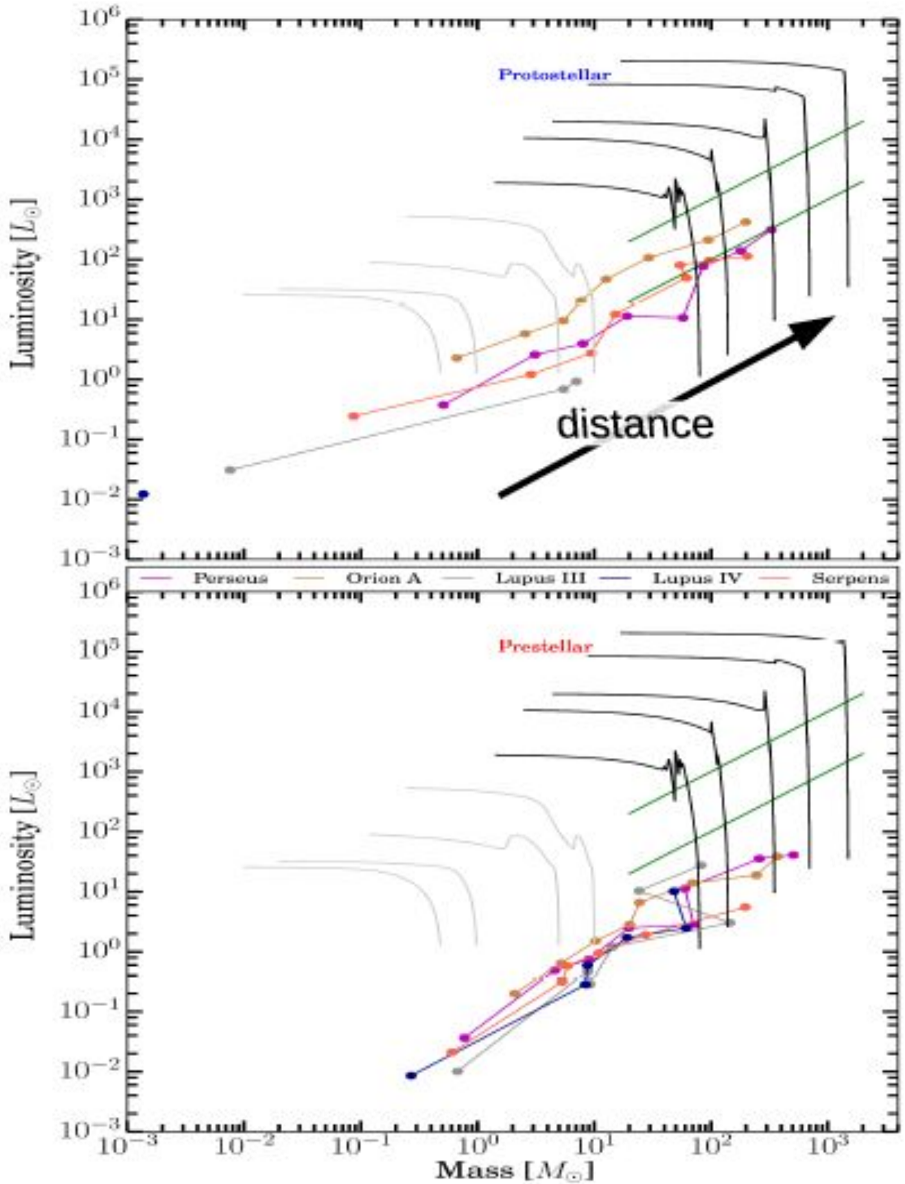

Barycenter of *M* and *L* at each probed distance

Constant slope

Orion A

Perseus

Serpens

Lupus III

Lupus IV

L_{bol}/L_{submm} ratio

***L_{submm}* calculated for *λ* > 350 μm**

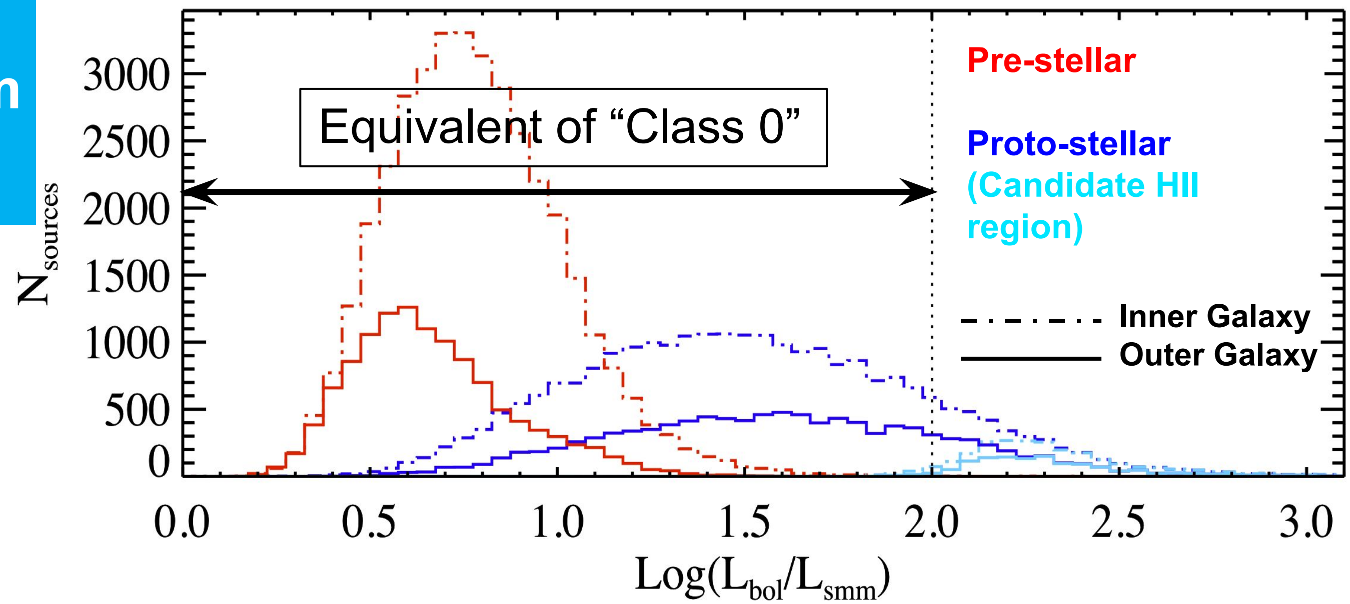

Bolometric temperature

$$T_{bol} = 1.25 \times 10^{-11} \frac{\int_{-\infty}^{\infty} \nu F_\nu \, d\nu}{\int_{-\infty}^{\infty} F_\nu \, d\nu}$$

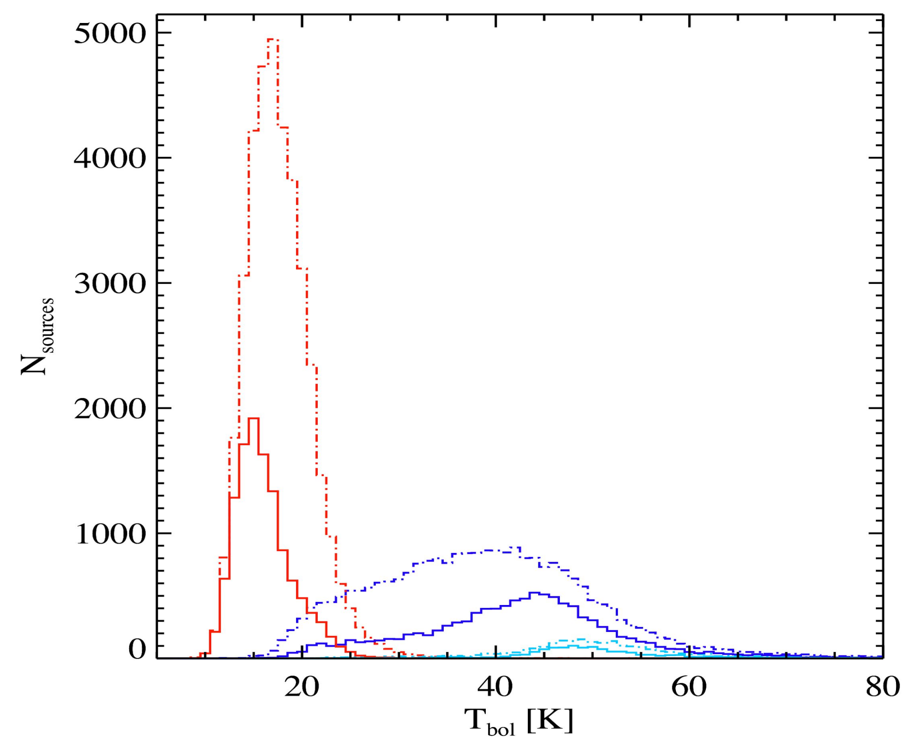

Surface density vs evolutionary stage

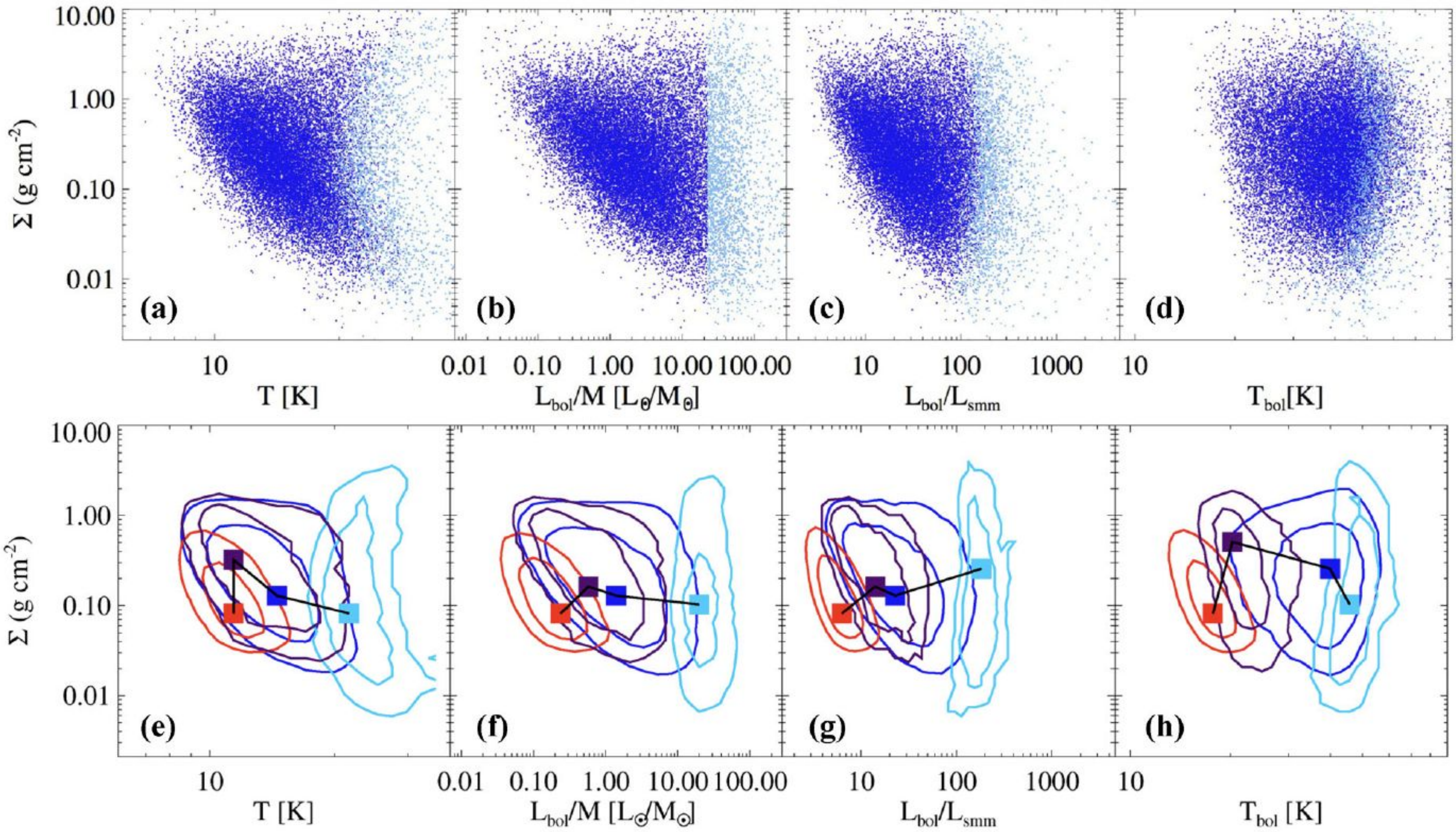

A synoptic view of evolutionary parameters

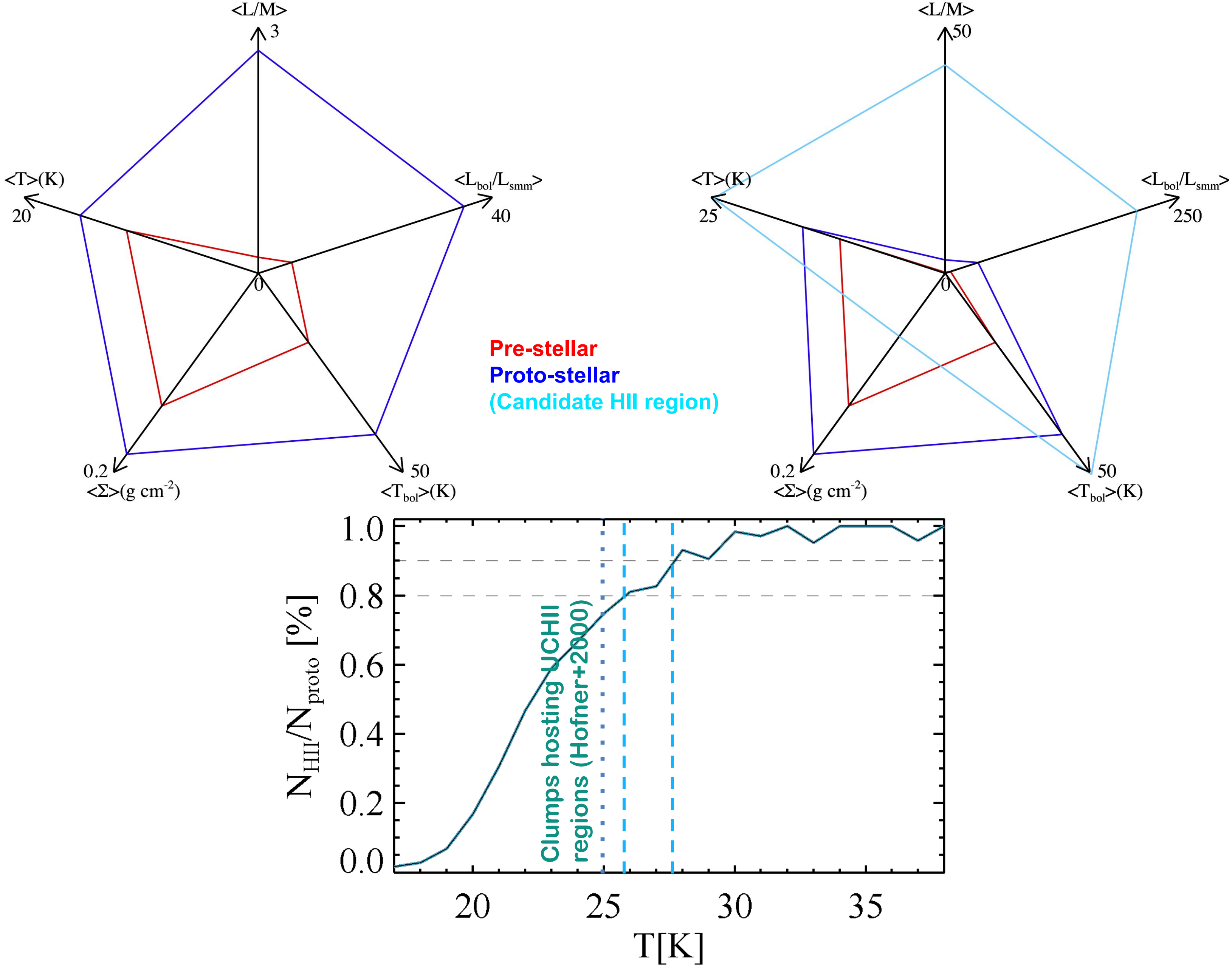

Inner vs Outer Galaxy

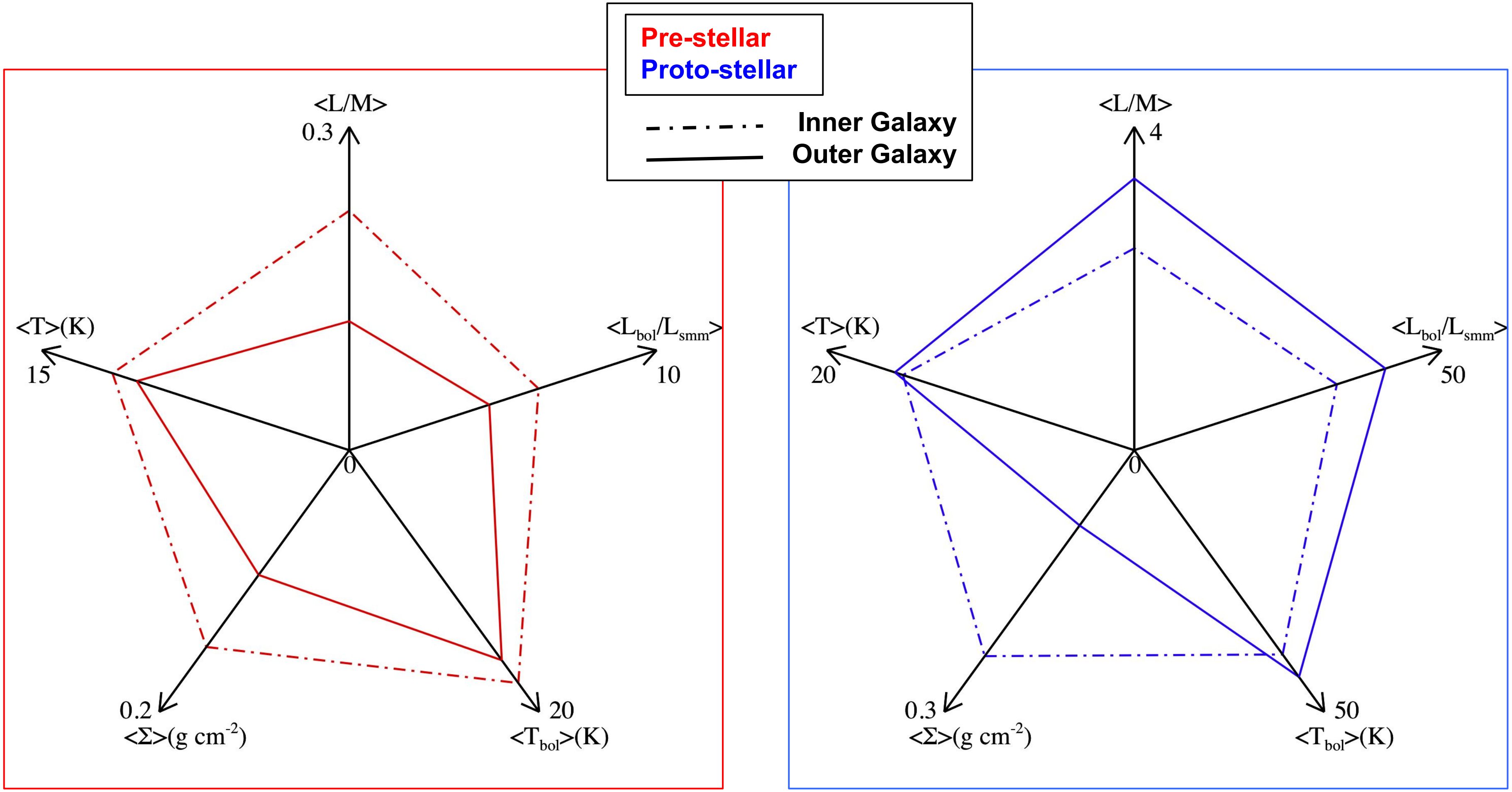

Pre-stellar sources seems to be on average less evolved in the inner Galaxy than in the outer, and the other way around for protostellar.

Possible confusion effect at 70 μm in the latter case?

ISRF and pre-stellar clump temperature

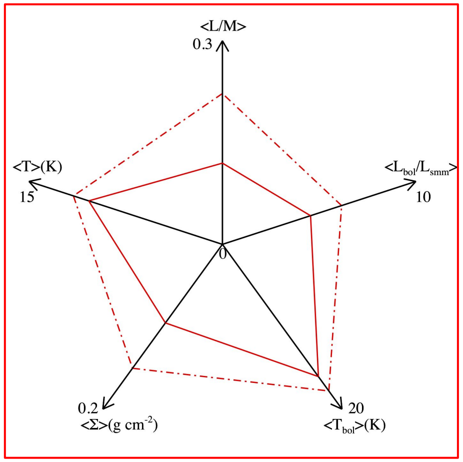

Averages of <I_{70}> and T in 1°-bins.

<I_{70}>: the PACS 70 μm intensity over a 61 °x 61 pixel (~3.25 °x 3.25 arcmin^2) subframe centred on the source centroid.

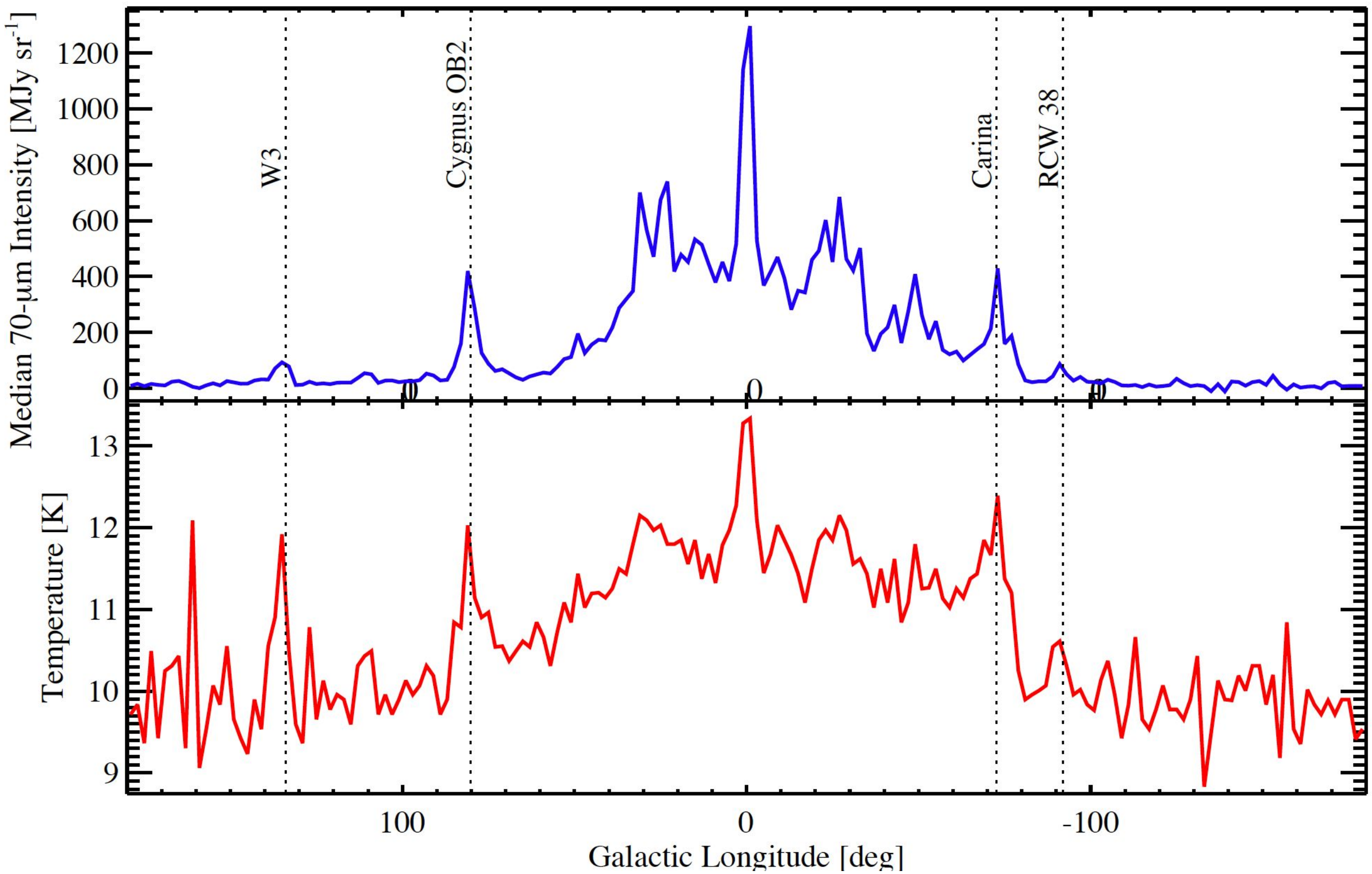

Pre-stellar/Proto-stellar confusion

	Inner Galaxy	Outer Galaxy
T (K)	15.2	15.3
L/M ($L_\odot/M_\odot$)	2.6	3.1
T_{bol} (K)	39.5	43.4
Σ (g cm^{-2})	0.21	0.10

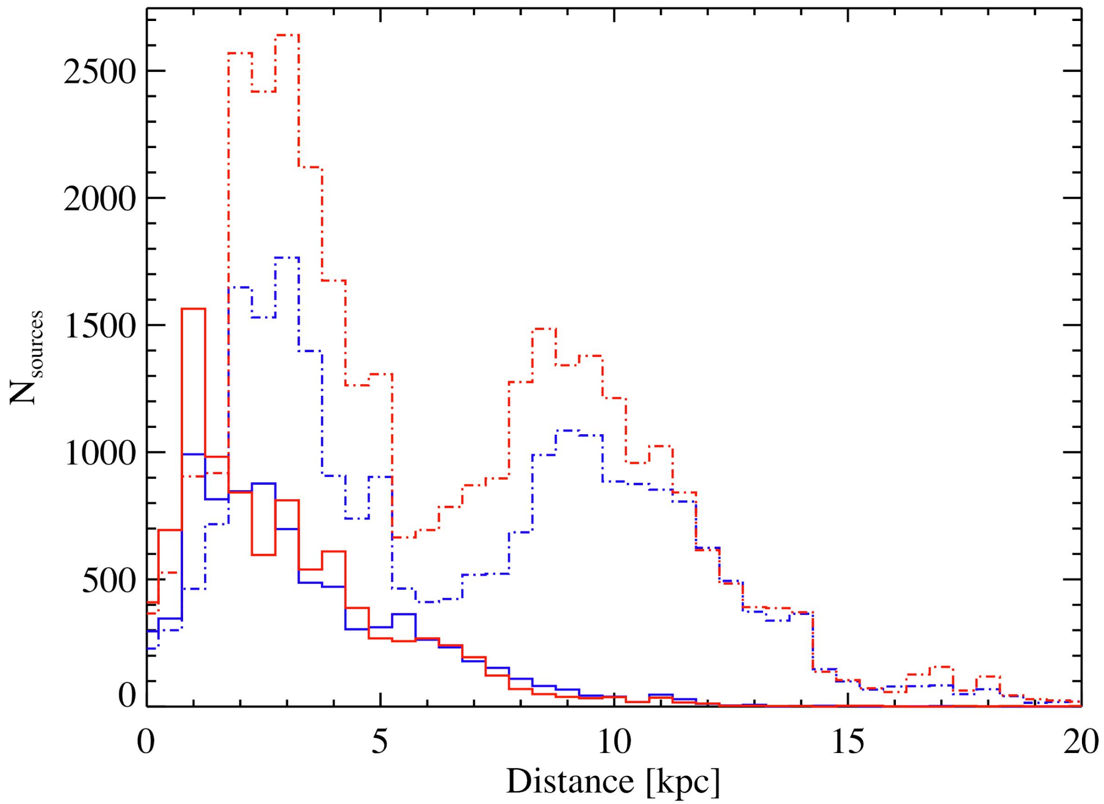

Larger Hi-GAL source distances imply larger level of blending.

Sources getting blended after this operation define a new unresolved source that assumes a protostellar character if at least one of its original components was protostellar.

<u>Considering only sources at *d* < 5 kpc, both in the inner and in the outer Galaxy, the above discrepancies get reconciled.</u>

Pre-stellar/Proto-stellar confusion

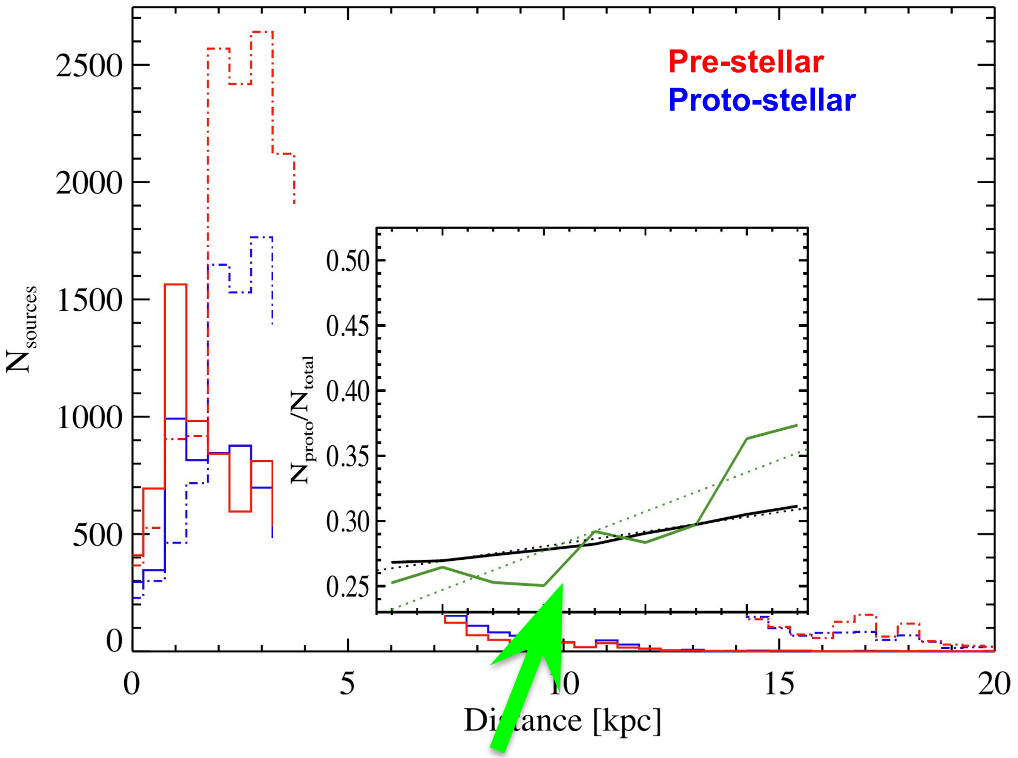

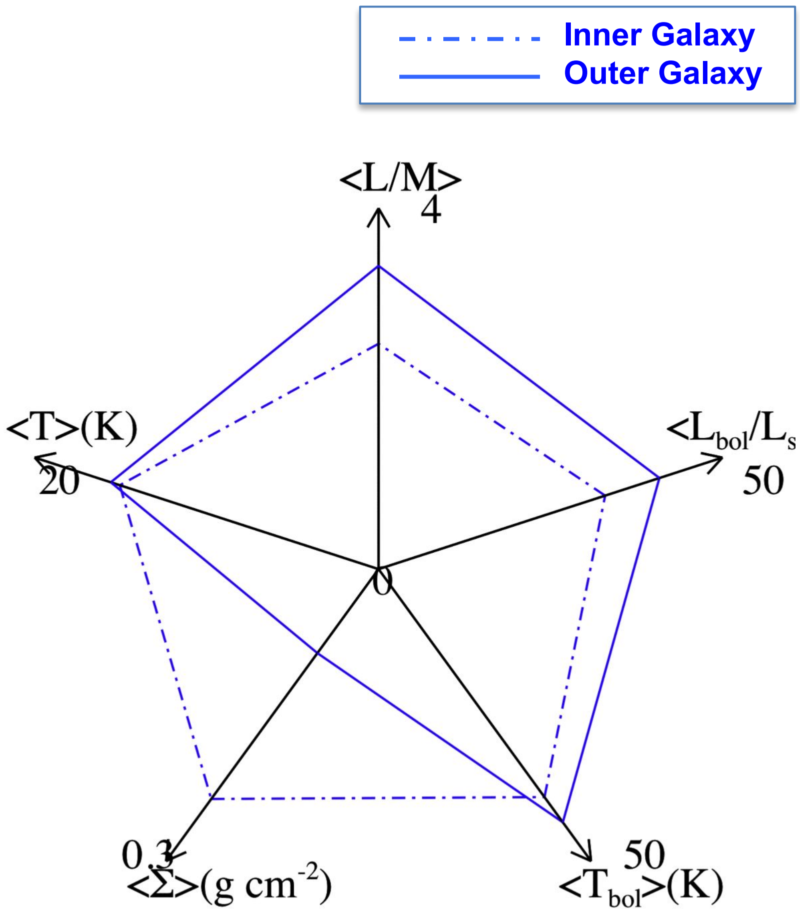

All the Hi-GAL sources located within *d* = 4 kpc have been virtually moved to larger distances, starting from *d* = 5 kpc, and their mutual separation re-evaluated accordingly. Sources getting blended after this operation define a new unresolved source that assumes a protostellar character if at least one of its original components was protostellar.

Trends with Galactocentric radius

Pre-stellar

Proto-stellar — MIR-dark / HII region candidates

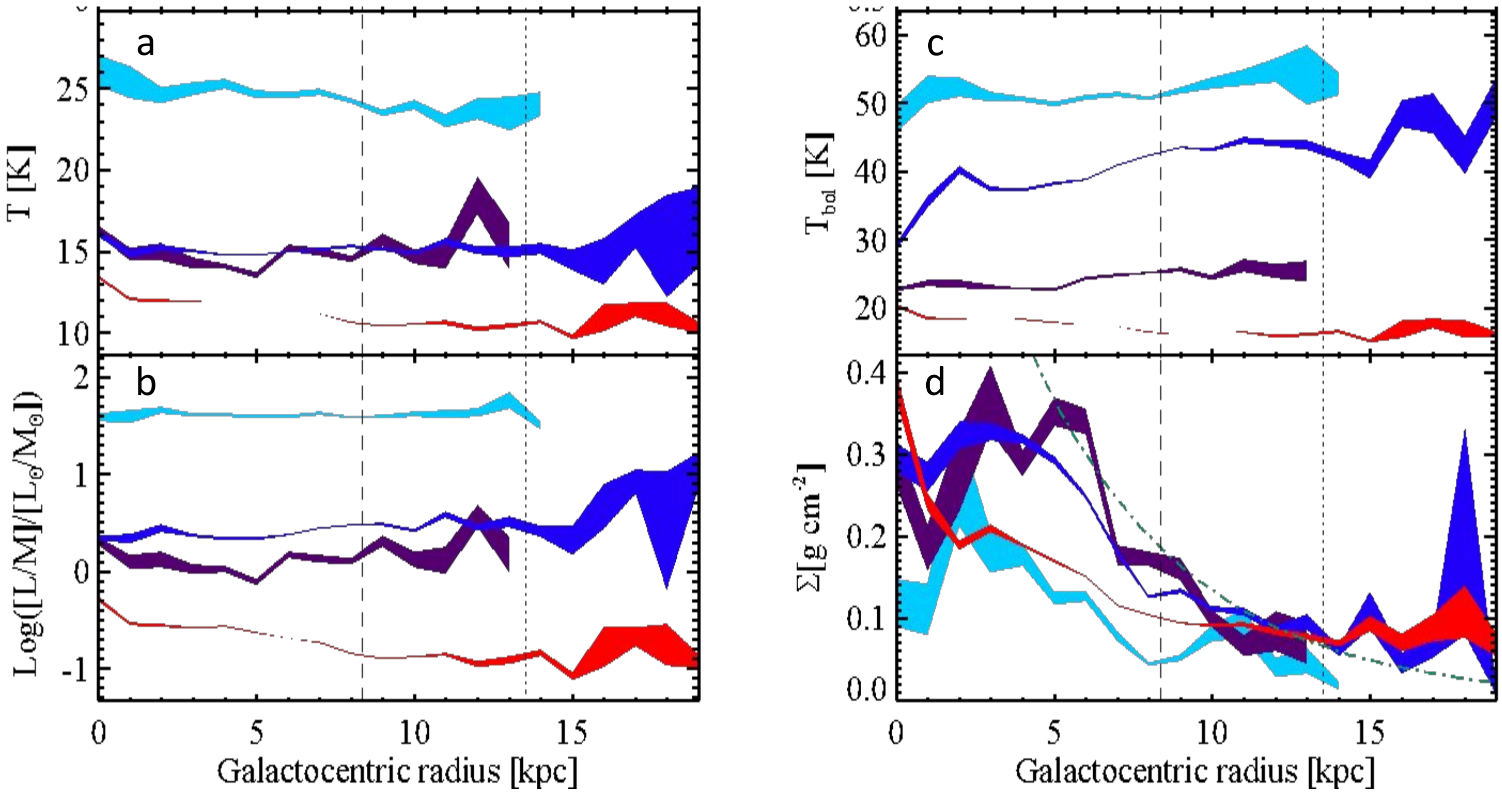

Medians of:

- **Temperature** (a)
- ***L / M*** (b)
- **Bolometric temperature** (c)
- **Surface density** (d)

…as a function of R_{gal}

No correspondence with spiral arm positions!

Milky Way metallicity profile

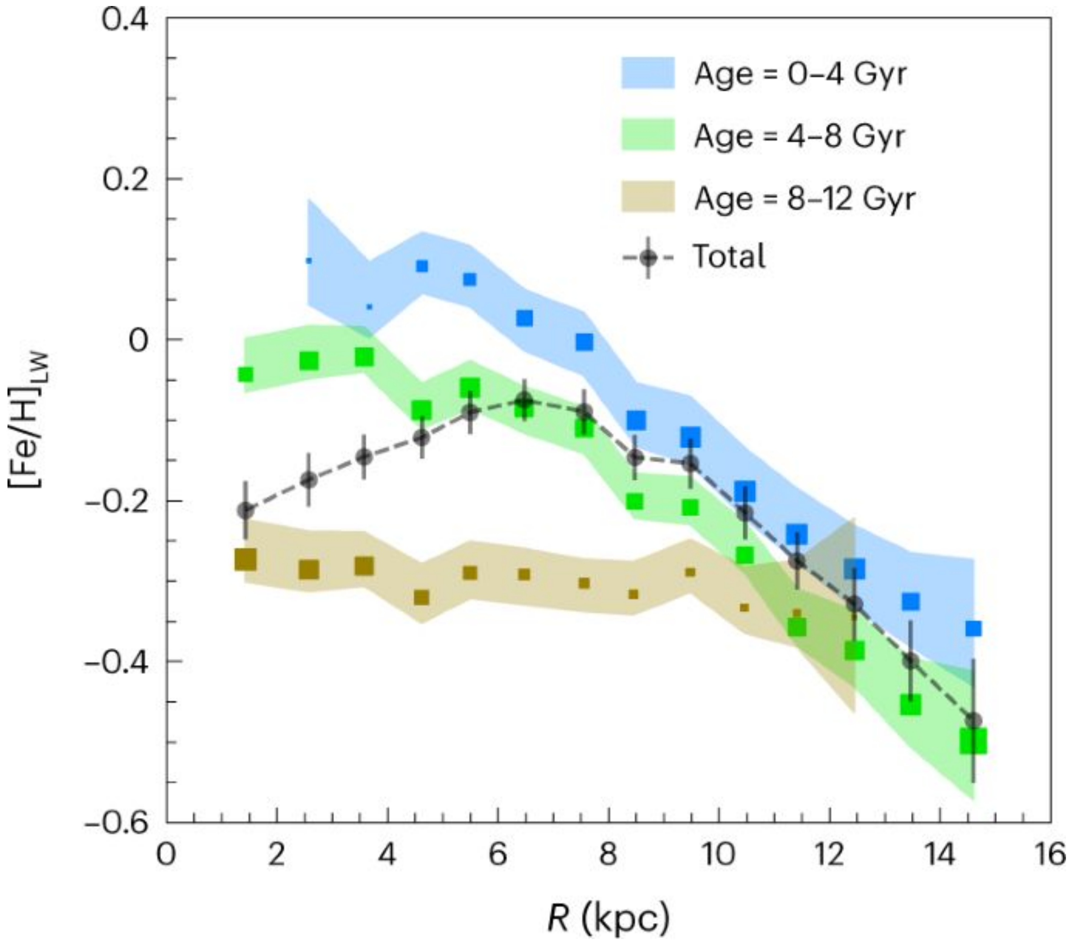

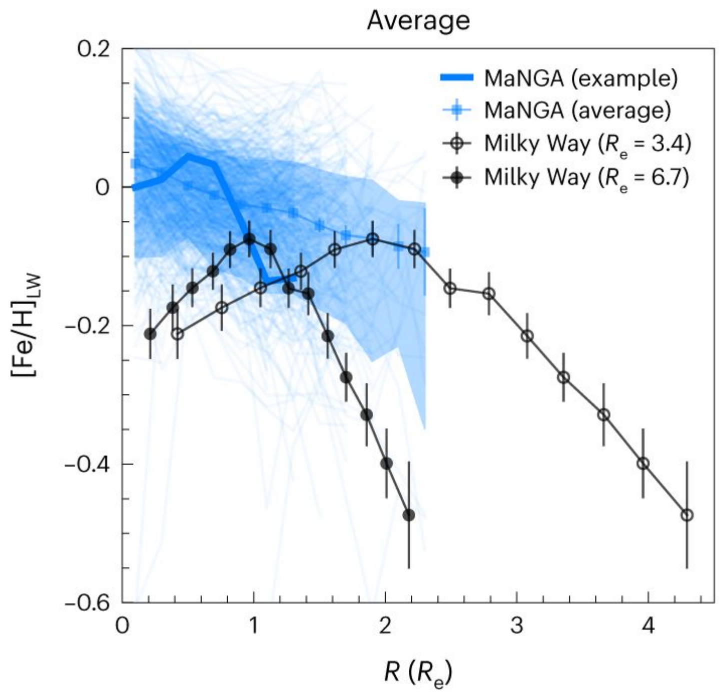

** Galaxy effective radius is the distance at which half of the total light of a galaxy is emitted.*

The integrated stellar metallicity profile of the Milky Way has a ∧-like broken shape, with a mildly positive gradient inside a Galactocentric radius of 7 kpc and a steep negative gradient outside. This broken integrated metallicity profile of the Milky Way is not unique but is not common among Milky Way-mass star-forming galaxies observed in the MaNGA survey (Lian+2023).

Measuring the MW SFR through FIR emission

Method	SFR $M_\odot\ yr^{-1}$	Reference
Ionization rate from radio free-free	0.35[a]	Smith et al. (1978)
Ionization rate from radio free-free	2.0 ± 0.6[a]	Guesten & Mezger (1982)
Ionization rate from radio free-free	1.6 ± 0.5[a]	Mezger (1987)
Ionization rate from [N II] 205 μm (COBE)	2.6 ± 1.3[a]	Bennett et al. (1994)
Ionization rate from [N II] 205 μm (COBE)	2.0 ± 1.0[a]	McKee & Williams (1997)
O/B Star Counts	1.8 ± 0.6[a]	Reed (2005)
Nucleosynthesis from ^{26}Al (INTEGRAL)	2.0 ± 1.2[a]	Diehl et al. (2006)
Continuum emission at 100 μm (COBE)	1.9 ± 0.8[a]	Misiriotis et al. (2006)
Ionization rate from microwave free-free (WMAP)	2.4 ± 1.2[a]	Murray & Rahman (2010)
YSO counts (*Spitzer*)	1.1 ± 0.4[a]	Robitaille & Whitney (2010)
YSO counts (MSX)	1.8 ± 0.3	Davies et al. (2011)
Combination of literature values	1.9 ± 0.4	Chomiuk & Povich (2011)
Continuum emission at 70 μm (*Herschel*)	2.1 ± 0.4	Noriega-Crespo (2013)
Combination of literature values	1.65 ± 0.19	Licquia & Newman (2015)
FIR clump counts (*Herschel*)	1.96 ± 0.74	Elia et al. (2022)

The star formation rate (SFR) predicted for Milky Way if all the clouds identified in CO surveys are collapsing at freefall exceeds the observed rate by at least two orders of magnitude.

With a total molecular mass of $1 \times 10^9\ M_\odot$ (Heyer & Dame 2015) and a free-fall time of 3.34×10^6 yr, taking a characteristic density of 100 cm^{-3}, if all molecular gas ($M_{mol,tot}$) forms stars with complete efficiency in a freefall time ($t_{ff,mol}$), the freefall SFR would be $SFR_{ff} = M_{mol,tot}/t_{ff,mol} = 300\ M_\odot\ yr^{-1}$. Instead

Measuring the MW SFR through FIR emission

The huge discrepancy between predicted and observed SFR is one of the most embarrassing in the field of star formation. It has been identified as the first of the three "big problems" in star formation, along with understanding stellar clustering and the origin of the initial mass function (Krumholz 2014).

The problem cannot be solved by rotational stabilization, as rotational energies are far less than gravitational or turbulent energies. Some combination of magnetic fields, turbulence, and feedback is generally invoked to explain why star formation is slow, but simulations with comparable gravitational and turbulent energies have difficulty matching the observations (SFR_{ff}/SFR_{obs} = 0.006), instead producing $SFR_{ff}/SFR_{obs} \gtrsim 0.1$, unless turbulence is continuously driven (with an artificial stirring force) and/or very strong magnetic fields are included.

Recently, Evans et al. (2022) demonstrated that the observed star formation rate of the Milky Way can be explained by applying a metallicity-dependent factor to convert CO luminosity to molecular gas mass and a star formation efficiency per freefall time that depends on the virial parameter of a molecular cloud, with the idea that the conversion of CO luminosity into mass is unlikely to be the same in all environments.

Star Formation Rate from protostellar clump counts

A first attempt in deriving the SFR in the two Hi-GAL SDP fields *l*=30°and *l*=59° (<u>Veneziani+2013</u>), comparing YSO statistics for <u>PROTOSTELLAR</u> clumps in the L_{bol} vs M_{env} plot against evolutionary predictions (McKee & Tan 2003, Molinari+2008).

Prescriptions updated to account for cluster formation with MC rather than single massive stars (Molinari+2019).

Each clump is associated to:

- **final ZAMS masses $M_{i,ZAMS}$**
- **formation times t_i**

$$SFR_c = \sum_i M_{i,ZAMS} / \tau_i$$

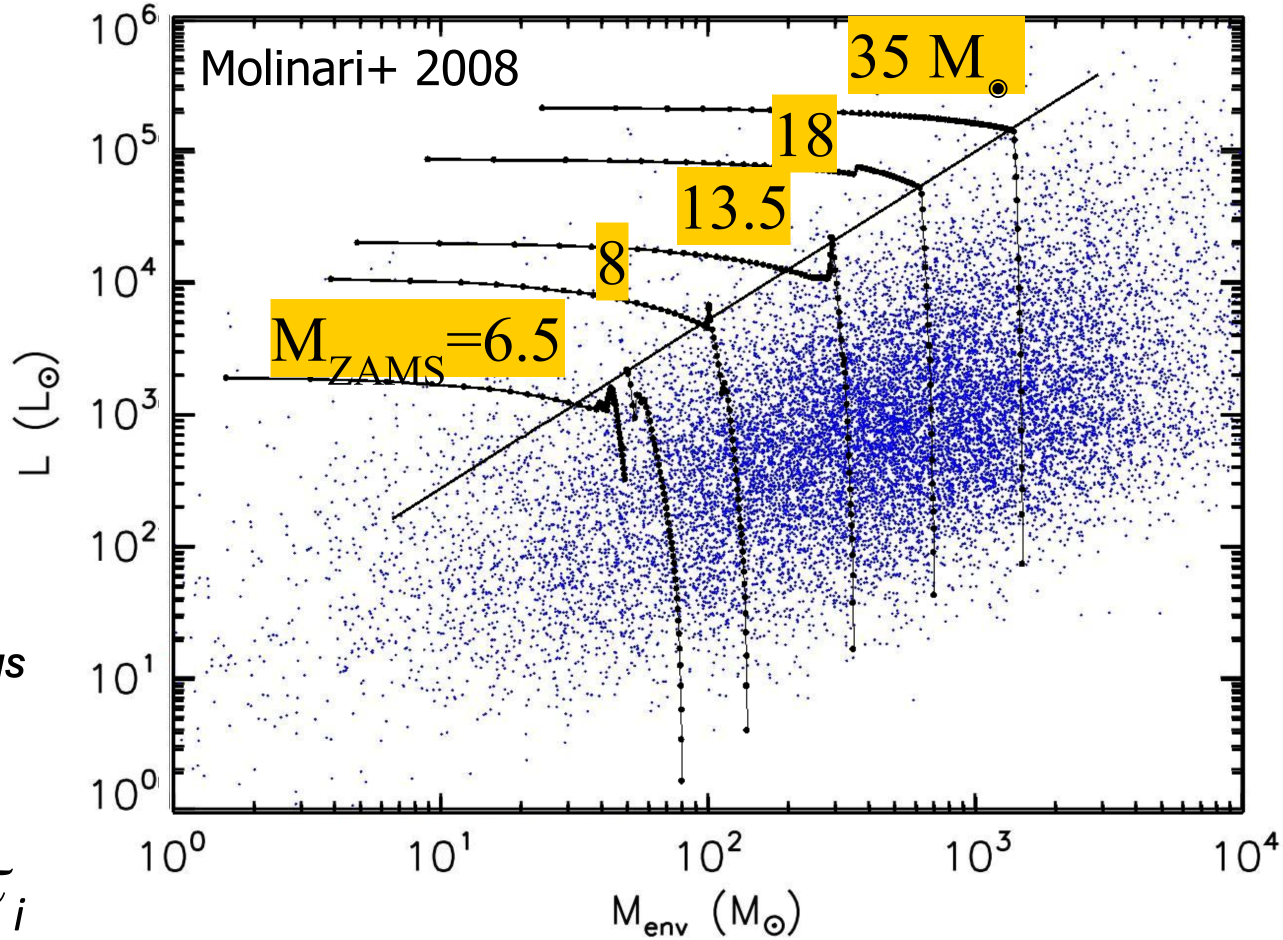

Global MW Star Formation Rate

SFR ≈ 1.7 ± 0.6 $M_\odot$ yr^{-1}

(84% of which from within the Solar circle)

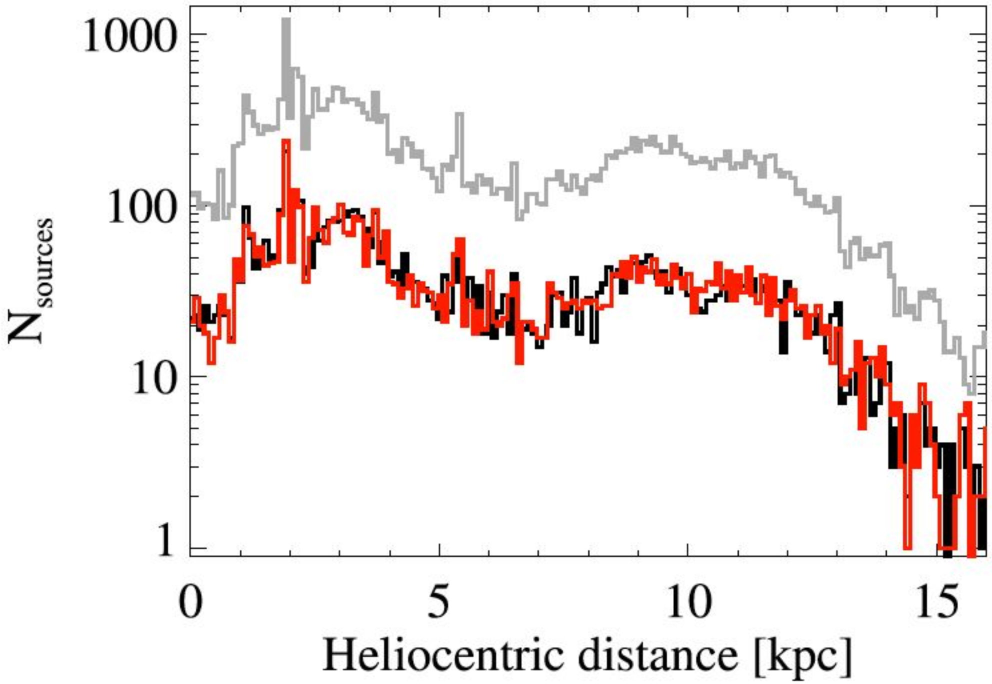

Trying to consider also the contribution of the "distanceless" clumps,

SFR ≈ 2.0 ± 0.7 $M_\odot$ yr^{-1}

Elia et al. (2022)

Is Milky Way SFR computation biased by the distance?

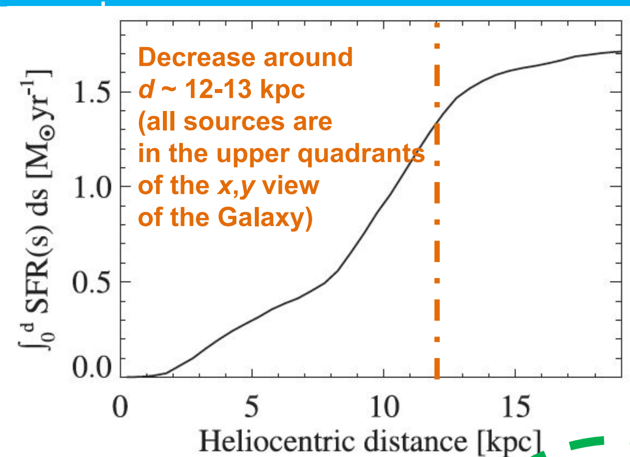

SFR calculated for nearby Gould Belt star forming regions does not change dramatically with simulated increasing distance (Baldeschi+2017b)

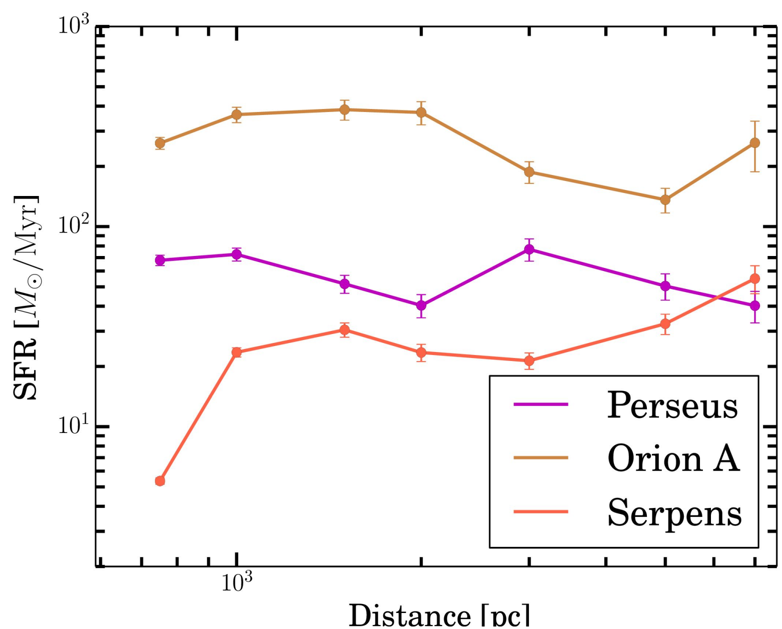

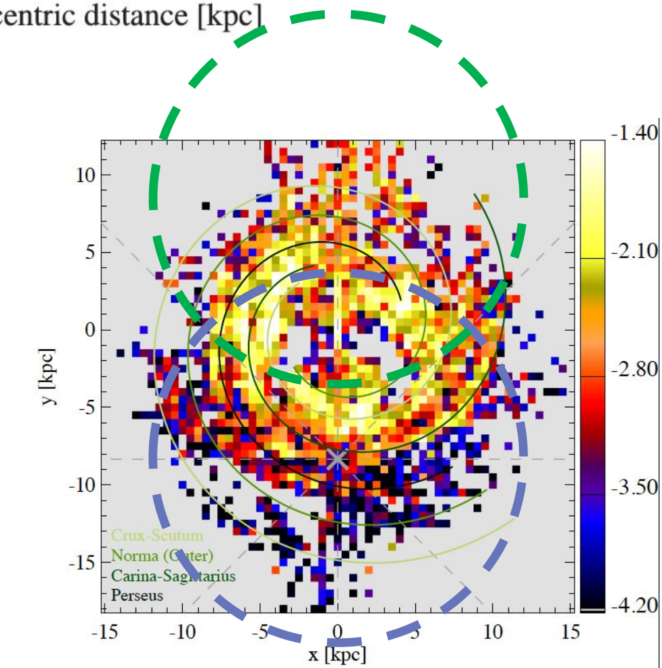

$SFR_{d>12kpc}$ = 0.45 $M_\odot$ yr^{-1}; $SFR_{symmetric}$ = 0.6 $M_\odot$ yr^{-1}.
Assuming symmetry w.r.t. GC, the difference corresponds to 8% of 1.7 $M_\odot$ yr^{-1} total SFR.

SFR in the CMZ

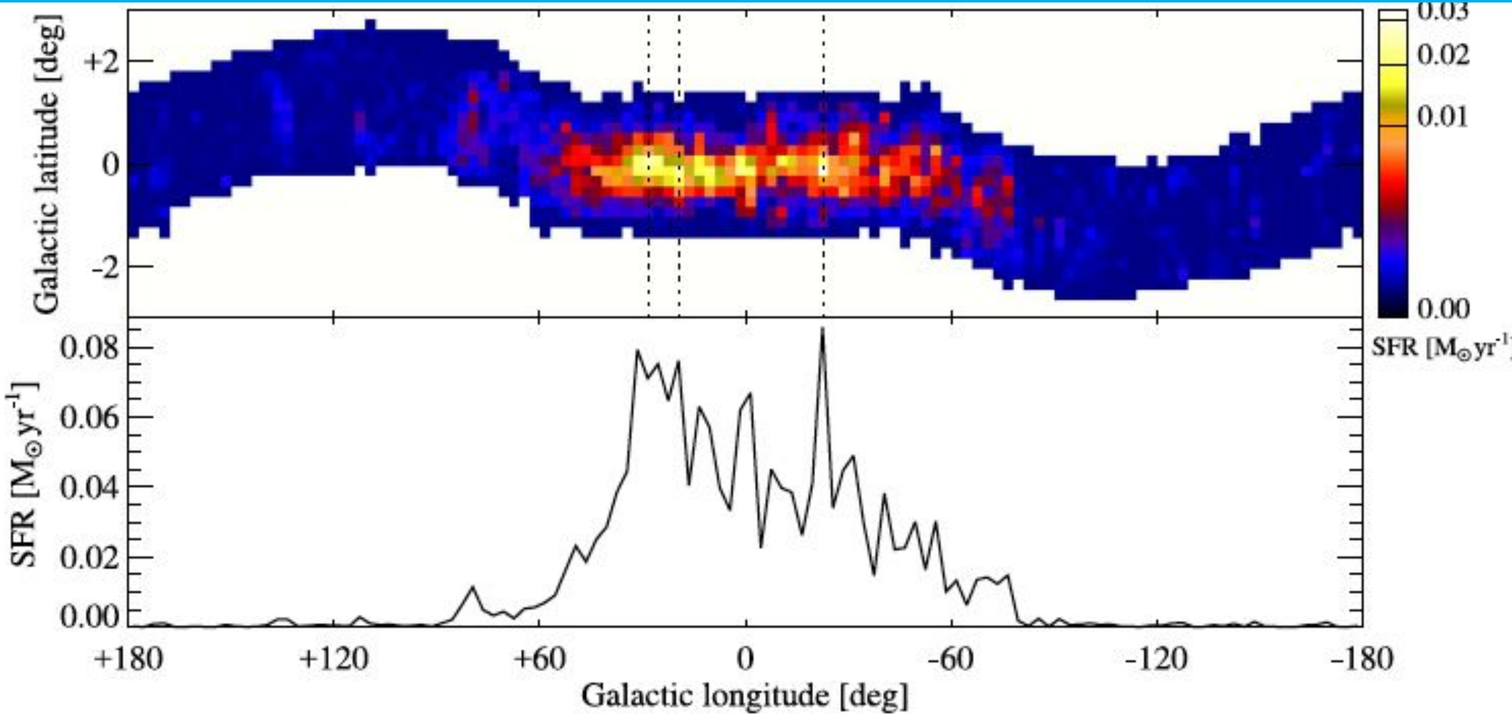

Star Formation Rate Estimates for the Central Molecular Zone

Method	Area Boundaries	SFR_{CMZ} (lit.) ($M_\odot$ yr^{-1})	References	SFR_{CMZ} (Elia+2022) ($M_\odot$ yr^{-1})
YSO counts (Spitzer)	$\lvert\ell\rvert < 1°$, $\lvert b\rvert < 10'$	0.14	Yusef-Zadeh et al. (2009)	0.04 ± 0.02
Continuum emission at 60, 100 μm (IRAS)	$\lvert\ell\rvert < 3°$, $\lvert b\rvert < 1°$ [a]	0.12	Crocker et al. (2011)	0.12 ± 0.05
Continuum emission at 60, 100 μm (IRAS)	$\lvert\ell\rvert < 0.8°$, $\lvert b\rvert < 0.3°$	0.08	Crocker et al. (2011)	0.04 ± 0.02
YSO counts (Spitzer)	$\lvert\ell\rvert < 1.5°$, $\lvert b\rvert < 0.5°$	0.08	Immer et al. (2012)	0.08 ± 0.03
Ionization rate from radio free–free	$2.5° < \ell < 3.5°$, $\lvert b\rvert < 0.5°$	0.035	Longmore et al. (2013)	0.11 ± 0.04
Ionization rate from radio free–free	as above, but $\lvert b\rvert < 1°$ for $\lvert\ell\rvert < 1°$	0.06	Longmore et al. (2013)	0.12 ± 0.05
Continuum emission at 24 μm (Spitzer)	$\lvert\ell\rvert < 1°$, $\lvert b\rvert < 0.5°$	0.09 ± 0.02		
Continuum emission at 70 μm (Spitzer)	$\lvert\ell\rvert < 1°$, $\lvert b\rvert < 0.5°$	0.10 ± 0.02	Barnes et al. (2017) [b]	0.06 ± 0.02[c]
Cont. emission at 5.8–500 μm (Spitzer, Herschel)	$\lvert\ell\rvert < 1°$, $\lvert b\rvert < 0.5°$	0.09 ± 0.03		

SFR distribution throughout the Galactic plane

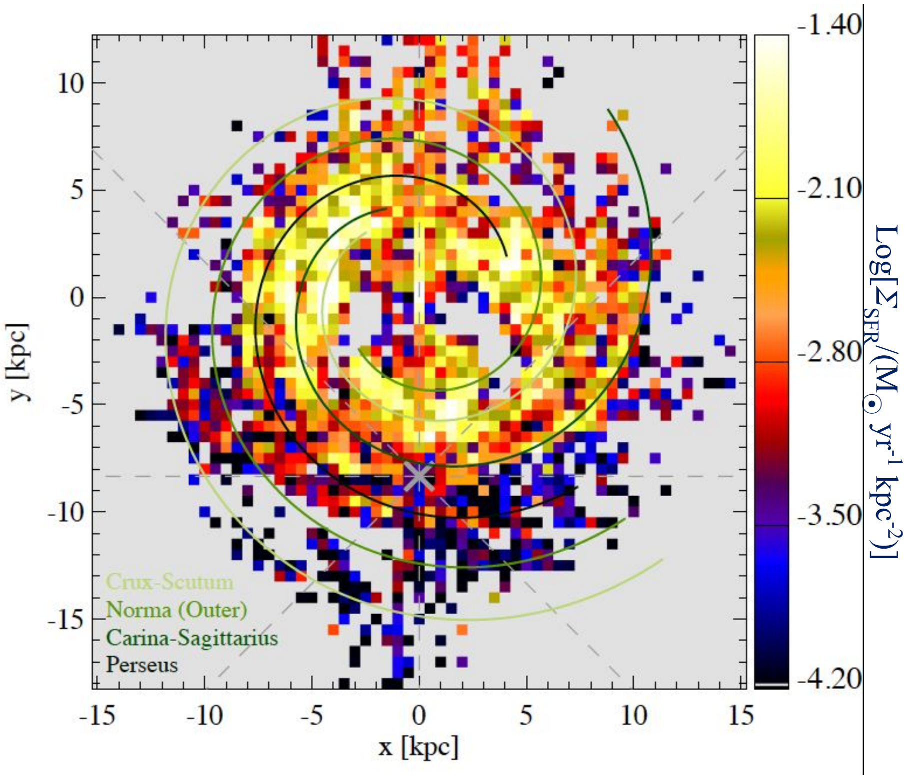

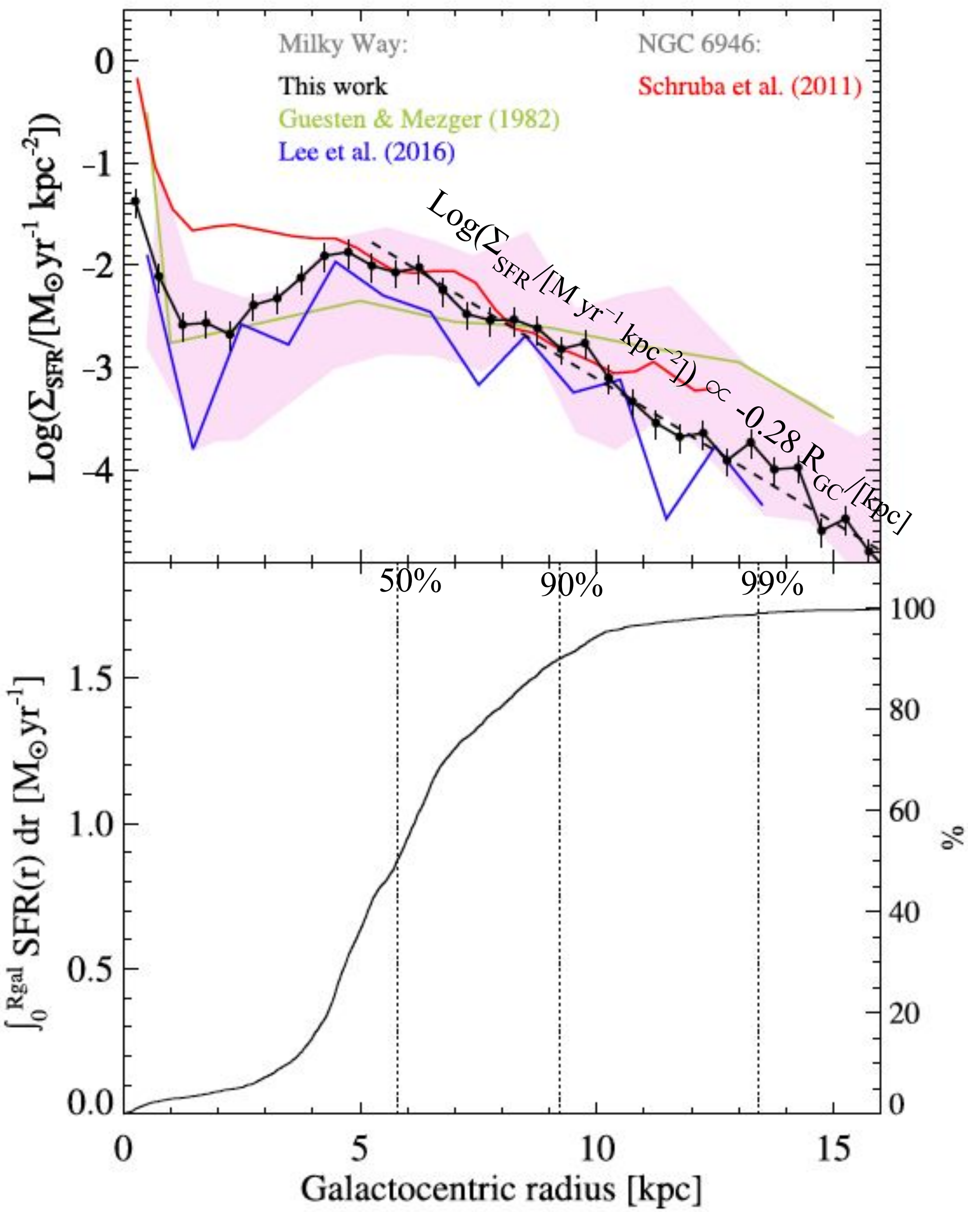

16% of total SFR comes from outside the Solar circle, and 1% from the far outer Galaxy (R_{GC} > 13.5 kpc).

SFR distribution throughout the Galactic plane

Zari+(2023) mapped the SFR distribution within a 6 x 6 kpc^2 box centered on the Sun, by using O-, B-, and A-type stars.
Soler+(2023) compared their Galactocentric profile with the one derived from clump counts.

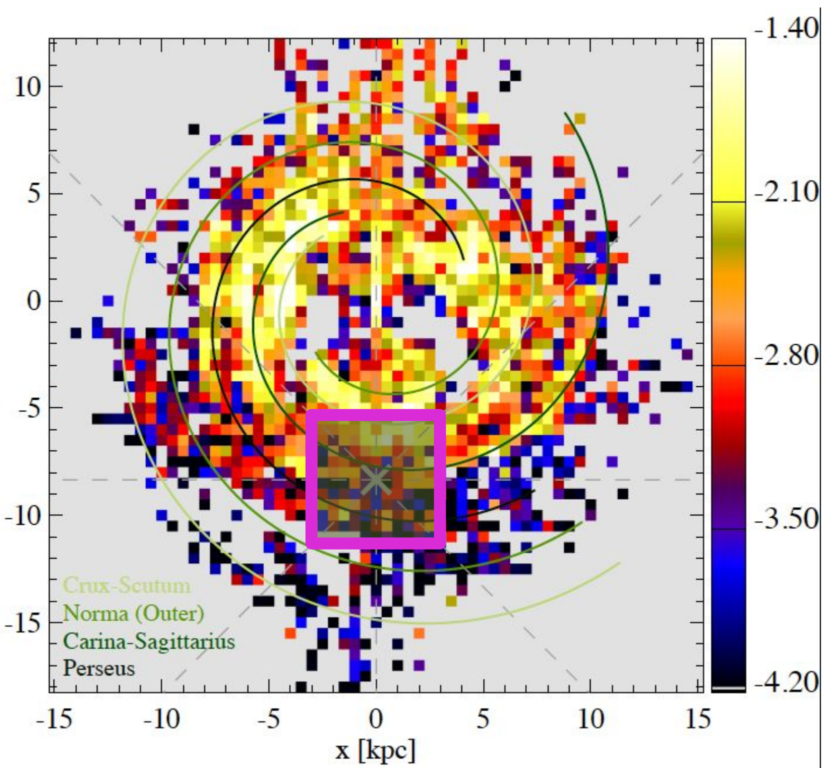

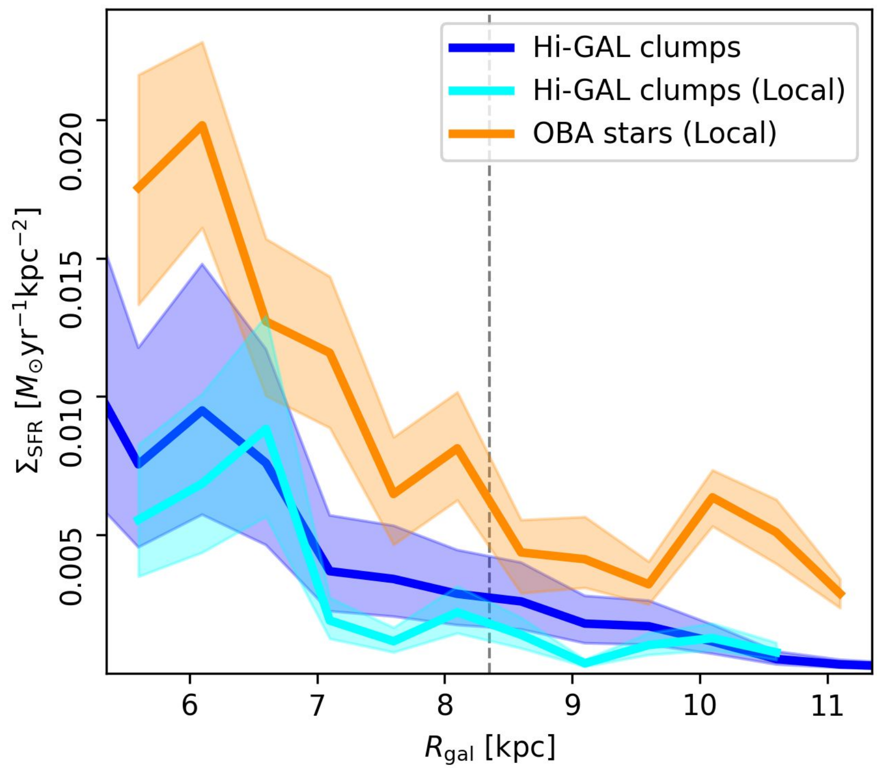

Soler+(2023)

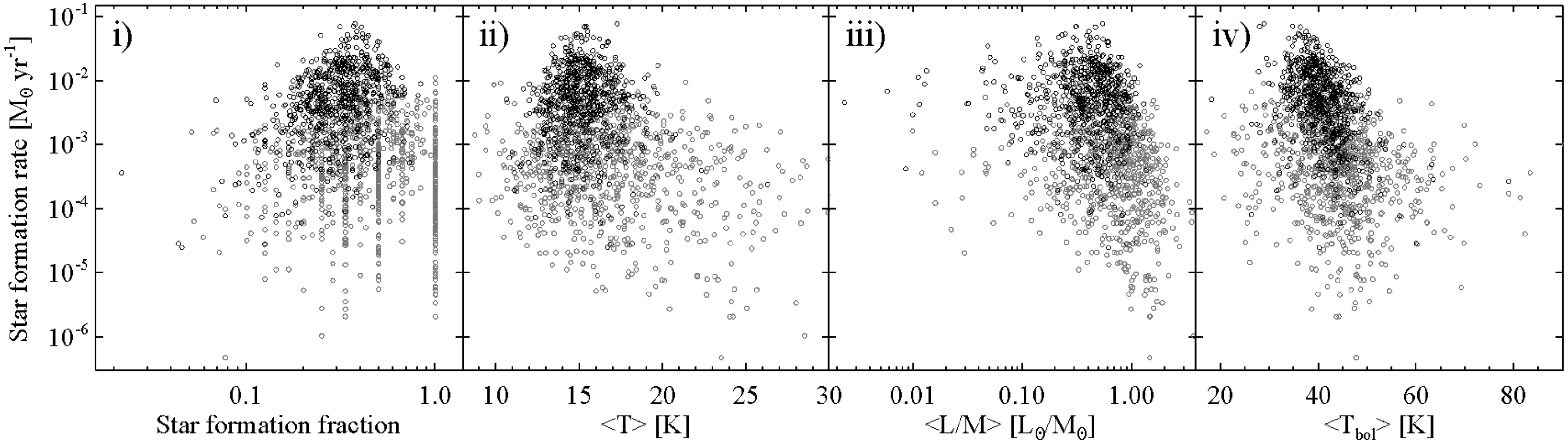

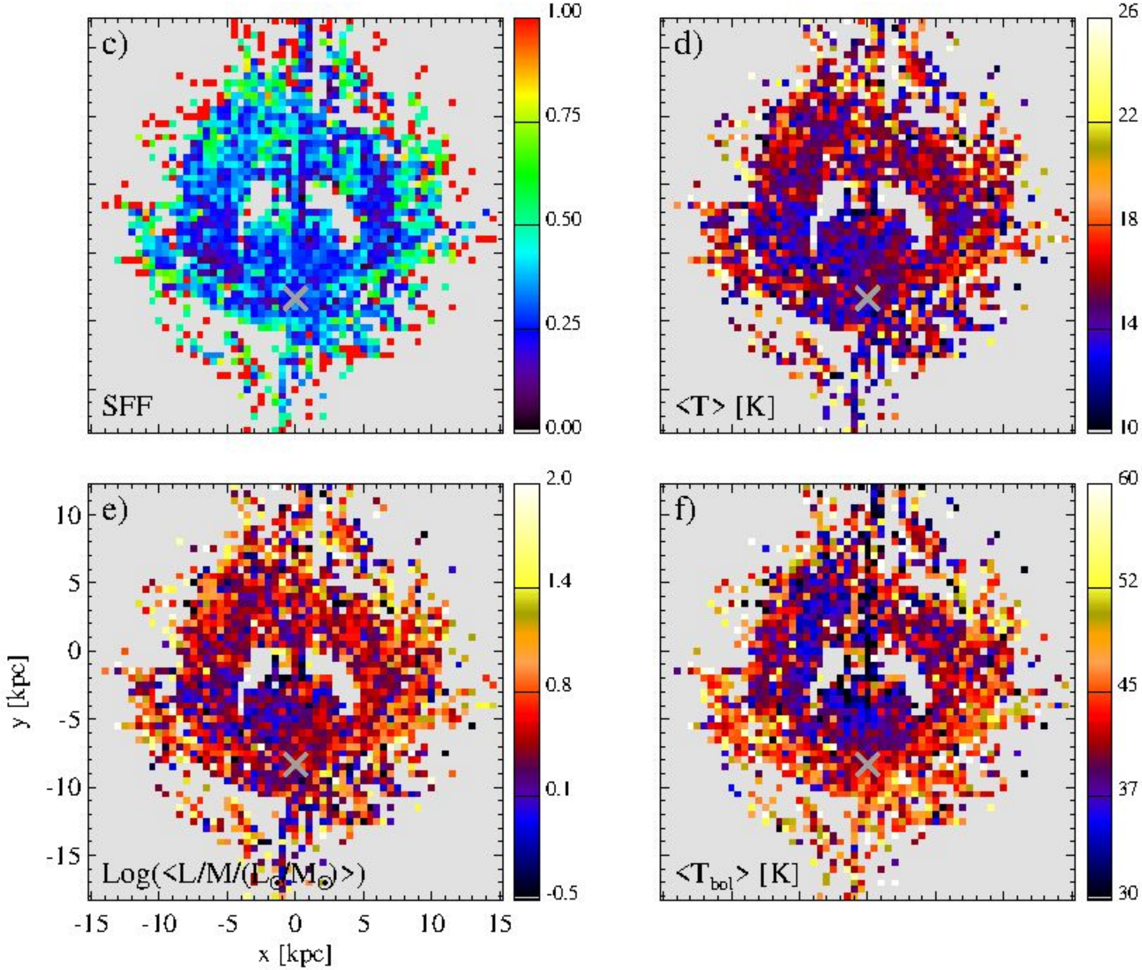

Comparing the maps of SFR in the Galactic plane with those of other observables considered indicative of the mean local evolutionary stage of clumps, no clear trends emerge.

Therefore, the SFR seems to be locally determined by mass availability itself much more than by evolutionary conditions.

Searching for recipes on the SFR…

A key ingredient in the understanding and modelling of galaxy evolution is the relationship between the large-scale star formation rate (SFR) and the physical conditions in the interstellar medium (ISM).

Most current galaxy formation and evolution models treat star formation using simple ad hoc parametrizations, and our limited understanding of the actual form and nature of the SFR-ISM interaction remains as one of the major limitations in these models.

Measurements of the star formation law in nearby galaxies can address this problem in two important respects, i) by providing empirical "recipes" that can be incorporated into analytical models and numerical simulations, and ii) by providing clues to the physical mechanisms that underlie the observed correlations.

The Kennicutt-Schmidt law

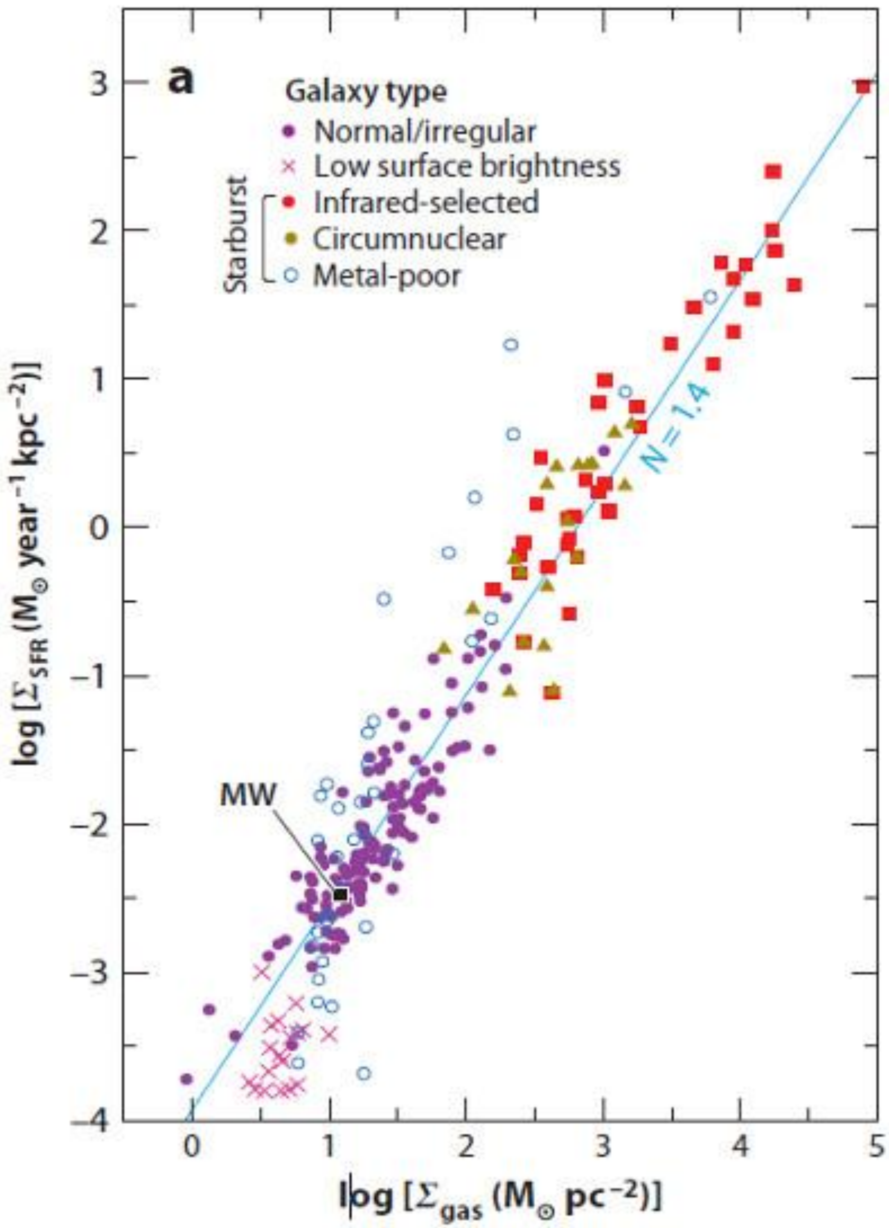

The most widely applied star formation law remains the simple gas density power law introduced by Schmidt (1959), which for external galaxies is usually expressed in terms of the observable surface densities of gas and star formation rate:

$$\Sigma_{SFR} = A\,\Sigma_{gas}^{N}$$

Hi-GAL K-S relation for Galactocentric rings

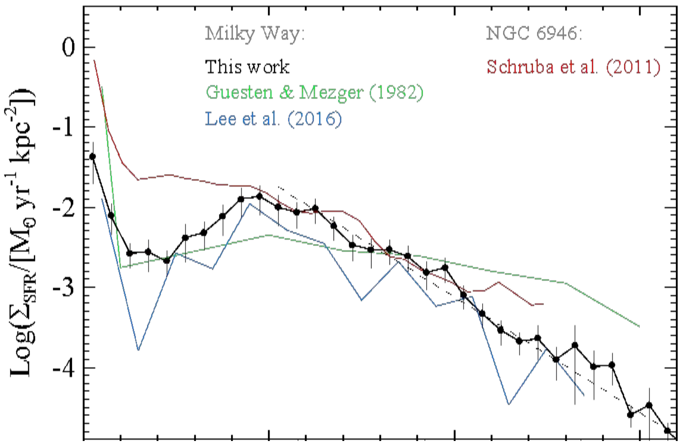

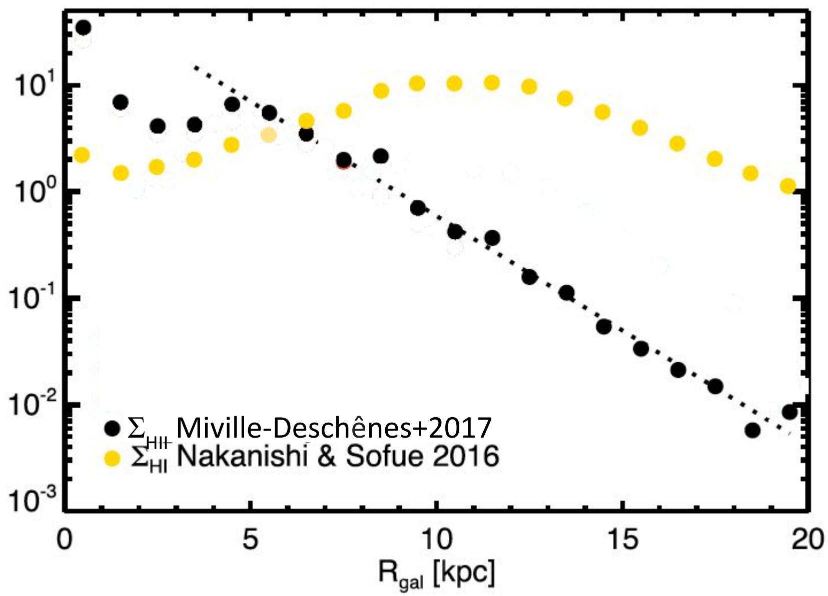

$$\Sigma_{SFR} \propto \Sigma_{H2}^{\ n}$$

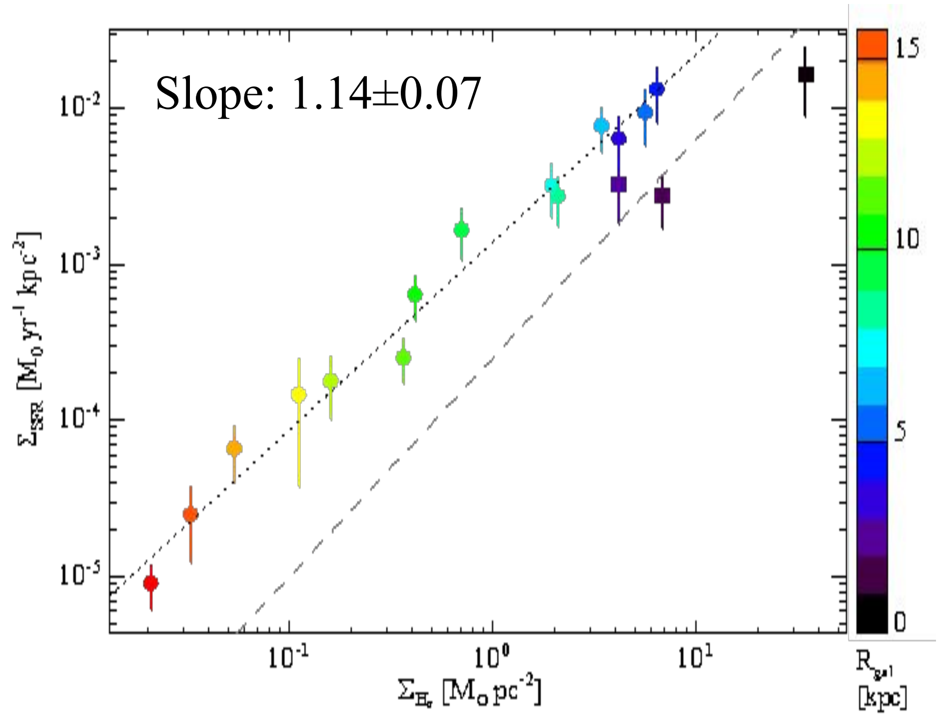

A power-law between Σ_{SFR} and Σ_{HII} is found for R_{GC} > 3 kpc, whereas this doesn't work with Σ_{HI}.